

MAGNETIC-AMPLIFIER ANALYSIS USING A
GENERALIZED MODEL FOR THE SATURABLE
REACTOR CORE

by

HERBERT HORACE WOODSON

S.B., Massachusetts Institute of Technology
(1952)

S.M., Massachusetts Institute of Technology
(1952)

SUBMITTED IN PARTIAL FULFILLMENT OF THE
REQUIREMENTS FOR THE DEGREE OF
DOCTOR OF SCIENCE

at the

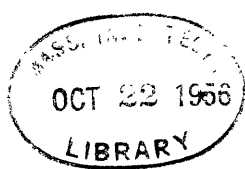
MASSACHUSETTS INSTITUTE OF TECHNOLOGY
(1956)

Signature of Author
Department of Electrical Engineering, May 14, 1956

Certified by

Accepted by ..
Chairman, Departmental Committee on Graduate Students

E6
Tenne
1956



DEPARTMENT OF ELECTRICAL ENGINEERING

MASSACHUSETTS INSTITUTE OF TECHNOLOGY
CAMBRIDGE 39, MASSACHUSETTS

May 8, 1956

Mr. H. H. Woodson
Room 10-098
M.I.T.

Dear Mr. Woodson:

This letter is to give you permission to print additional copies of your thesis by the multilith process, and to submit to the Department of Electrical Engineering copies thus produced, in lieu of the typed copies normally required.

A copy of this letter is to be reproduced by the same process and is to be placed in each copy of the thesis immediately following its title page.

Sincerely yours,

S. H. Caldwell
for the
Department Graduate Committee

SHC:mm

MAGNETIC-AMPLIFIER ANALYSIS USING A
GENERALIZED MODEL FOR THE SATURABLE
REACTOR CORE

by

HERBERT HORACE WOODSON

Submitted to the Department of Electrical Engineering on
May 14, 1956, in partial fulfillment of the requirements
for the degree of Doctor of Science.

ABSTRACT

A mathematical representation for a polycrystalline, thin-tape, ferromagnetic metal is derived for the operating conditions found during flux resetting in a magnetic amplifier. The starting point for the derivation is the dynamic behavior of the magnetization process in ferromagnetic single crystals reported in the literature. The general reactor representation is simplified to a form which is suitable for magnetic-amplifier analysis, and the simplified representation is verified experimentally. The constants which describe the reactor characteristics are obtained from a constant current switching characteristic of the type used for describing reactors in the digital-computer field.

The simplified reactor representation is applied to the analysis of a single-core, self-saturating magnetic-amplifier circuit with a direct resetting voltage and arbitrary reset circuit resistance. The results of the analysis yield reasonably accurate predictions of the amplifier input-output characteristic over wide ranges of supply frequency and reset circuit resistance. In addition, the reset circuit parameters necessary for maximum power gain are obtained in terms of the reactor constants and supply frequency. At the same time, the analysis yields a measure of the relative reset circuit resistance necessary for operation with so-called current control and voltage control. This provides an answer to the problem of whether reset circuit resistance is high or low.

Thesis Supervisor: David C. White
Title: Associate Professor of Electrical Engineering

✓

ACKNOWLEDGMENTS

A research of this type would be impossible without the encouragement and assistance of many people. The author would like to thank Professor David C. White for his support, encouragement, and patience in the supervision of this thesis. Thanks are due to Professors Kusko and Epstein for their helpful comments on the work, and especially to Professor Epstein and his colleagues in the Laboratory for Insulation Research who helped the author over many rough spots in the theory of ferromagnetism.

Miss Evelyn Fraccastoro was very helpful with the typing of the first draft in record time. The superb skill of Mrs. Bertha Hornby made the task of typing the final draft an easy one. Mr. Lund and Mr. Kelley, of the M.I.T. Illustration Service, have been most helpful with the figures.

The author appreciates the support extended by the Energy Conversion Group of the Servomechanisms Laboratory under Air Force Contract No. AF33(616)3242, without which this research would not have been possible.

TABLE OF CONTENTS

	Page
ABSTRACT	iii
CHAPTER I INTRODUCTION	
1.0.0 Objectives	1
1.1.0 Present Status of Magnetic-Amplifier Theory ..	2
1.1.1 Brief History of Magnetic Amplifiers ..	2
1.1.2 Operation of the Single-Core Circuit ..	7
1.1.3 Previous Analyses of the Single- Core Circuit	8
1.2.0 Theory of Ferromagnetism	13
1.2.1 Processes of Nucleation	15
1.2.2 Domain Wall Motion	18
CHAPTER II THE MATHEMATICAL REPRESENTATION FOR A REACTOR	
2.0.0 Introduction	23
2.1.0 Single-Domain Behavior	24
2.1.1 Plane Wall in Rectangular Specimen	24
2.1.2 Cylindrical Wall in Cylindrical Specimen	28
2.1.3 General Form of Equations Describing Single-Domain Behavior	31
2.2.0 Mathematical Representation for a Polycrystalline Material	35
2.2.1 Distribution of Starting Fields	36
2.2.2 Definition of an Average Normalized Domain Dimension	38
2.2.3 Rate of Change of Flux	40
2.3.0 Experimental Verification of the Representation	43
2.3.1 Switching with Large Constant Field ...	43
2.3.2 Switching with Small Constant Field ...	45
2.3.3 Switching with Slowly Varying Field ...	51
2.4.0 Variation of ID/OD Ratio	55

TABLE OF CONTENTS (continued)

	Page
CHAPTER III MAGNETIC-AMPLIFIER ANALYSIS USING THE REACTOR REPRESENTATION	
3.0.0 Introduction	58
3.1.0 "Exact" Analysis, Constant-Current Reset	63
3.1.1 Calculation of Reset Flux	65
3.1.2 Calculation of Normalized Input-Output Characteristic	66
3.1.3 Experimental Verification of "Exact" Analysis	66
3.2.0 Approximate Analysis	67
3.2.1 Constant-Current Reset	70
3.2.2 Constant Voltage Reset with Finite Resistance	72
3.2.3 Maximization of the Power Gain	74
3.2.4 Normalized Input-Output Characteristics, Finite Resistance ...	76
CHAPTER IV RESULTS AND CONCLUSIONS	
4.0.0 Introduction	80
4.1.0 The Mathematical Representation for a Reactor	83
4.1.1 Switching with Large Constant Field ..	87
4.1.2 Switching with Small Fields	88
4.2.0 Magnetic-Amplifier Analysis	91
4.2.1 "Exact" Magnetic-Amplifier Analysis ..	92
4.2.2 Approximate Magnetic-Amplifier Analysis	94
4.3.0 Conclusions	100
4.3.1 Material Quality	100
4.3.2 Application of Existing Reactors	102
4.4.0 Areas of Future Work	104
APPENDIX I DERIVATION OF SINGLE-DOMAIN BEHAVIOR	106
APPENDIX II INPUT-OUTPUT CHARACTERISTIC, "EXACT" ANALYSIS, CONSTANT-CURRENT RESET	112

TABLE OF CONTENTS (continued)

	Page
APPENDIX III MAXIMIZATION OF THE POWER GAIN	116
APPENDIX IV NORMALIZATION OF INPUT-OUTPUT CHARACTERISTICS	119
BIOGRAPHICAL NOTE	122
BIBLIOGRAPHY	123

ILLUSTRATIONS

<u>Fig. No.</u>	<u>Title</u>	<u>Page</u>
1-1	Saturable reactor circuits	4A
1-2	Φ -F characteristic of ideal saturable reactor	4A
1-3	Series-connected saturable reactor with feedback	6A
1-4	Examples of self-saturating circuits	6A
1-5	Doubler circuit using two cores	6B
1-6	Single-core self-saturating circuit	6B
1-7	Single-core circuit	6B
1-8	Dynamic B-H loop for 2-mil Orthonol 60 cps sinusoidal flux	6C
1-9	Voltage-current characteristic of silicon junction rectifier	8A
1-10	Φ -F loop of saturable reactor	8A
1-11	Domain configurations	12A
1-12	Specimen shape for mathematical representation	12A
1-13	Specimen with surface imperfection	16A
1-14	Processes of flux change	16A
1-15	Energy as a function of wall position	16A
2-1	Structure for plane-wall movement	24A
2-2	Definition of co-ordinates for plane- wall motion	24A
2-3	Normalized rate of change of flux vs wall position for a plane wall in a rectangular specimen with eddy-current damping only	26A
2-4	Structure for cylindrical domain dynamics	26A
2-5	Definition of variables for cylindrical wall ...	28A
2-6	Voltage waveform for expanding cylindrical domain in cylindrical specimen with constant applied field and eddy-current damping	28A

ILLUSTRATIONS (continued)

<u>Fig.No.</u>	<u>Title</u>	<u>Page</u>
2-7	Voltage waveform for expanding cylindrical domain in cylindrical specimen with constant applied field and spin-relaxation damping	30A
2-8	Nucleation at two sites	30A
2-9	Illustrating distortion of domain wall	30A
2-10	Demonstrating distribution of nucleating sites and shape of nucleated domains in simplified representation	36A
2-11	Number of domain walls moving as a function of applied field	36A
2-12	Distribution of moving walls with applied field	38A
2-13	Area of reversed magnetization as a function of the average normalized dimension r	38A
2-14	One type of distribution of starting fields	44A
2-15	Switching characteristics at high applied fields	44A
2-16	Shape of voltage pulse for constant applied field	44A
2-17	Plots of $(d\varphi/dt)_{pk}$ vs $(H-H_c)$ for three reactors	50A
2-18	Circuit for checking representation with slowly varying field	52A
2-19	Approximation for $G(H)$ to yield switching characteristics that vary as the square of the effective field	52A
2-20	Plots of $(d\varphi/dt)_{pk}$ vs $(H-H_c)$ for various values of N_r^2/R_r	54A
2-21	Core configuration for investigating the effect of ID/OD ratio	56A
3-1	Single-core self-saturating magnetic-amplifier circuit	56A
3-2	Operating φ -F loop	58A
3-3	Typical waveforms in circuit	58A
3-4	Reset waveforms	64A

ILLUSTRATIONS (continued)

<u>Fig.No.</u>	<u>Title</u>	<u>Page</u>
3-5	Normalized rate of change of flux as a function of ωt for various values of ω_r	66A
3-6	Normalized input-output characteristic of the amplifier	66B
3-7	Experimental arrangement for input-output characteristics with constant-current reset and variable frequency	66C
3-8	Illustrating the flattening of the reset waveform with increasing N^2/R	66C
3-9	Comparison of theoretical and experimental input-output characteristics for constant-current reset, approximate analysis	70A
3-10	Theoretical and experimental power gain as a function of the relative reset N^2/R	76A
3-11	Experimental arrangement for input-output characteristics with variable reset N^2/R and variable frequency	76B
3-12	Theoretical and experimental input-output characteristics for $\gamma = 0.343$	76C
3-13	Theoretical and experimental input-output characteristics for $\gamma = 1.0$	76D
3-14	Normalized current gain as a function of relative reset conductance	78A
4-1	Qualitative plot of the distribution of domain wall starting fields	86A

Chapter I

INTRODUCTION

1.0.0 Objectives

In the analysis of a self-saturating magnetic amplifier, the flux resetting characteristic of the saturable reactor must be described analytically. In most analyses of the past, the reactor characteristic has been represented by a single-valued relation between flux and magnetomotive force. Such a restrictive representation does not yield correct predictions of magnetic-amplifier performance over wide ranges of supply frequency and control-circuit resistance. In order to obtain such predictions, a more general representation of the reactor characteristic must be used. Consequently, the objectives of this research are: (1) to obtain a more general reactor representation, and (2) to apply this representation to the analysis of a single-core, self-saturating magnetic amplifier.

. Mathematically, the generalization of the reactor representation must be obtained by the use of one or more variables in addition to flux and magnetomotive force. These additional variables, which must describe the physical processes active in the reactor material, will be obtained from a consideration of the dynamics of ferromagnetic domains. Although little detailed information is available about the magnetization process in polycrystalline specimens, several studies of single-crystal specimens in which agreement between theory and experiment was good have been reported in the literature. Consequently, the equations describing domain wall dynamics in

single crystals will be used as a starting point for the derivation of a representation for a polycrystalline reactor material. The representation in its most general form will be too complicated for simple inclusion in a magnetic-amplifier analysis; consequently, the general representation will not be checked experimentally. Several simplifications will be made in the representation to facilitate circuit analyses. These simplified representations will be experimentally verified for simple types of excitation.

The magnetic-amplifier analysis yields predictions of magnetic-amplifier characteristics over wide ranges of supply frequency and control-circuit resistance. The predictions with respect to control-circuit resistance also give information about the maximum power gain obtainable with a given reactor as a function of supply frequency. In addition, a definition of "high" and "low" control-circuit resistance, with an adequate description of the transition region, will be obtained. Such a definition is not available in the literature.

1.1.0 Present Status of Magnetic-Amplifier Theory

In order to define the ferromagnetic problem to be solved, magnetic-amplifier theory must be reviewed. Consequently, a brief history of magnetic amplifiers will be given along with the types of analyses used and the limitations of each analysis.

1.1.1 Brief History of Magnetic Amplifiers

A magnetic amplifier is defined by the AIEE Magnetic Amplifier Committee as "a device using saturable reactors

either alone or in combination with other circuit elements to secure amplification or control."^{1*} The phenomenon used "to secure amplification or control" is the flux saturation property of ferromagnetic materials. Thus the above definition includes all circuits utilizing controllable saturable reactors regardless of whether or not useful power gain is obtained. The primary objective of this research is the analysis of the self-saturating magnetic amplifier which provides a useful power gain; consequently, the historical description will be limited to those magnetic-amplifier circuits which provide useful power gain.

The earliest magnetic amplifiers were the so-called series- and parallel-connected saturable-reactor circuits shown schematically in Fig. 1-1. These circuits were first used during the early years of the twentieth century.^{2,3} There was little nonlinear-circuit analysis at that time; consequently, experimental curves for existing amplifiers were used for application purposes. A short time later, a piece-wise linear analysis having application to saturable-reactor circuits was presented by Boyajian.⁴ He applied the analysis to saturable-reactor circuits using a piece-wise linear approximation to the normal magnetization curve of the reactor. The cores used in the early saturable-reactor circuits were constructed of stacked laminations of transformer steel; thus the magnetic paths contained relatively large air gaps. Reactors constructed by the use of such cores were accurately described by normal magnetization curves.

*

The superscript numerals refer to the bibliography.

During the 1930's and 1940's, better ferromagnetic materials were developed, along with improved techniques of core fabrication to reduce air gaps. It was determined that improvements in core materials beyond a certain quality gave no further improvement in magnetic-amplifier performance. This resulted because the saturable-reactor circuits have definite limits of operation even for perfect reactors:^{5,6,7} i.e., reactors having zero saturated impedance, infinite unsaturated impedance, and no losses, as shown in Fig. 1-2. The analysis given by Johannessen⁵ showed that when the reactor characteristics are improved beyond the point where the unsaturated reactor impedance is large compared to the load resistance, no further improvement in amplifier characteristics is obtained.

At the same time that core materials were being improved, better dry rectifiers became available. These rectifiers were first used to rectify the output of the magnetic-amplifier circuits for the purpose of obtaining d-c output. This mode of operation did not appreciably affect the magnetic-amplifier characteristics. However, when the rectified load current was made to flow through a winding in such a way as to aid the control current, both the power gain and the speed of response were improved.⁸ The use of the load current in this way was termed "feedback"; however, the results (increase of gain and decrease of time constant) are not consistent with conventional feedback amplifier theory. Johannessen⁵ removed the inconsistency by pointing out that the increase in power gain results because the addition of the rectifiers to provide "feedback" effectively raises the input impedance of the device, while

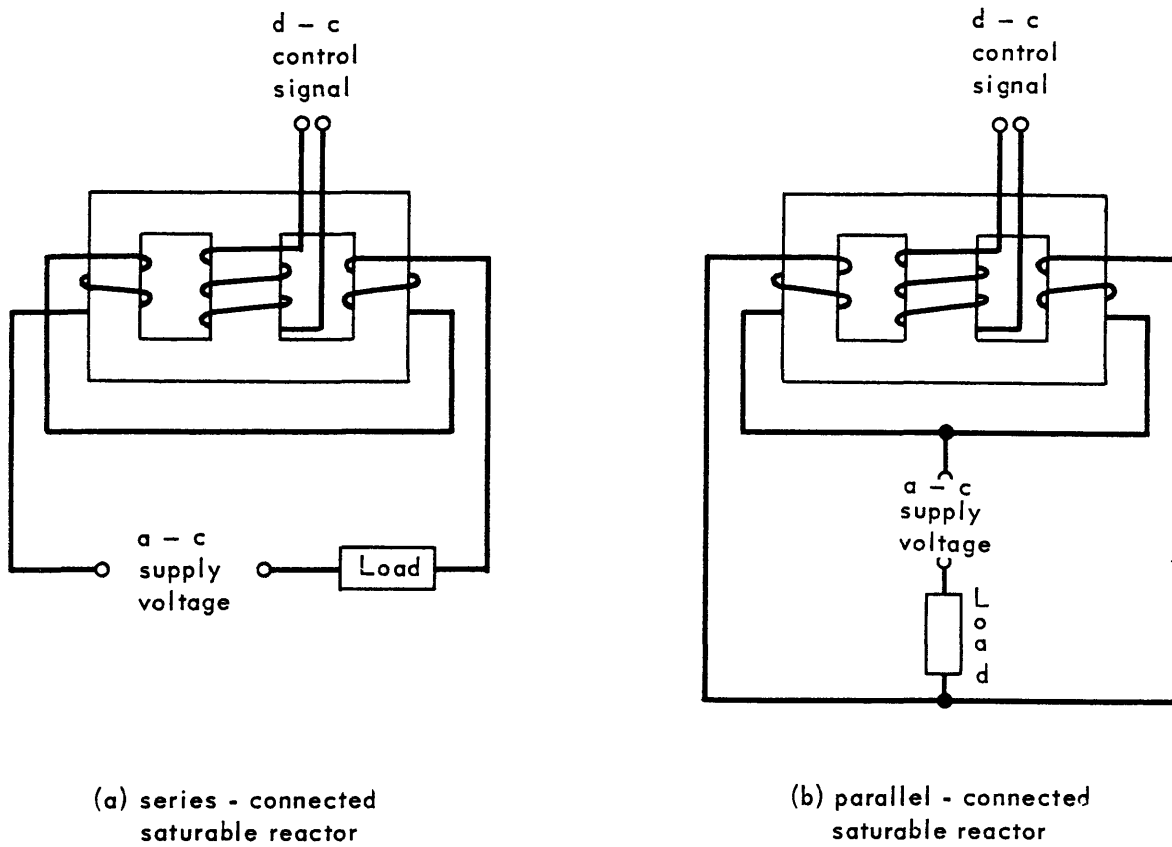
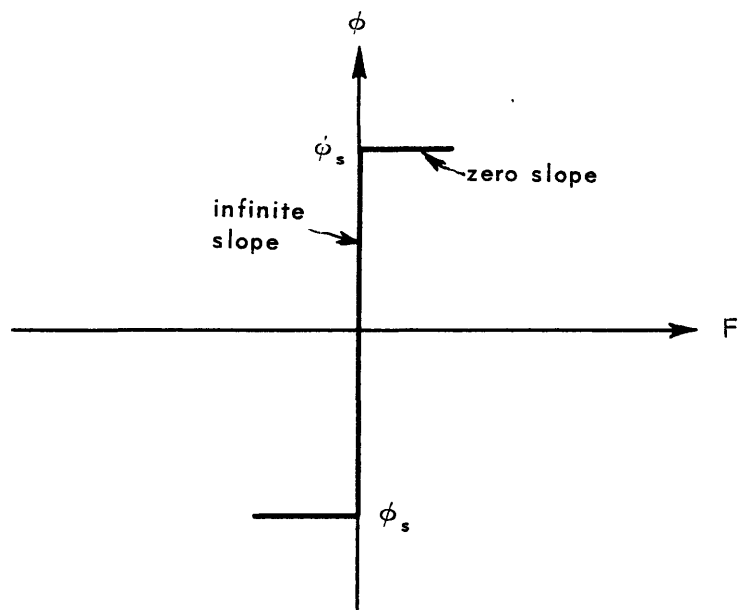


Fig. 1.1. Saturable reactor circuits

Fig. 1.2. ϕ - F characteristic of ideal saturable reactor

the volt-time integral (flux) necessary for control remains the same. By the same token, the time constant is reduced, because the apparent inductance of the control circuit remains the same, while the input impedance is increased. A series-connected saturable-reactor circuit with external "feedback" is shown schematically in Fig. 1-3.

When the discovery was made that rectified load-current feedback improved the dynamic performance of magnetic amplifiers, several investigations were made into the extent of improvement possible. With the highly rectangular B-H loop materials and 100 percent feedback (feedback turns equal to load turns), it was expected that the circuit would have practically infinite gain. The gain was much lower than the analyses indicated⁹ for any feedback above 80 percent.¹⁰ The reduction in gain from the high level expected occurred because the high level of feedback increased the input impedance until it was limited by either reactor or rectifier characteristics. It was found that practical circuits could be designed in which the rectifier operation was essentially ideal; thus the ultimate limitation on magnetic-amplifier performance was shown to be the dynamic reactor characteristics.

Experiments performed with 100 percent feedback showed that essentially the same dynamic performance could be obtained by eliminating the feedback winding and by placing rectifiers in series with the load-circuit windings in the parallel-connected saturable reactor.¹¹ A circuit operating in this manner is called a self-saturating circuit. Several different self-saturating circuits then evolved, two examples of which

are shown schematically in Fig. 1-4. At this time, in magnetic-amplifier development, gapless toroidal cores fabricated by spirally winding thin metal tapes became available. In order to apply these new cores in the circuits using the three-legged core construction, it was only necessary to wind a control winding on each core separately or on both cores together after the power windings had been placed on the separate cores. An example of a self-saturating magnetic amplifier using two separate cores is shown in Fig. 1-5.

In any self-saturating magnetic-amplifier circuit there is a rectifier associated with the load winding which is coupled to each magnetic circuit. Consequently, a multi-core magnetic-amplifier circuit can be treated as an interconnection of simple circuits, each containing one rectifier and one magnetic circuit. Such a simple circuit is known as a single-core, self-saturating circuit, and is shown schematically in Fig. 1-6.

With the advent of the self-saturating magnetic amplifier, there appeared in the literature a great many analyses of a large number of self-saturating circuits. The usual procedure has been to attempt an analysis of the single-core circuit, and then to infer the operation of a more complicated circuit from the result. The principal shortcoming of each of these analyses has been that the operation of the reactor has been approximated by a mathematical representation of insufficient generality to allow accurate description of the operation in a magnetic amplifier. These mathematical representations were usually derived empirically from some measured terminal characteristic under simplified excitation conditions, and no

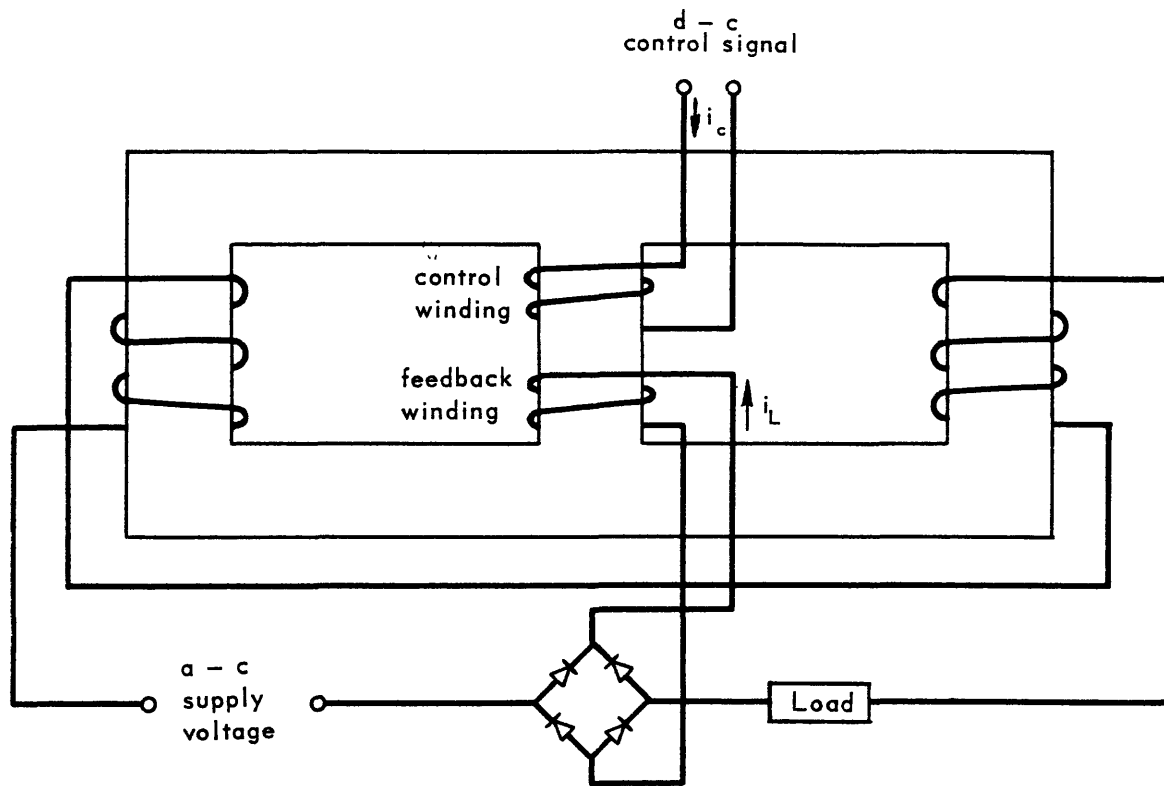


Fig. 1.3. Series-connected saturable reactor with feedback

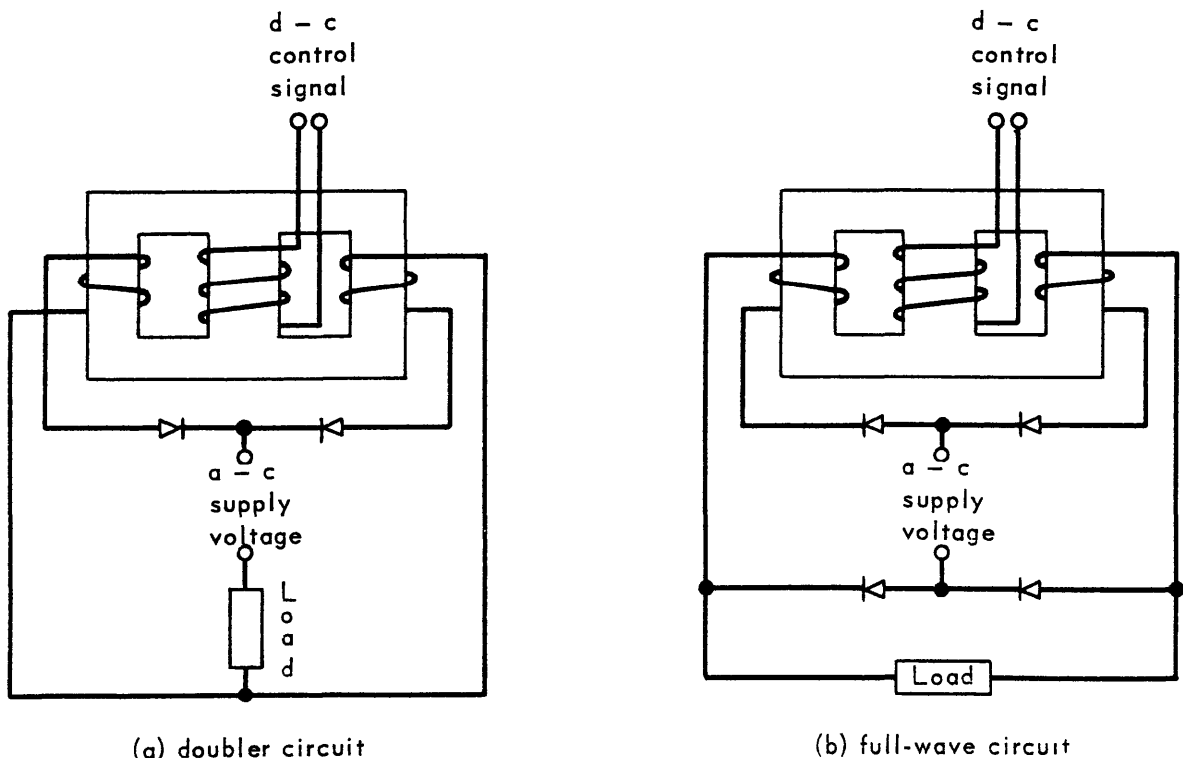


Fig. 1.4. Examples of self-saturating circuits

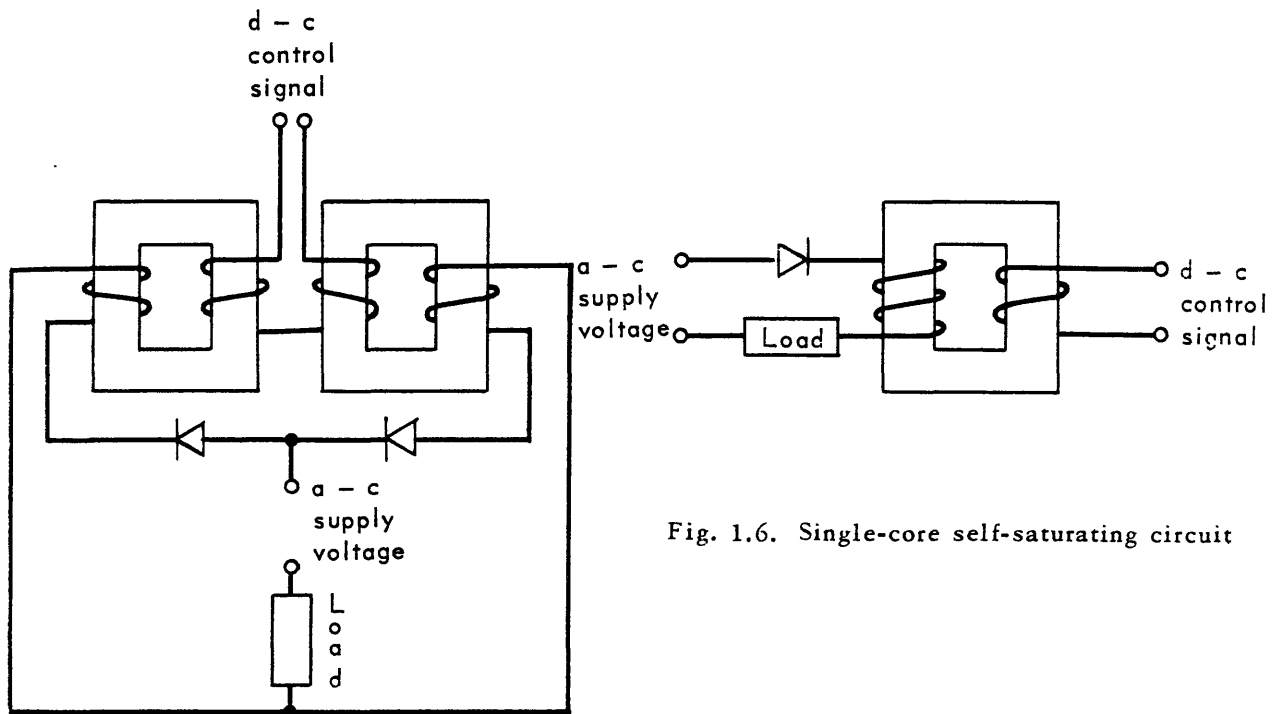


Fig. 1.5. Doubler circuit using two cores

Fig. 1.6. Single-core self-saturating circuit

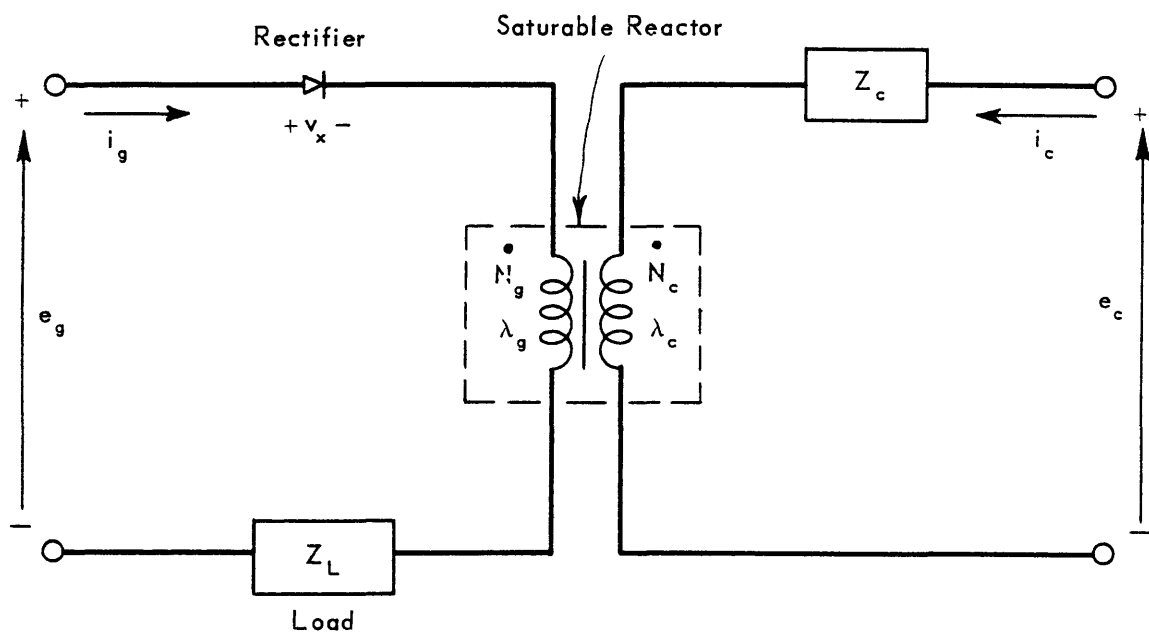


Fig. 1.7. Single-core circuit

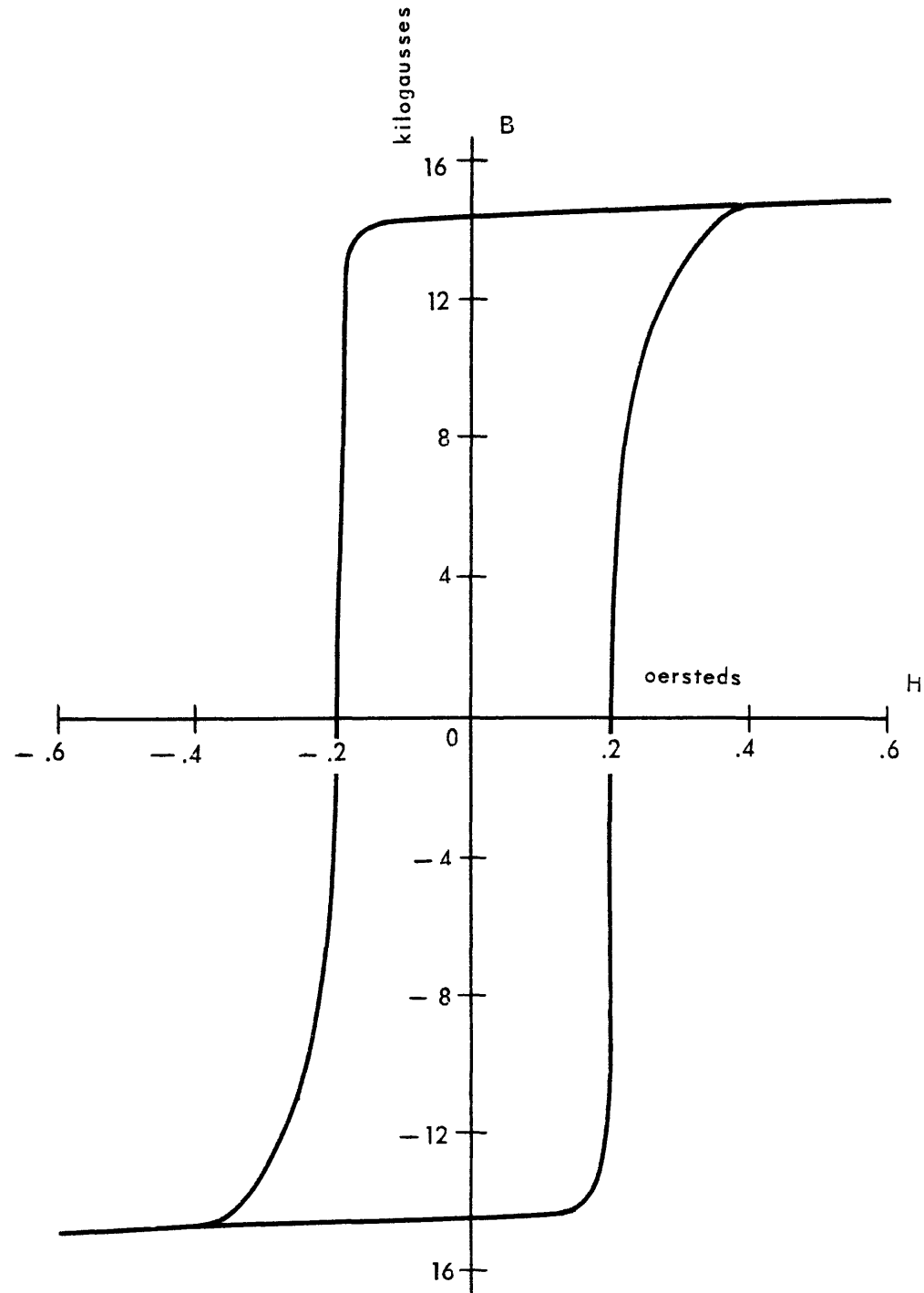


Fig. 1.8. Dynamic B-H loop for 2-mil Orthonol, 60 cps sinusoidal flux

consideration was given to the physical processes active in the core material. The result has been that each analysis was valid only for the particular experimental arrangement used, and attempts to generalize the results to other circuit conditions were usually doomed to failure. Two notable areas of failure of presently available analyses are: accurate predictions of gain with changes in control-circuit impedance level, and with changes in supply frequency.

Before specifically treating these previous analyses of the single-core, self-saturating magnetic amplifier, a brief description of the circuit will be given. In addition, a simple analysis of the circuit will be made to indicate the type of information about the reactor which is necessary for solution of the equations.

1.1.2 Operation of the Single-Core Circuit

The single-core, self-saturating magnetic-amplifier circuit is shown in detail schematically in Fig. 1-7. The saturable reactor is assumed to have a flux saturation characteristic which is abrupt enough so that switching occurs when the reactor saturates. A dynamic B-H loop for a typical reactor core material is shown in Fig. 1-8. Similarly, the rectifier is assumed to have a reverse-to-forward impedance ratio high enough to be considered as a switch. A characteristic curve for a typical rectifier is shown in Fig. 1-9. The supply voltage e_g is usually sinusoidal, while the control voltage e_c is usually unidirectional.

With these approximations and definitions, the operation of the circuit of Fig. 1-7 is as follows. At the start of an

interval of time during which the supply voltage e_g has the polarity shown in Fig. 1-7, there is a flux ϕ_o in the reactor, as shown on the ϕ -F loop of Fig. 1-10. The rectifier conducts, and practically all the supply voltage appears across winding N_g as a rate of change of flux linkages. This condition holds while the core operation traverses path ab in Fig. 1-10. When point b is reached, the reactor saturates and switches the supply voltage to the load. At the end of the positive alternation of supply voltage, the reactor operation returns to the region of residual flux. As the supply voltage goes negative, the rectifier blocks, and the control voltage drives the core flux negative along some path ca to the flux level ϕ_o at the start of the next positive alternation of the supply voltage. Thus it is evident that the rectifier acts as a switch to give a low impedance while power is delivered to the load, and a high impedance when the control signal is causing flux change from saturation. The amount of flux change from saturation is determined by the control signal. Since the control signal is effective during a negative alternation of the supply voltage, and the output determined by this signal occurs during a positive alternation of the supply voltage, a dead-time occurs between the application of a control signal and the appearance of an output.

1.1.3 Previous Analyses of the Single-Core Circuit

Before treating the previous attempts at analysis of this circuit, considerable simplification can be accomplished by an enumeration of the assumptions common to all the analyses. These assumptions can best be given in terms of the circuit

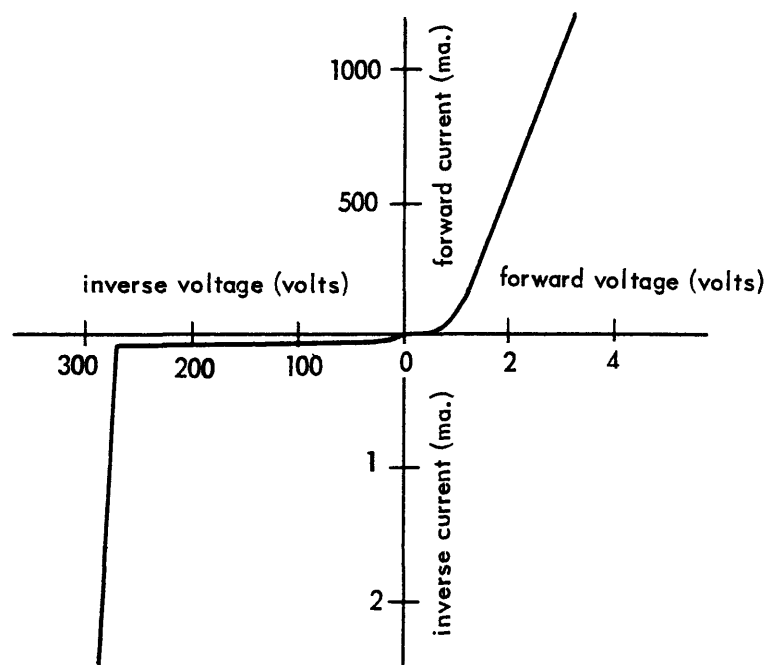


Fig. 1.9. Voltage-current characteristic of Silicon Junction Rectifier IN336

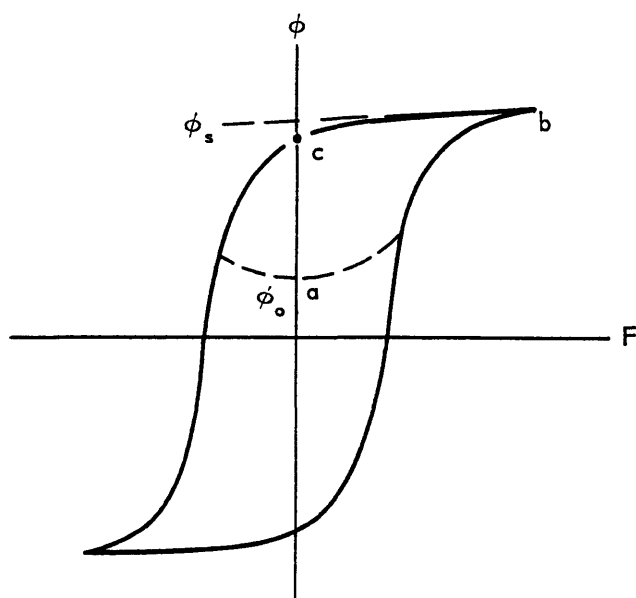


Fig. 1.10. ϕ -F loop of saturable reactor

equations. Referring to the circuit of Fig. 1-7, the voltage equations are:

$$e_g = v_x + Z_L i_g + \frac{d\lambda_g}{dt} \quad (1-1)$$

$$e_c = Z_c i_c + \frac{d\lambda_c}{dt} \quad (1-2)$$

where the winding resistances are included in the impedances.

The assumptions made in the analyses to be discussed are:

(1) The load impedance is resistive.

(2) The control impedance is resistive except in cases where the control source is a current source, and then Z_c is immaterial.

(3) The rectifier is assumed resistive, such that

$$v_x = R_x i_g \quad (1-3)$$

where R_x is either the forward resistance R_f or the reverse resistance R_r . In some cases the additional assumptions are made that $R_f = 0$ and $R_r = \infty$.

(4) Leakage flux is neglected, so that unity coupling occurs between windings when the reactor is unsaturated, giving:

$$\frac{\lambda_g}{N_g} = \frac{\lambda_c}{N_c} = \emptyset \quad (1-4)$$

(5) When the reactor is saturated, no additional flux change occurs, so that

$$\frac{d\lambda_g}{dt} = \frac{d\lambda_c}{dt} = 0 \quad (1-5)$$

This assumption neglects the air-core inductance of the windings.

(6) Sinusoidal supply voltage:

$$e_g = E_g \sin \omega t \quad (1-6)$$

(7) Uni-directional control voltage, either a direct voltage or a rectified sinusoidal voltage.

The assumptions given above yield simplifications of Eqs. (1-1) and (1-2) to:

$$e_g = R_x i_g + R_L i_g + N_g \frac{d\phi}{dt} \quad (1-7)$$

$$e_c = R_c i_c + N_c \frac{d\phi}{dt} \quad (1-8)$$

These two equations are the basis for the analyses that have been made. Note that Eqs. (1-7) and (1-8) contain three unknowns: i_g , i_c , and ϕ . Thus an additional equation is needed to allow solution. This additional equation must be determined by the characteristics of the reactor, because it must relate the mmf's applied to the reactor and the resultant flux in the reactor.

In early attempts at analyzing the single-core, self-saturating magnetic-amplifier circuit, the control source was assumed to be a current source, and some single-valued magnetization curve was assumed.^{8,12,13} Such a single-valued magnetization characteristic gave poor results with reactors containing gapless cores. The next improvement in analysis came when it was noted that the transfer characteristic of the single-core circuit looked more like the back side of a dynamic B-H loop.¹⁴ Consequently the assumption was made that the reactor operated on a major B-H loop, and the differential equations were solved graphically.¹⁵ The results were still not very accurate, and the type of error encountered varied among core materials. Next, the reactor core was assumed to operate along a major dynamic B-H loop for high saturation, and along the normal

magnetization curve for low saturation.¹⁶ The upper and lower limits were plotted, and a straight line was drawn between them. The results of this analysis were not widely applicable.

The several attempts to relate the non-symmetrical operation in the self-saturating magnetic amplifier to symmetrical core characteristics were not very gratifying. Consequently, attempts were made to measure core properties while the core was operating in a self-saturating circuit. The first attempt at this was the work of Lehman.¹⁷ He used a calibrated oscilloscope to measure the reset flux from saturation as a function of control mmf with the core operating in a single-core, self-saturating circuit. The shortcoming of this approach was the lack of any method of predicting how this reset flux curve would change with changes in external conditions: i.e., control-circuit resistance, control-source waveform, supply frequency, etc. Work along this line was performed by Roberts in connection with a circuit for core testing and grading.¹⁸ He points out the problem of rectifier "backfiring," the conduction of the load-circuit rectifier during the reset half-cycle, in limiting reset flux. Like the work done before, the resulting curves were applicable only if the external circuit conditions were not changed drastically.

Additional study of the behavior of reactors in magnetic amplifiers was performed by Lord.^{19,20} These studies were primarily experimental investigations of the apparent operating ϕ -F loops in magnetic-amplifier circuits with different levels of control-circuit impedance. No analytical expressions were

derived to describe the core materials in these experiments, although the experiments demonstrated that variables, in addition to flux and current, are needed to describe a core material. A study similar to Lord's studies was made by Huhta.²¹ In this study, the rate of change of flux as a function of time was investigated for several materials with current-source excitation. The effects of the resulting voltage waveforms on the operation of a single-core, self-saturating magnetic amplifier were discussed graphically. No analytical expressions describing the core material were derived or used.

The references cited represent essentially all the published methods of analysis of magnetic amplifiers. The disadvantage of all the analyses is the lack of a mathematical representation of the reactor core material which is sufficiently general to describe the amplifier under a variety of external circuit conditions. The representation is so restricted that the curves obtained by Lehman¹⁷ and Roberts¹⁸ with current sources for control cannot be generalized, even by model theory, to other control sources. Thus a generalized representation for the core material is needed to allow accurate prediction of magnetic-amplifier characteristics under a variety of operating conditions.

Before a mathematical representation of the core material can be derived, the physical processes active in the core material must be understood. Thus a brief review of the theory of ferromagnetism will be given.

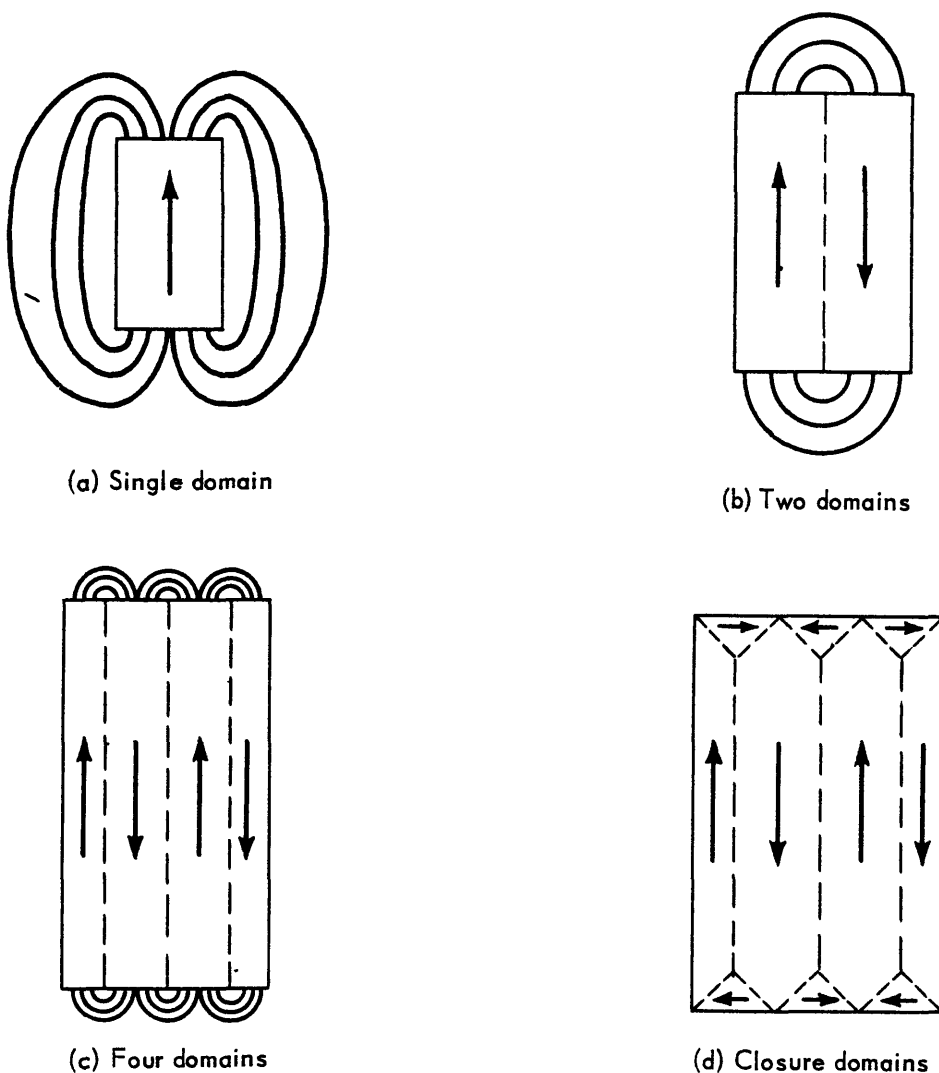


Fig. 1.11. Domain configurations

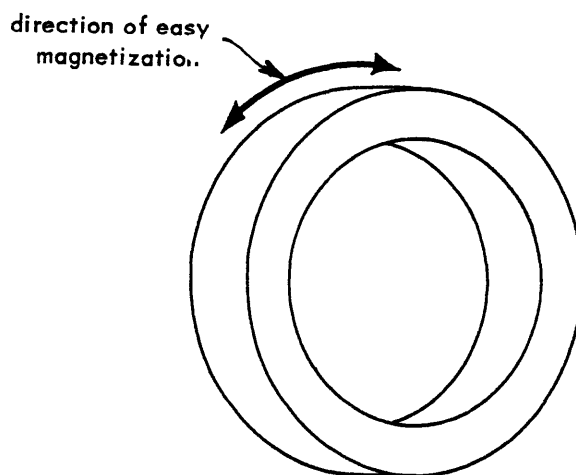


Fig. 1.12. Specimen shape for mathematical representation.

1.2.0 Theory of Ferromagnetism

The present-day theory of ferromagnetism is based on quantum mechanics. The ferromagnetism in materials is due to a spontaneous alignment, below the ferromagnetic Curie temperature, of unpaired electron spins. These unpaired spins, occurring at the 3d level in iron, cobalt, and nickel, are held in alignment by quantum mechanical exchange forces.²²

Ferromagnetic materials form in small crystals; consequently, the properties can be discussed in terms of a single crystal. Of course, practically all technical ferromagnetic devices are polycrystalline; and account must be taken of the nonuniformity of the crystals.

For the purpose of discussion, consider a rectangular, single-crystal, ferromagnetic specimen. The quantum mechanical exchange forces tend to align all the unpaired spins to form the bar magnet shown in Fig. 1-11a. The closure field external to the crystal requires considerable energy. A configuration requiring less energy in the closure field is that shown in Fig. 1-11b. In this case the unpaired electron spins are aligned within two limited regions called domains, the direction of alignment of the spins being different in the two domains. The transition region between the two domains, where the change in direction of the electron spins takes place, is called a domain wall or Bloch wall. In this case the transition region is a 180-degree wall, because the spins are rotated 180° through the wall. The amount of energy required in the closure fields is reduced further in the domain configuration of Fig. 1-11c.

Since energy is required to establish the domain walls, the stable domain configuration for a particular specimen will be one in which the decrease in closure field energy due to the creation of additional domain walls equals the energy required to establish the additional walls. In the case where a material has two easy directions of magnetization, a stable configuration can be that shown in Fig. 1-11d, where the external closure fields are reduced to zero. The triangular closure domains are bounded by 90-degree Bloch walls.²³

Ferromagnetic crystals exhibit easy and hard directions of magnetization. The additional amount of energy necessary to change the state of magnetization from an easy to a hard direction is called the magnetic anisotropy energy. Consequently, whether or not closure domains form as shown in Fig. 1-11d depends on whether the anisotropy energy in the closure domains is larger or smaller than the energy of external closure fields that exist when the closure domains are not present.

The domain walls have thicknesses determined by two types of energy. The quantum mechanical exchange energy is a minimum when adjacent spins are aligned; thus it tends to make the walls thick. The magnetic anisotropy energy is a minimum when all spins are aligned along easy directions; hence it tends to make the walls thin. The combination of these two energy terms gives the wall thickness:²³ In 3.8% Si-Fe, for instance, the wall thickness is of the order of 300 atomic diameters.²⁴

The magnetization in a specimen occurs in domains each of which is saturated in a particular direction; consequently, a

change in the net magnetization of the specimen will occur through a change in domain pattern by the movement of the domain walls, so that domains with orientation in the direction of the applied field grow at the expense of the domains with magnetization opposite to the applied field. When a specimen is saturated in one direction so that it is one large domain, small domains of reverse magnetization must be formed before walls can be moved to reverse the magnetization. The process by which domains of reverse magnetization are formed is called the process of nucleation.²⁴ Since the reactor flux is reset from near residual in a self-saturating magnetic-amplifier circuit, and since the reactors used have gapless cores with highly rectangular B-H loops, the two problems of nucleation and wall movement must be considered in the treatment of the resetting characteristics of the reactor.

1.2.1 Processes of Nucleation

Consider an annular ring of ferromagnetic material having an easy direction of magnetization along the circumference, as shown in Fig. 1-12. If a field is applied which is strong enough to completely magnetize the specimen in one direction, then when the field is removed, if the specimen is pure enough, the single-domain configuration will remain. If the field is reversed and increased slowly from zero, no change will take place until a critical field is reached at which field-strength domains of reverse magnetization form. At this point, domain walls are available for reversal of magnetization by movement of the walls through the material. This movement will be treated in the next section.

The process of nucleation takes place when the nucleated configuration is energetically favorable with respect to the unnucleated configuration, and when there is no insurmountable energy barrier between the two configurations. If an energy barrier does exist between the two configurations, then thermal agitation might be sufficient to cause the transition. For a perfect crystal, Dijkstra²⁵ has shown that the temperature necessary to cause nucleation is several orders of magnitude higher than the ferromagnetic Curie temperature. In fact, any process of nucleation in a perfect crystal will require fields much greater than those found experimentally to be necessary for nucleation.²⁵ In view of this result, nucleation field strength, as measured experimentally, does not appear to be an inherent property of a material.

If nucleation field strength is not an inherent property of a material, it must depend on the configuration of the specimen. When a specimen contains an imperfection such as a notch in the surface, as shown in Fig. 1-13a, so-called free magnetic poles form where the magnetization intersects a material discontinuity. Since energy is associated with the formation of the free poles, the system energy can be reduced by the formation of closure domains as illustrated in Fig. 1-13b when the material has two directions of easy magnetization. These closure domains may be a source of mobile domain walls; thus the formation of the closure domains can be considered as a nucleation process. An experimental result in support

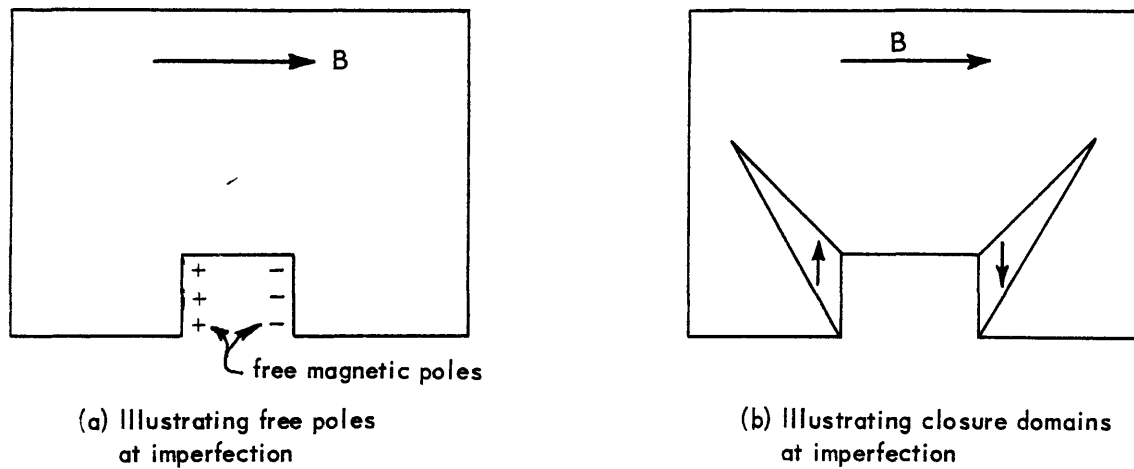


Fig. 1.13. Specimen with surface imperfection

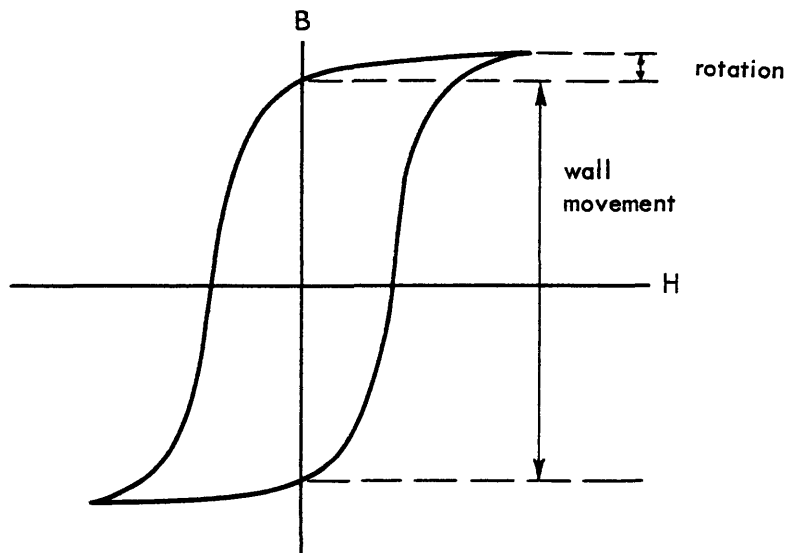


Fig. 1.14. Processes of flux change

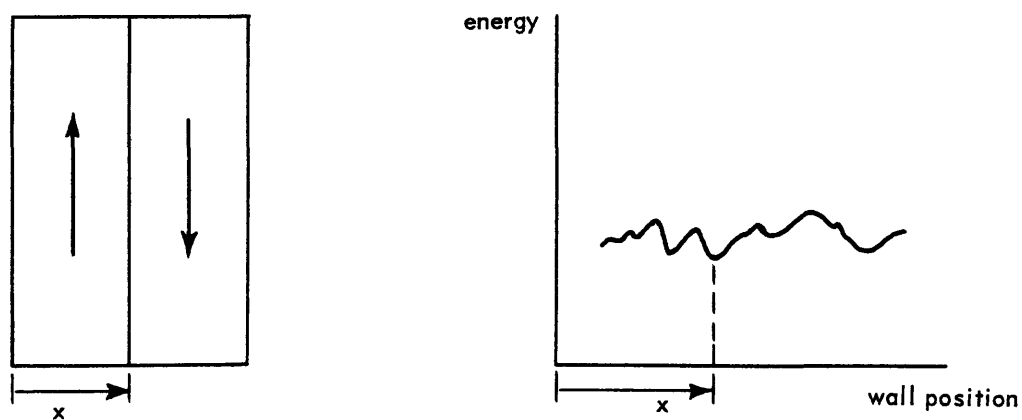


Fig. 1.15. Energy as a function of wall position

of this viewpoint was reported by Williams.²⁴ In this particular experiment, the nucleating field strength for a perminvar ring sample was reduced by a factor of two by cutting a notch in the surface of the specimen. This result was cited by Williams²⁴ in support of the theory that nucleation in a ferromagnetic specimen occurs at lattice imperfections. Goodenough²⁶ has made order-of-magnitude calculations for four types of possible nucleation sites in polycrystalline materials: (1) granular inclusions, (2) lamellar precipitates, (3) grain boundaries, and (4) crystalline surfaces. Of these four possible nucleation sites, the most probable sites for the formation of mobile domain walls, as indicated by a comparison of theoretical and experimental nucleating field strengths, are the grain boundaries and crystalline surfaces.

In a polycrystalline specimen, nucleation at grain boundaries indicates a volume process, while nucleation at crystalline surfaces indicates a surface process. Friedlander²⁷ presents experimental evidence with different thicknesses and widths of Orthonol* to indicate that nucleation is primarily a surface process. However, if the thin tapes tested by Friedlander were only one grain thick, and if the grain surface size stayed constant with thickness, then nucleation at grain boundaries would appear essentially as a surface process.

Thus, in the thin-tape, grain-oriented, high-permeability polycrystalline ferromagnetic metals treated in this research, nucleation will be assumed to occur at grain boundaries and at crystalline surfaces.

* Trademark of Magnetics, Inc., Butler, Pa. for highly grain-oriented and annealed 50 Ni-50 Fe.

1.2.2 Domain Wall Motion

There are two processes by which the magnetization of a specimen can be changed: rotation of the spin directions within a domain through a small angle, and movement of domain walls which rotates spins through a large angle in a limited region. In the highly grain-oriented rectangular B-H loop materials, the rotation process contributes very little flux change, usually accounting for the flux change from remanence to saturation in the same direction as indicated in Fig. 1-14. This difference is usually an indication of the departure from perfect grain orientation. For the most part, the reversal of flux from remanence is accomplished by domain wall movement. Since in a magnetic amplifier the flux reset from near remanence must be found, the domain wall movement will be the only process of flux change considered.

Domain wall movement occurs in two forms: reversible and irreversible. When a domain wall exists in a specimen with no field applied, the system energy as a function of wall position will be irregular and will have a shape something like that depicted in Fig. 1-15. With no field applied, the wall will come to rest at a minimum of energy. If a small field is applied such that the wall does not move over a peak of energy, and then the field is removed, the wall will return to its initial position. This is reversible domain wall movement. If, on the other hand, a field is applied such that the wall moves past a peak of energy, then when the field is removed, the wall will not return to its initial position but will move to the (energetically) nearest minimum. This is irreversible domain wall movement.

When a field is applied to a specimen to change the flux a specified amount less than saturation, the accuracy with which the flux can be set is determined by the distance between minima of the energy curve of Fig. 1-15. Experiments performed by Pittman²⁸ on a pulse-counting circuit indicate that in the rectangular B-H loop, 50% Ni-50% Fe materials normally used in magnetic amplifiers, the distance between minima is very small and of the order of one percent of the total distance a wall must move to complete the flux reversal. Consequently, only irreversible wall movement will be considered in the mathematical representation, and it is expected that less than one-percent error will appear in calculated flux changes due to the neglect of reversible wall movements.

In a magnetic-amplifier reactor core, as in other applications, the flux must be changed during a specified period of time; therefore the processes impeding domain wall motion must be known in order to allow the calculation of flux change with time.

Four processes which affect wall motion have been discussed in the literature. First there is a mechanism known as spin-relaxation damping. This is the dissipative mechanism that makes the electron spins spiral into the direction of an applied field when no macroscopic eddy-current losses occur. The mechanism of spin-relaxation damping is not completely understood; however, it has been attributed to "relativistic effects,"²⁹ microscopic eddy currents, and other phenomena. At any rate, such a damping mechanism was first postulated by Landau and Lifshitz,²⁹ and the resulting equation of motion

was solved. Several investigators have used this approach in the prediction of the behavior of domain walls in ferrites where macroscopic eddy currents are so small that spin relaxation damping is the limiting mechanism for domain wall motion. Among the investigators, Galt³⁰ showed that this approach gave reasonable results for Fe_3O_4 , although in all cases some of the material constants were rather difficult to determine.

A second mechanism impeding the movement of domain walls is macroscopic eddy currents. The flow of macroscopic eddy currents depends on the bulk resistivity of the material; consequently, eddy-current damping appears most markedly in ferromagnetic metals. Eddy currents occur because the rate of change of flux caused by the motion of the domain wall generates a voltage in the material. The resulting current flow creates a field in opposition to the applied field which reduces the net field acting on the domain wall. This viewpoint of reduced field is not normally used in calculations of eddy-current damping. The usual procedure is to equate eddy-current power losses to input power, and obtain the rate of change of flux and hence the domain wall velocity from the resulting expression. Williams, Shockley, and Kittel³¹ have calculated the effect of eddy-current damping in a single crystal of 3.8 percent silicon-iron cut in the form of a picture frame with the easy directions of magnetization along the sides of the frame. They calculated the domain wall behavior for two limiting cases. The first case was for very

low fields where the domain wall moved as a plane wall through the material. They obtained the result that the wall velocity was linear with applied field. A generalization of this treatment will be given in Chap. II, where it will be shown that the velocity of the wall at a particular point in the material is linear with applied field, but the constant of proportionality varies with wall position. The second limiting case treated was for very high applied fields where the domain walls become curved and move as collapsing cylinders. The result obtained showed that for the range of very high fields, the velocity of the domain wall at any wall position in the reversal process was linear with applied field. A similar result was obtained by Menyuk and Goodenough³² and later by Menyuk³³ for ultra-thin tapes of polycrystalline metals.

At intermediate fields between the limiting cases where the domain wall is still curved, a force is exerted on the wall by surface tension. The wall possesses a certain amount of energy per unit area; thus, work must be performed to increase the wall area. This is the source of the surface tension. The surface-tension forces are independent of applied field, but nonetheless they impede or aid the domain wall motion, depending on whether the cylinder is expanding or collapsing. A force similar to surface tension can occur when many lattice imperfections are present in the specimen. A closure domain which is present at an imperfection and which is anchored firmly to the imperfection can become attached to the moving wall. As the wall moves, the closure domain is

stretched to greater length, and a retarding force arises because additional wall area is being created in the closure domain boundaries.

It has been found that domain walls possess an apparent mass which can affect the dynamic behavior of the wall.³⁴ However, this inertia effect appears only at much higher wall velocities than occur in magnetic-amplifier operation.³⁵ Consequently, the apparent domain wall mass will be neglected in the mathematical representation of Chap. II.

When a domain wall is present in a ferromagnetic specimen, a certain minimum applied field is necessary to start the wall moving. This field, known as the starting field, was found to be the d-c coercive field in the single-crystal experiments of Williams, Shockley, and Kittel.³¹ The structure of a polycrystalline specimen is such that the material properties vary from point to point. Thus it is reasonable to expect that the starting field for a domain wall will vary as a function of the wall location. In view of this, a distribution of starting fields over the large number of domains in a polycrystalline specimen will be considered in the derivation of Chap. II.

The mechanisms affecting domain wall motion discussed above will be used in Chap. II to derive a mathematical representation of a saturable reactor which can be applied in a simple manner to the analysis of a single-core, self-saturating magnetic amplifier over wide ranges of supply frequency and control-circuit resistance.

TABLE I*
MAGNETIC AMPLIFIER CORE MATERIALS

TRADE NAMES	COMPOSITION	GRAIN STRUCTURE	SATURATION FLUX DENSITY w/m ²	REMANENCE FLUX DENSITY w/m ²	APPROXIMATE d-c COERCIVE oe	RESISTIVITY microhm-cm
Hg Mu 80 4 - 79 Permalloy Mo Permalloy	79% Ni 17% Fe 4% Mo	"Random"	0.87	0.60	0.02	57
48 Alloy Carpenter 49 Allegheny 4750 Hypernik	48% Ni 52% Fe	Random	1.60	1.00	0.10	45
Orthonol Orthonik Permeron Deltamax Hypernik V	50% Ni 50% Fe	oriented	1.55	1.44	0.10	45
Magnesil Armco Oriented T Hypersil Orthosil Silectron	97% Fe 3% Si	oriented	2.00	1.42	0.30	48

* Information for Table I taken from Tables A and B of Catalog TWC-100, Magnetics, Inc., Butler, Pa.

Chapter II

THE MATHEMATICAL REPRESENTATION FOR A REACTOR

2.0.0 Introduction

The purpose of this chapter is to describe the derivation of a mathematical representation for a saturable reactor which is both simple enough for analytical inclusion in a magnetic-amplifier analysis and general enough to make the analysis give accurate predictions of performance over a wide range of operating conditions. First a general representation for a polycrystalline specimen is derived by averaging single-domain equations over the polycrystalline specimen. This general representation is derived without reference to any particular type of material. Simplifications are necessary before the representation can be readily applied to a circuit analysis. The simplifications are made with reference to the types of materials used in magnetic amplifiers and to the mode of operation found in magnetic amplifiers. The simplified representation is checked experimentally by resetting the reactor flux from near residual by a constant voltage in series with a variable resetting resistance.

The core materials most commonly used in magnetic amplifiers are high-permeability, sometimes grain-oriented, ferromagnetic metals, and the cores are constructed as toroids of spirally wound thin tape. Some common types of materials and their trade names are listed in Table I. The thicknesses of tape used at power-supply frequencies of 60 cps to about 2000 cps range from one to four mils. By far the most useful material

for handling moderate amounts of power at normal power frequencies is the 50% Ni-50% Fe material (see Table I).

The mode of operation of a reactor in a self-saturating magnetic amplifier has been described in Section 1.1.2 of Chap. I. The discussion of that section indicates that the reactor representation must describe the reactor flux as a function of time, as the flux is reset from near remanence by a control or resetting signal after the flux has been driven into saturation by the load current.

2.1.0 Single-Domain Behavior

Before considering the mathematical representation for a polycrystalline specimen, several examples of single-domain wall behavior in single crystals will be considered for simple, easily solvable geometries. These results will be used to obtain the form of the equations to be averaged over the polycrystalline structure.

In the single-crystal examples to be considered, the starting field will be assumed greater than the nucleating field; thus, whenever the starting field is reached or exceeded, the domain wall will move and the state of magnetization will change.

2.1.1 Plane Wall in Rectangular Specimen

Consider the annular ring of rectangular cross-section shown in Fig. 2-1. The thickness d of the ring is assumed to be much smaller than the radius r_i , so that the field does not vary appreciably inside the material. The easy direction of magnetization is along the circumference. The specimen is

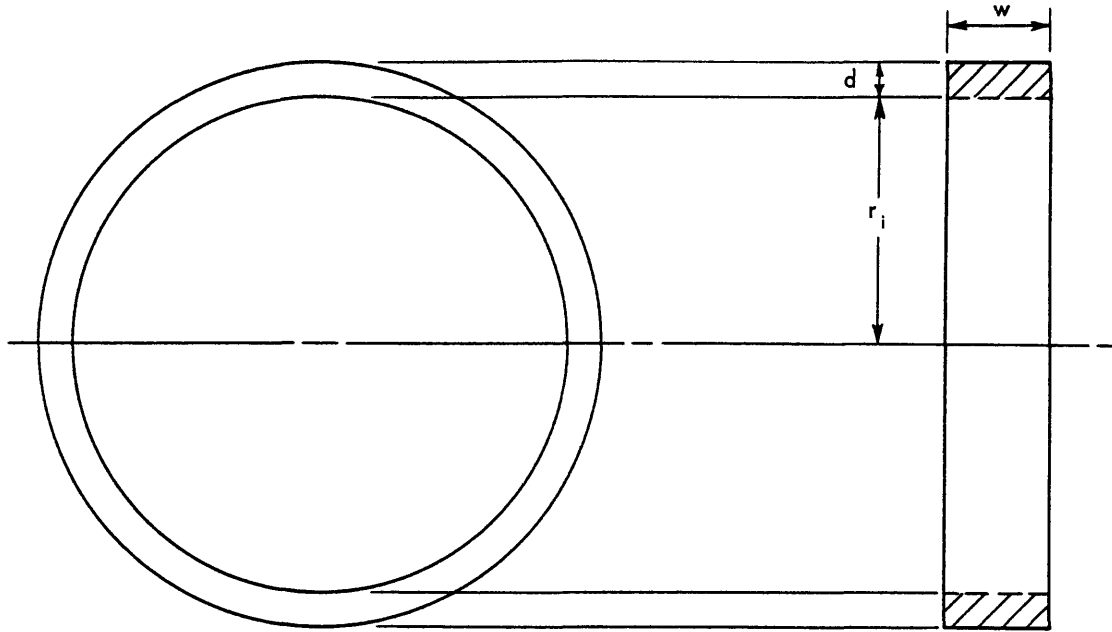


Fig. 2.1. Structure for plane-wall movement

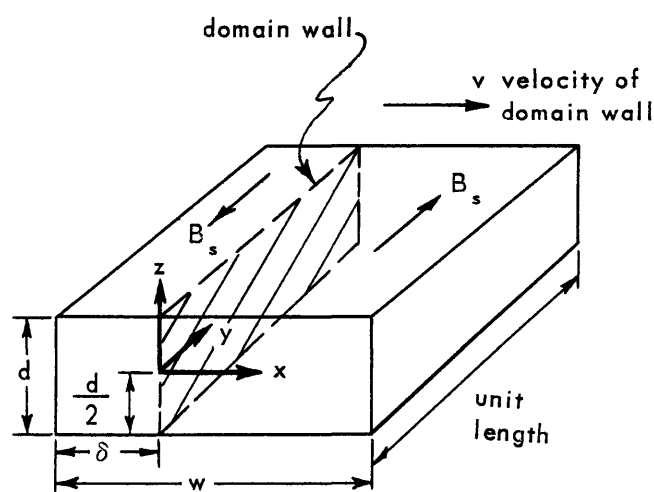


Fig. 2.2. Definition of coordinates for plane-wall motion

assumed to be a single crystal; and at low fields, flux change is assumed to occur by movement of a single, plane domain wall along the width w as depicted by the drawing in Fig. 2-2. This method of wall movement is energetically favorable with respect to the movement of a plane wall across the thickness d , because a domain wall possesses a certain energy per unit area which is characteristic of the material. The rectangular xyz co-ordinate system is fixed with respect to the specimen, and is located at the domain wall at the instant of time being considered. The domain wall is assumed to have a starting field H_0 which is constant over the whole specimen; thus the field acting on the wall is $(H - H_0)$ where H is the applied field. In general, the wall movement will be retarded by two types of damping forces, eddy-current, and spin-relaxation. These two types of damping will be considered separately.

When macroscopic eddy currents provide the only damping, the differential equation describing the wall position δ as a function of applied field is derived in Appendix I-A by equating instantaneous values of eddy-current power loss and electrical input power. The resulting expression is:

$$F(\delta) \frac{d\delta}{dt} = \frac{\pi^3}{8\sigma B_s d} (H - H_0) \quad (2-1)$$

with

$$F(\delta) = \sum_{n \text{ odd}} \frac{1}{n^3} \frac{\sinh \frac{n\pi w}{d}}{\cosh \frac{n\pi w}{d} + \cosh \frac{n\pi(2\delta - w)}{d}} \quad (2-2)$$

where rationalized mks units have been assumed and

- σ = conductivity in mhos/meter
 B_s = saturation flux density in webers/meter²
 d = thickness of specimen in meters
 w = width of specimen in meters
 δ = distance of wall from one edge of specimen in meters (see Fig. 2-2)
 H = applied field in amperes/meter
 H_0 = starting field in amperes/meter

This is a generalization of the problem solved by Williams, Shockley, and Kittel;³¹ and the result, Eq. (2-1), reduces to their result when the wall is in the center of the specimen ($\delta = \frac{w}{2}$).

The rate of change of flux in the specimen is given by:

$$\frac{d\phi}{dt} = 2B_s d \frac{d\delta}{dt} \quad (2-3)$$

Thus the dynamic description of a plane domain wall in a rectangular specimen, under the damping action of macroscopic eddy currents, is contained in Eqs. (2-1), (2-2), and (2-3).

When the domain wall velocity is eliminated from Eqs. (2-1) and (2-3), the normalized rate of change of flux is obtained:

$$\frac{4\sigma}{\pi^3(H - H_0)} \frac{d\phi}{dt} = \frac{1}{F(\delta)} \quad (2-4)$$

This expression, shown plotted in Fig. 2-3, represents the rate of change of flux as a function of wall position for constant applied field and eddy-current damping. Note that at any wall position the rate of change of flux is linear with applied field.

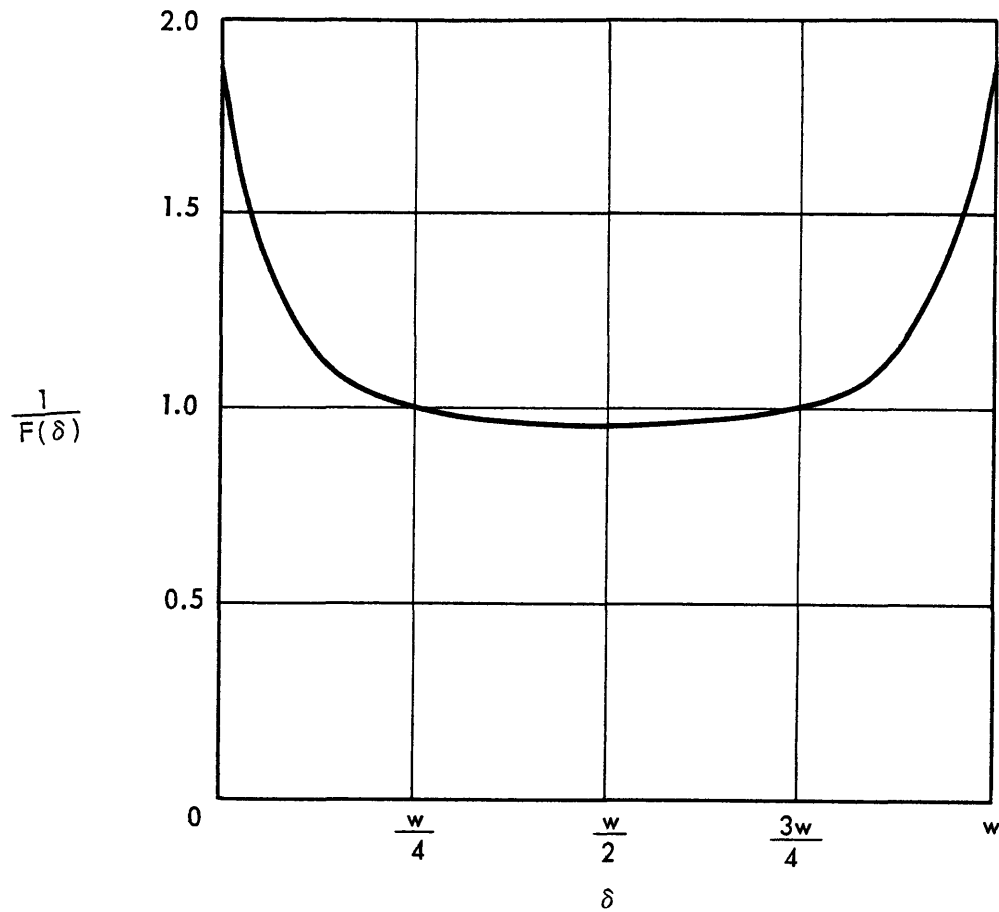


Fig. 2.3. Normalized rate of change of flux vs. wall position for a plane-wall in a rectangular specimen with eddy current damping only

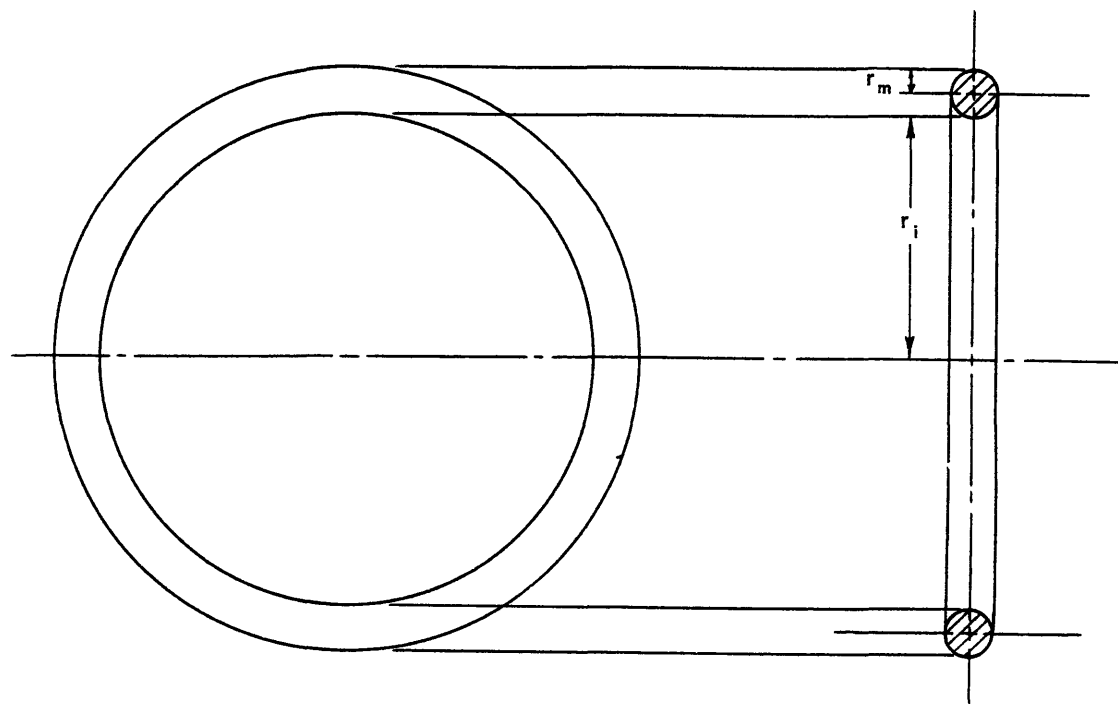


Fig. 2.4. Structure for cylindrical domain dynamics

Now consider the same configuration with only spin-relaxation damping to impede wall motion. Spin-relaxation damping is characterized by a constant β_r which expresses the force per unit lateral wall area per unit velocity, and in the mks system is

$$\beta_r \frac{n \text{ sec}}{m^3}$$

With the assumption of a plane wall in a specimen of rectangular cross-section, as depicted in Figs. 2-1 and 2-2, with only spin-relaxation damping to retard the wall motion, and with a constant starting field H_0 throughout the material, the wall velocity is found in Appendix I-B by equating input power to power dissipated by the damping. The result is:

$$v = \frac{d\delta}{dt} = \frac{2B_s}{\beta_r} (H - H_0) \quad (2-5)$$

This expression, in combination with the rate of change of flux given by Eq. (2-3), describes the dynamic behavior of a plane wall in a rectangular specimen under the action of spin-relaxation damping.

In this particular case the wall position can be eliminated entirely, to yield the single expression:

$$\frac{d\phi}{dt} = \frac{4B_s^2 d}{\beta_r} (H - H_0) \quad (2-6)$$

Since this expression describes a voltage which varies linearly with a current, the excitation characteristic of this specimen can be represented by a resistive circuit. Thus, if a polycrystalline specimen has plane walls which are subject only to spin-relaxation damping, and if all the walls have the

same starting field, the inclusion of the core characteristics in a magnetic-amplifier analysis will be quite simple. Unfortunately, the polycrystalline cores used in magnetic amplifiers are not so well behaved; however, in some cases an approximation of this sort will yield useful results.

2.1.2 Cylindrical Wall in Cylindrical Specimen

When a domain of reverse magnetization is nucleated inside a material, the domain will probably have a circular cross-section, because a circle has a maximum enclosed area for a given circumference. Thus the domain with circular cross-section contains a maximum amount of flux for a given domain wall area, and thus a given domain wall energy. Consequently, for nucleation within a specimen, the dynamics of the flux change can be treated by considering an expanding cylindrical domain. The problem is simplified when the domain is assumed nucleated in the center of a cylindrical specimen; consequently, the physical arrangement assumed for the treatment of expanding cylindrical domains is the toroid of cylindrical cross-section shown in Fig. 2-4. The radius r_m of the cross-section is very small compared with the radius r_i , in order that the field can be considered constant throughout the specimen. The specimen is assumed to contain a concentric domain wall which is expanding with the velocity v , as shown in Fig. 2-5. The starting field H_0 for the domain wall is assumed to be constant throughout the specimen.

Consider the case of eddy-current damping only. The differential equation relating wall position δ to applied field H

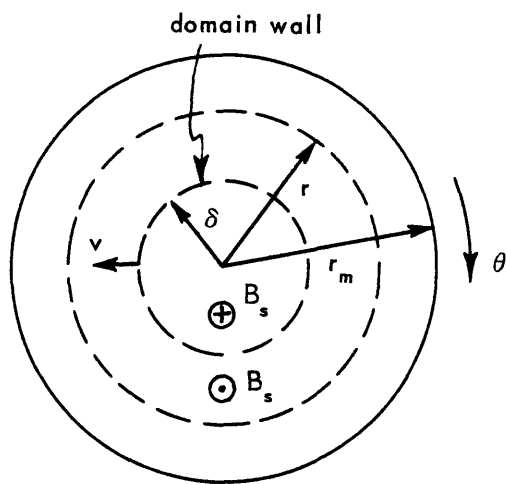


Fig. 2.5. Definition of variables for cylindrical wall

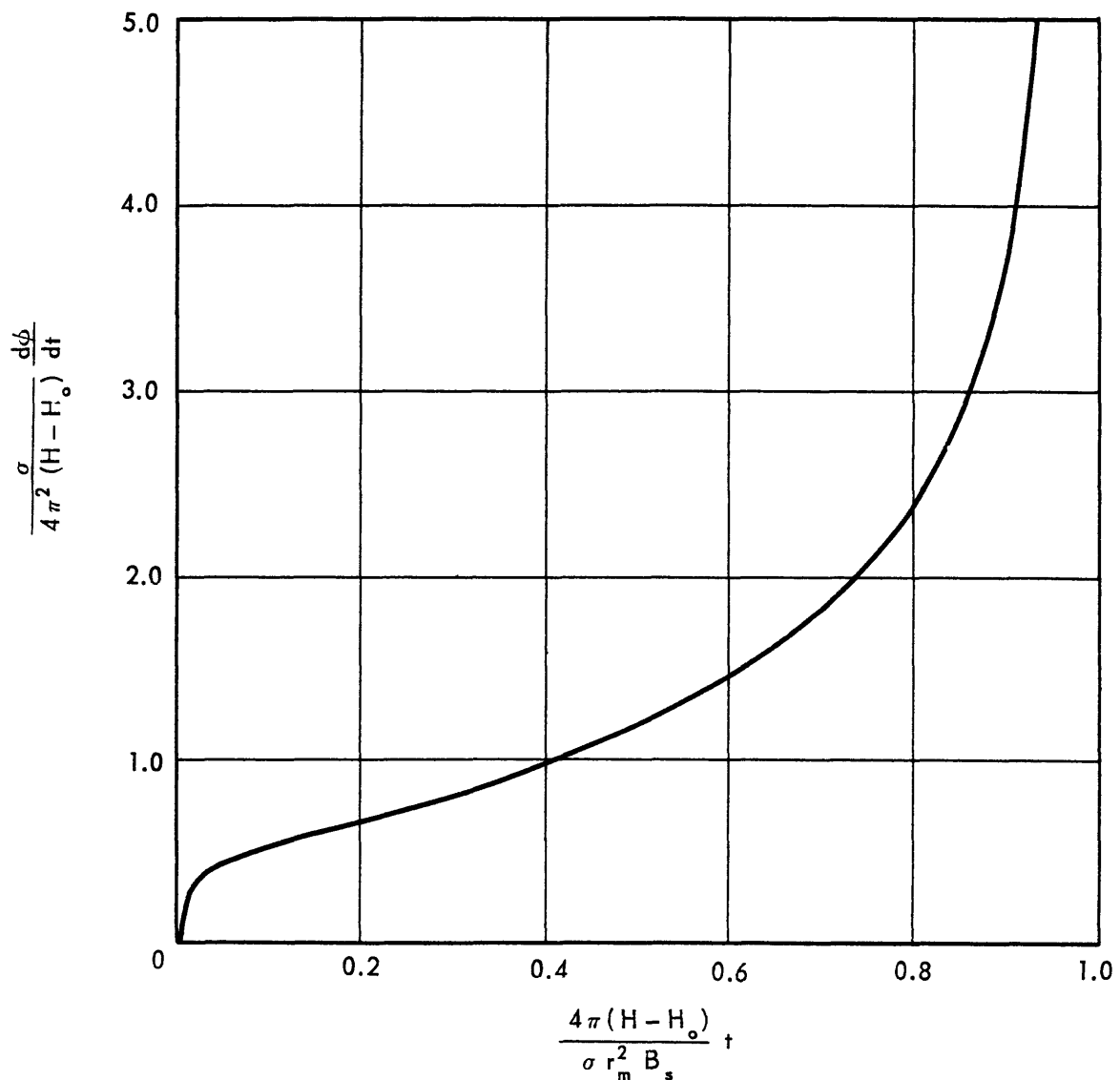


Fig. 2.6. Voltage waveform for expanding cylindrical domain in cylindrical specimen with constant applied field and eddy current damping

is derived in Appendix I-C by equating the power dissipated in eddy currents to the input power. The resulting equation is:

$$\delta \ln \frac{r_m}{\delta} \frac{d\delta}{dt} = \frac{1}{2B_s \sigma} (H - H_o) \quad (2-7)$$

The rate of change of flux in the specimen is given as Eq. (I-23) of Appendix I-C as:

$$\frac{d\phi}{dt} = 4\pi B_s \delta \frac{d\delta}{dt} \quad (2-8)$$

The expressions of Eqs. (2-7) and (2-8) give a dynamic description of the magnetic characteristics of the specimen.

These equations are substantially the same as those of Williams, Shockley, and Kittel³¹ for collapsing cylindrical domains, and of Menyuk and Goodenough³² for expanding cylindrical domains.

The simultaneous solution of Eqs. (2-7) and (2-8), with the applied field H a constant, yields the normalized rate of change of flux as a function of time shown in Fig. 2-6. When this specimen is switched with constant field, the shape of the pulse is always that shown in Fig. 2-6, with the height of the pulse varying linearly with applied field, and the time to any point on the pulse varying inversely as the applied field.

When the cylindrical domain wall described above for eddy-current damping is assumed to be expanding against only a spin-relaxation damping force, the differential equation relating the wall position to the applied field, as derived in Appendix I-D, is:

$$\frac{d\delta}{dt} = \frac{2B_s}{\beta_r} (H - H_o) \quad (2-9)$$

The additional equation needed to relate the flux and applied field is the rate of change of flux given by Eq. (2-8).

When a constant field H is applied to this specimen after it has been completely magnetized in one direction, the rate of change of flux after nucleation at $t = 0$ is given by

$$\frac{d\phi}{dt} = \frac{16\pi B_s^3}{\beta_r^2} (H - H_o)^2 t \quad (2-10)$$

for $0 < t < \frac{r_m \beta_r}{2B_s(H - H_o)}$

Equation (2-10) can be normalized as

$$\frac{\beta_r}{8\pi B_s^2 r_m (H - H_o)} \frac{d\phi}{dt} = \frac{2B_s}{r_m \beta_r} (H - H_o) t \quad (2-11)$$

The relation of Eq. (2-11) is shown plotted in Fig. 2-7.

When this specimen is magnetized with a constant applied field, the rate of change of flux at any wall position varies linearly with applied field, and the time required for the wall to traverse a given distance varies inversely with applied field.

In the model describing a cylindrical domain wall, the domain wall area changes with domain wall position. Thus, since the domain wall possesses a certain energy per unit area, there must be a surface-tension force on the domain wall tending to collapse it. The pressure on the wall varies inversely with wall position from the center of the cylindrical structure; and at a critical domain radius, the surface-tension force becomes equal to the force of the starting field. Consequently, all domains having radii smaller than this critical

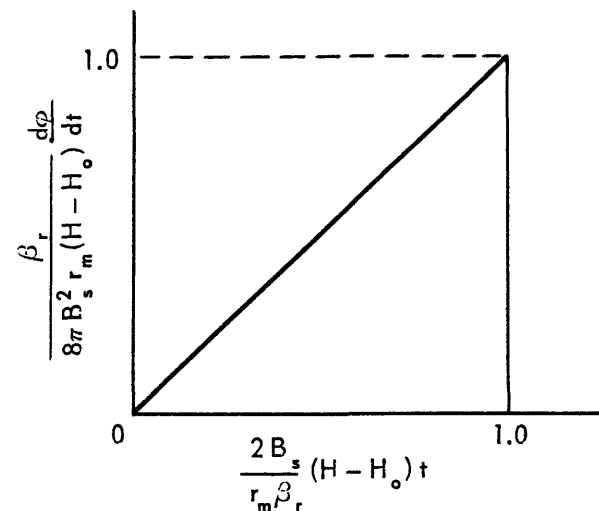


Fig. 2.7. Voltage waveform for expanding cylindrical domain in cylindrical specimen with constant applied field and spin relaxation damping

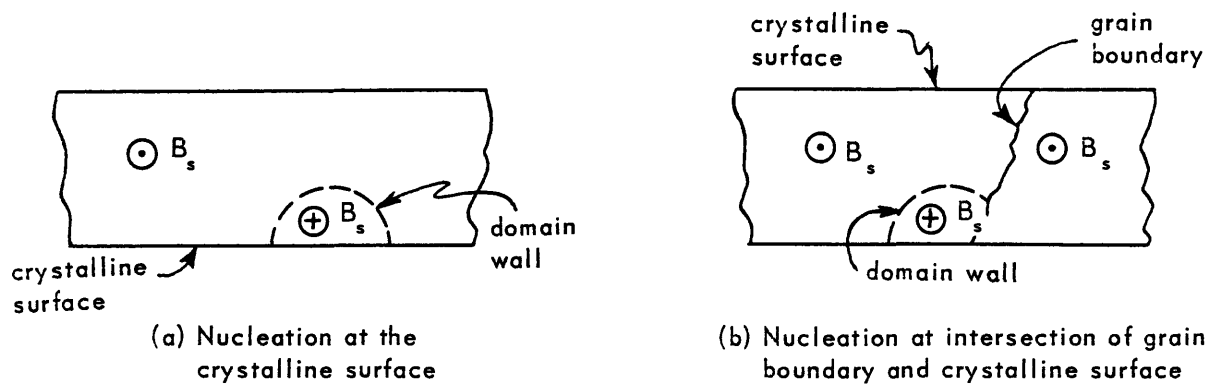


Fig. 2.8. Nucleation at two sites

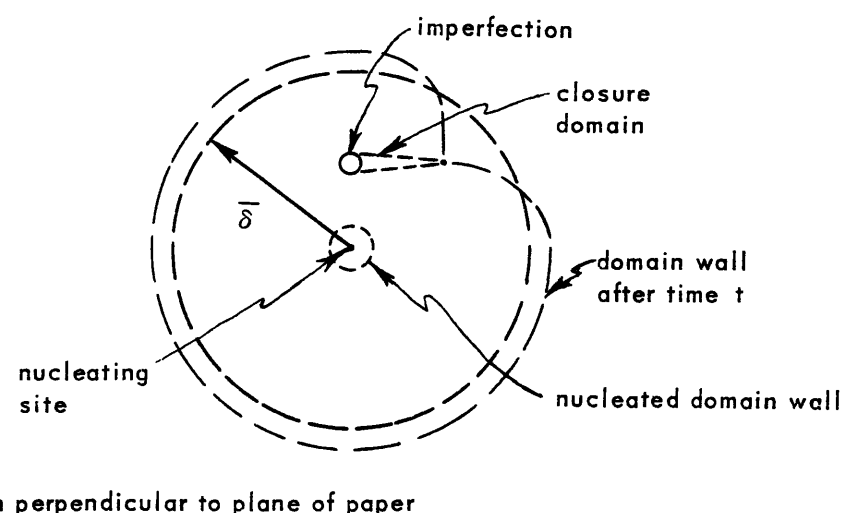


Fig. 2.9. Illustrating distortion of domain wall

radius would collapse upon removal of an external field. Such an occurrence would result in a flux instability over at least part of the flux range. Although this instability has been noted in some materials,³⁶ it apparently does not occur in the 50% Ni-50% Fe material commonly used in magnetic amplifiers, as evidenced by the resolution obtained in pulse counters as cited in Chap. I.²⁸ Therefore, surface-tension forces will be neglected in the derivation of the mathematical model for the polycrystalline material.

2.1.3 General Form of Equations Describing Single-Domain Behavior

In the preceding two sections, the dynamics of several types of domain wall motion have been described. The physical structures and domain wall configurations assumed were simple, in order to illustrate the form of the differential equations describing the magnetization process. In a polycrystalline specimen, the domain walls will not in general have the simple configurations treated in Sections 2.1.1 and 2.1.2. A domain may nucleate at the crystalline surface, in which case it may have a semicircular cross-section as illustrated in Fig. 2-8a. If the nucleation occurs within the material, and the nucleated domain has a circular cross-section, the domain wall will not be moving in a specimen concentric with the domain wall. In addition, during the movement of the domain wall it may come in contact with the crystalline surface, thus annihilating part of the wall. Also the domain wall may come in contact with a wall of another domain, in which case part of both walls will be annihilated and the two domains will merge and act as a single domain.

In view of the above discussion, it is apparent that in a polycrystalline material the nucleated domains will not necessarily have simple mathematical shapes, and in the subsequent wall motion the domains will not maintain the same shape until flux reversal is completed. In spite of this difficulty, the behavior of a single domain wall in a polycrystalline material will be assumed to be governed by equations of the same form as those of Sections 2.1.1 and 2.1.2. The same form means that the domain wall damping depends only on the wall position, and the damping force is linear with the field in excess of the starting field, as demonstrated in Eqs. (2-1), (2-5), (2-7), and (2-9). The average domain dimension $\bar{\delta}$ is defined as the average distance from the nucleating site to all parts of the domain wall at time t . The definition of an average dimension is necessary because, as a domain wall moves away from the nucleating site, it may become distorted by a closure domain at an impurity or an imperfection, in which case all points on the domain wall will not be the same distance from the nucleating site, as illustrated by Fig. 2-9. Then, if the retarding forces on the wall are caused by eddy-current damping and spin-relaxation damping, the average domain dimension is assumed to be related to the applied field by the equation:

$$f(\bar{\delta}) \frac{d\bar{\delta}}{dt} = K_1(H - H_s) \quad (2-12)$$

where H_s is the starting field for the domain wall in question and it is assumed constant throughout the movement of the domain wall. The function $f(\bar{\delta})$ describes the damping of the

domain wall motion as a function of wall position, and the constant K_1 is a constant of the specimen.

The rate of change of flux due to a single domain in a grain-oriented material is

$$\frac{d\varphi_1}{dt} = 2B_s \frac{dA_d}{dt} \quad (2-13)$$

where A_d is the cross-sectional area included within the domain of reverse magnetization. In general, the area A_d will be a function of the average domain dimension $\bar{\delta}$; consequently the rate of change of flux can be written as

$$\frac{d\varphi_1}{dt} = 2B_s \frac{dA_d}{d\bar{\delta}} \frac{d\bar{\delta}}{dt} \quad (2-14)$$

When the definition is made that

$$\frac{dA_d}{d\bar{\delta}} = g'(\bar{\delta}) \quad (2-15)$$

the expression of Eq. (2-14) becomes:

$$\frac{d\varphi_1}{dt} = 2B_s g'(\bar{\delta}) \frac{d\bar{\delta}}{dt} \quad (2-16)$$

This expression has the same form as the rates of change of flux in the simplified mathematical models treated earlier [see Eqs. (2-3) and (2-8)]: that is to say, the rate of change of flux is linear with $\frac{d\bar{\delta}}{dt}$ and also depends on $\bar{\delta}$ through the function $g'(\bar{\delta})$.

The two relations, Eqs. (2-12) and (2-16), could be used as a mathematical representation for a reactor. In the most general case, the two equations could be used to describe the motion of the domain wall at each nucleating site, in which case a different damping function $f(\bar{\delta})$, shape function $g'(\bar{\delta})$,

and starting field H_s would have to be defined for each nucleating site. There would be a number of variables equal to the number of nucleating sites, in addition to the terminal variables, flux, and field. Thus, for any excitation, a differential equation of the form of Eq. (2-12) would have to be solved for each nucleating site, and then the rate of change of flux given by Eq. (2-16) would have to be summed over all nucleating sites. Such a general representation is not feasible at present, because no detailed information is available about nucleating sites and domain patterns in polycrystalline materials. In addition, such a large number of variables would make circuit analysis extremely cumbersome.

One type of simplification from this general representation has been made by Friedlander.²⁷ He assumed that all domains have the same damping function, shape function, and starting field. Then, by assuming two types of distribution of nucleating sites, random and uniform, he calculates the shape of the voltage pulse for constant-field switching. The agreement between Friedlander's experimental and theoretical results was good, but the mathematical expressions that were used cannot be easily included in a circuit analysis. Even though he considered that all domains had the same starting field, in his calculations he did recognize the fact that for fields just larger than the coercive field the number of domains participating in the flux reversal appears to be a function of the applied field.

Another type of simplification from the general representation will be used in the derivation to follow. In this

case, all domains are assumed to have the same damping and shape functions, but different starting fields. The assumption of the same shape function $g'(\delta)$ means that the nucleating sites are considered as uniformly distributed in the material, and that all nucleated domains have the same shape, as shown in Fig. 2-10. The equation of motion for a typical domain wall is then averaged over all starting fields, to obtain a single equation which, on the average, describes all domain wall motion in the material. Then the representation is completed by summing the rate of change of flux over all domains.

Other types and degrees of simplification from the original equations could be used. The reason for the type of approximation chosen here is that the simplified representation retains enough detailed information about reactor characteristics to yield good predictions of magnetic-amplifier performance while not complicating the analysis excessively.

2.2.0 Mathematical Representation for a Polycrystalline Material

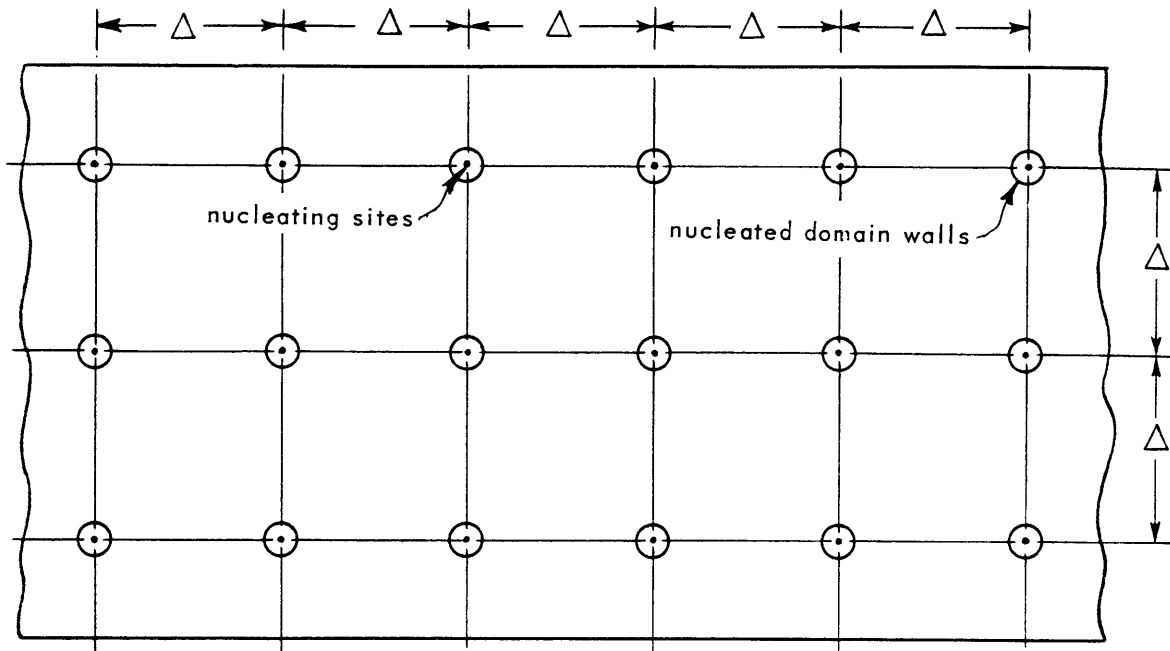
In the preceding treatments of single-domain behavior, the validity of the equations did not depend on the initial conditions: i.e., the initial position of the wall. In the treatment to follow, the distribution functions with which the single-domain behavior is averaged over the polycrystalline structure are strongly dependent on the initial conditions. In order that the initial conditions for the flux change shall always be the same, the restriction is placed on the operation that, just prior to the flux resetting

which the model describes, the reactor shall have been driven into saturation by a field strength at least five times the coercive field. If this requirement is not met in practice, some mobile domain walls may remain in the material at places other than the normal nucleating sites. The presence of these mobile walls will reduce the field required to reset the flux. When this phenomenon occurs, an instability of the magnetic amplifier results.³⁵ Such an instability is not predicted by the representation used here.

The requirement of previous strong saturation eliminates mobile domain walls from the specimen; consequently, before the flux can be reset, domains of reverse magnetization must be nucleated. In accordance with the discussion of Section 1.2.1 of Chap. I, the nucleation is assumed to occur at the grain boundaries and crystalline surfaces. The field required to nucleate a domain is, in general, different from the field required to move the domain wall away from the nucleating site. The nucleated domains are considered to be so small that the nucleation process does not yield an appreciable change in flux; therefore, the mathematical representation takes account of only the starting field for a domain wall.

2.2.1 Distribution of Starting Fields

A polycrystalline material is not homogeneous; the detailed characteristics of the material, such as grain size and structure, internal stress, size and distribution of impurities, etc. will vary from point to point. Thus it is



excitation perpendicular to plane of paper

Fig. 2.10. Demonstrating distribution of nucleating sites and shape of nucleated domains in simplified representation

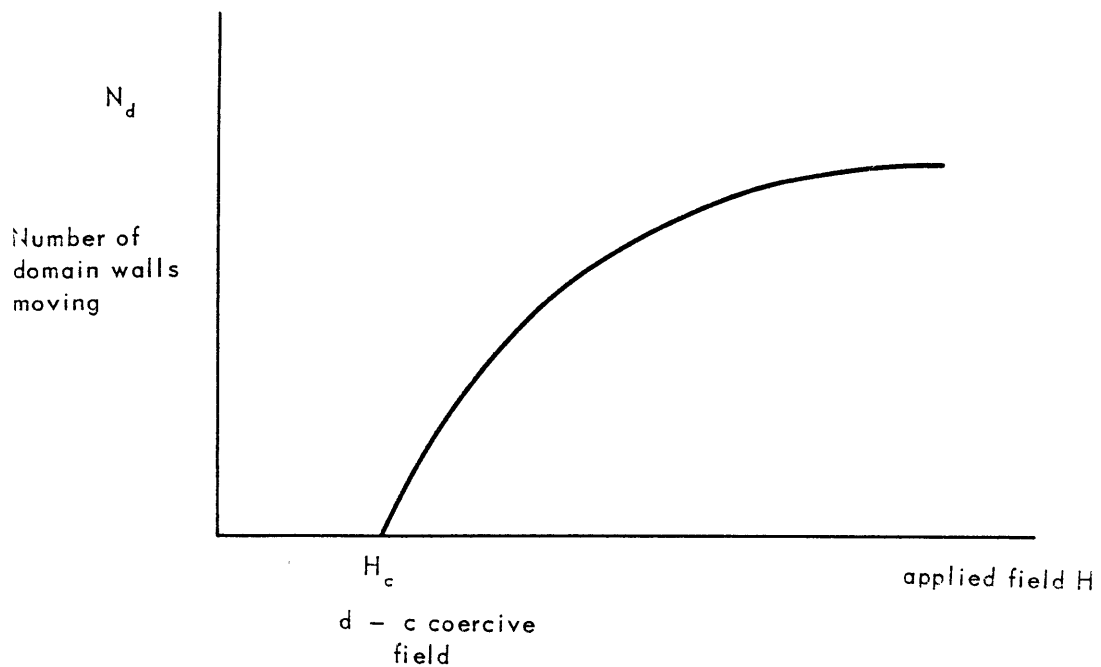


Fig. 2.11. Number of domain walls moving as a function of applied field

reasonable to assume that the walls of domains nucleated at different points in the material will have different starting fields. With the relatively fine grain structure found in the materials used in magnetic-amplifier reactors, the flux reversal at normal field strengths is probably accomplished by the movement of a large number of domain walls. Since each domain wall has a different starting field, the number of domain walls participating in the flux change will vary with applied field, perhaps as shown in Fig. 2-11. The curve is considered continuous because of the large number of domains involved.

With the assumption of a continuous curve for N_d as a function of H , the curve of Fig. 2-11 can be considered to be obtained by integration of a distribution function

$$N_d(H) = \int_{H_c}^H \frac{dN_d(H_s)}{dH_s} dH_s \quad (2-17)$$

where the number of domain walls which have starting fields between H_s and $H_s + dH_s$ is

$$G(H_s)dH_s = \frac{dN_d(H_s)}{dH_s} dH_s \quad (2-18)$$

The distribution function of Eq. (2-18) will have a shape perhaps like that shown in Fig. 2-12. Of course, for fields less than the d-c coercive field H_c , no domain walls will move.

The function $G(H)$ gives a qualitative idea of the structure and grain texture in a material: for instance, suppose

the grain sizes are all the same and there exists only one type of nucleating site. With this high degree of uniformity, the function $G(H)$ will be an impulse at H_c : that is to say, all domain walls will have the same starting field. On the other hand, suppose that there is a wide range of grain sizes and shapes in the material. In this case it is reasonable to expect that there will be a large variety of starting fields among the great variety of nucleating sites. Thus the function $G(H)$ will have an appreciable value over a wide range of fields. If the grain size varies, but each grain size is present in the same amount, then the function $G(H)$ should be relatively constant over a range of fields.

The distribution of starting fields given in Eq. (2-18) is independent of flux level. This result holds true only for the initial condition described in Section 2.2.0 of this chapter. That initial condition is: that the material has been saturated strongly before the flux resetting which the representation will describe. If the material is not saturated strongly enough to annihilate practically all mobile domain walls, the number of walls moving at a particular field strength will depend on the wall configuration prior to the resetting period. Thus the distribution function described by Eq. (2-21) is assumed to hold only when the initial condition of practically no mobile domain walls is satisfied.

2.2.2 Definition of an Average Normalized Domain Dimension

The domain dimension $\bar{\delta}$ in Eq. (2-12) is an average dimension of a single domain. In order to describe the polycrystalline

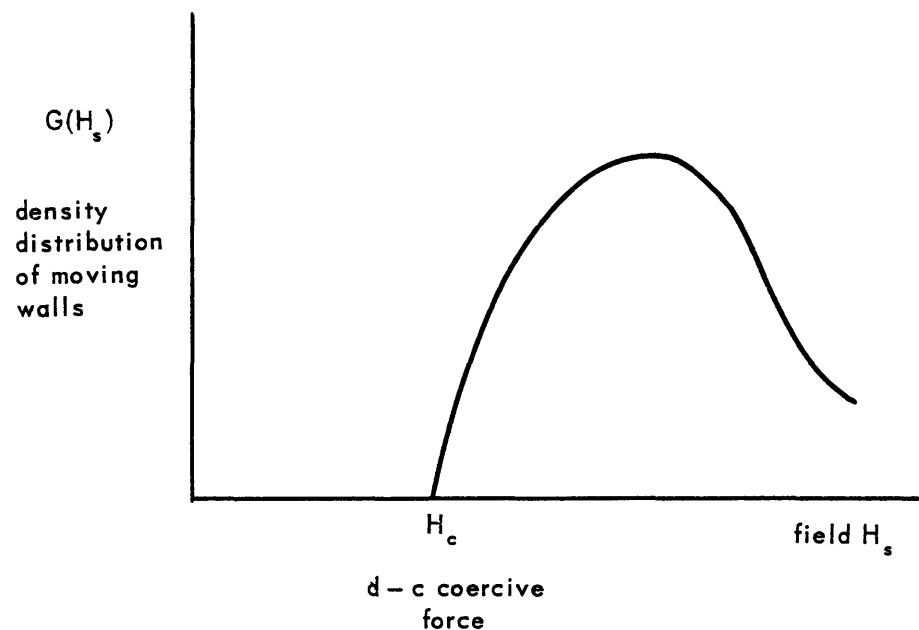


Fig. 2.12. Distribution of moving walls with applied field

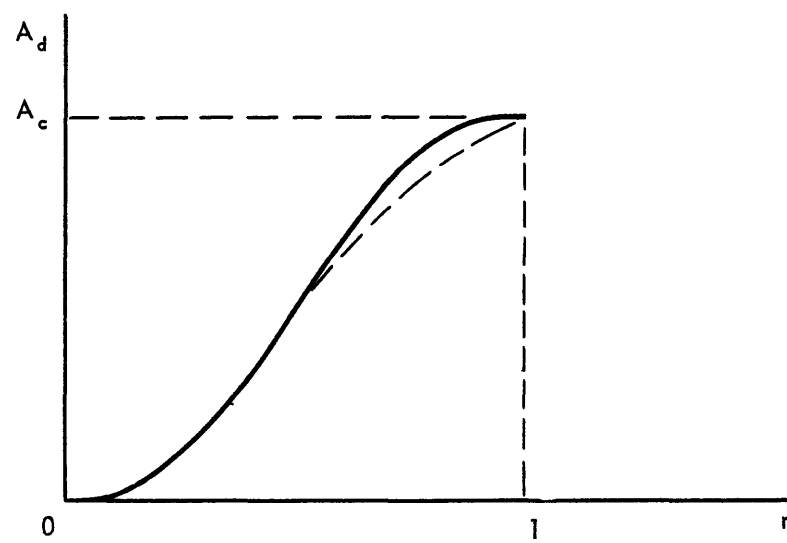


Fig. 2.13. Area of reversed magnetization as a function of the average normalized dimension r .

material, the average domain dimension \bar{x} is defined as the average domain dimension resulting from averaging over all the individual domains contributing to the flux reversal. Since the only difference among the individual domains is assumed to be in the starting field, the average domain dimension \bar{x} is defined from Eq. (2-12) by averaging the right-hand side over the number of domain walls moving to yield the result:

$$f(\bar{x}) \frac{d\bar{x}}{dt} = K_1 \frac{\int_{H_c}^H (H - H_s) G(H_s) dH_s}{\int_{H_c}^H G(H_s) dH_s} \quad (2-19)$$

On the average, the distance \bar{x}_{max} that a domain wall must move to complete the flux reversal will be inversely proportional to the number of domain walls moving; thus an average normalized domain dimension r can be defined

$$r = \frac{\bar{x}}{\bar{x}_{max}} = K_2 \bar{x} \int_{H_c}^H G(H_s) dH_s \quad (2-20)$$

The substitution of Eq. (2-20) into Eq. (2-19) yields:

$$\begin{aligned} f \left(\frac{r}{K_2 \int_{H_c}^H G(H_s) dH_s} \right) \left[\frac{dr}{dt} - \frac{rG(H)}{\int_{H_c}^H G(H_s) dH_s} \frac{dH}{dt} \right] &= \\ = K_1 K_2 \int_{H_c}^H (H - H_s) G(H_s) dH_s \end{aligned} \quad (2-21)$$

Equation (2-21) describes the dynamics of the average normalized domain dimension r as a function of the applied field H . From Eq. (2-20) it is evident that before the flux reversal starts, r is zero; and at the end of a complete flux reversal, r is unity.

The definitions of both the average domain dimension \bar{x} and the normalized dimension r imply a physical model considerably simpler than a random distribution of nucleating sites and domain shapes. The description of all domain wall motion by one differential equation, Eq. (2-21), implies that all the nucleated domain walls have the same shape, and that the nucleating sites are distributed uniformly throughout the material, as shown in Fig. 2-10. Also this implies that the damping on all domain walls is the same function of position.

2.2.3 Rate of Change of Flux

The rate of change of flux in a grain-oriented material depends on the rate of change of cross-sectional area included in the domains of reverse magnetization. As a domain starts to grow, the area included in its cross-section grows. This domain growth continues until the domain wall is completely annihilated at a crystalline surface or by collision with another domain wall. Thus the initial growth of the area of reversed magnetization will depend on the average domain dimension \bar{x} , as well as on the number of walls moving N_d . This growth will continue until wall annihilation sets in. If the majority of domain wall annihilation occurs through collision of two walls, then the distance a domain wall travels before

being annihilated will vary inversely with the number of domain walls moving. Thus the area of reversed magnetization can be assumed to be a function of the product of N_d and \bar{x} , thus:

$$A_d = A_d(N_d \bar{x}) \quad (2-22)$$

The variable $N_d \bar{x}$ is related to the average normalized domain dimension by a constant in Eq. (2-20); thus the area of reversed magnetization can be written

$$A_d = A_d(r) \quad (2-23)$$

As discussed in Section 2.2.2, the variable r is zero at the start of the flux reversal and unity at the end of the flux reversal. Thus

$$\begin{aligned} A_d(0) &= 0 \\ A_d(1) &= A_c \end{aligned} \quad (2-24)$$

where A_c is the cross-sectional area of the core.

According to the expression of Eq. (2-23), the area of reversed magnetization always proceeds along the same curve with respect to r , as shown qualitatively in Fig. 2-13. This assumes that the details of domain growth and annihilation always remain the same with respect to the variable r . The details of domain growth probably do remain the same; however, as the driving conditions are varied, the details of annihilation will probably change because of variation in density of nucleating sites throughout the material, as shown by the dotted curve in Fig. 2-13. Any variations of this sort will be neglected in this representation because, in magnetic-amplifier analysis, the initial portion of the curve is most

important, and experimental results published in the literature³² indicate that the variation is not very large.

The total rate of change of flux in the core is given by

$$\frac{d\varphi}{dt} = 2B_s \frac{dA_d}{dt} = 2B_s \frac{dA_d(r)}{dr} \frac{dr}{dt} \quad (2-25)$$

Thus, defining

$$\frac{dA_d(r)}{dr} = g(r) \quad (2-26)$$

the rate of change of flux becomes:

$$\frac{d\varphi}{dt} = 2B_s g(r) \frac{dr}{dt} \quad (2-27)$$

Equations (2-21) and (2-27) relate the flux in a reactor to the field applied to the reactor through the use of the auxiliary variable r . These two equations will be further simplified for the magnetic-amplifier analysis of Chap. III. Before these equations can be used to describe a particular reactor, the functions $f(\bar{x})$, $g(r)$, and $G(H_s)$, as well as the constants in the equations, must be known. These factors could conceivably be determined from a detailed knowledge of the structure and composition of the core material; however, with the limited amount and accuracy of such information at the present time, these factors can best be determined by suitable measurements made on the reactor. Such measurements will be made to obtain the necessary information for the model in the applications of later chapters. The functions $f(\bar{x})$, $g(r)$, and $G(H_s)$ will be chosen to obtain as close an approximation as possible to the reactor characteristics and at the same time to yield mathematical expressions simple enough to allow easy manipulation.

2.3.0 Experimental Verification of the Representation

The experimental verification of the reactor representation in its most general form has not been attempted. Some simple examples will be presented to show how the representation fits experimental results for certain simplified excitations. Sufficient verification will be made to indicate the applicability of the representation to magnetic-amplifier analysis.

2.3.1 Switching With Large Constant Field

When a saturable reactor is reset from residual by a constant applied field H , Eq. (2-21) simplifies to

$$f \left(\frac{r}{K_2 \int_{H_c}^H G(H_s) dH_s} \right) \frac{dr}{dt} = K_1 K_2 \int_{H_c}^H (H - H_s) G(H_s) dH_s \quad (2-28)$$

Consider the case of a material in which the range of starting fields is limited and the distribution function is as shown in Fig. 2-14. When the applied field is sufficiently large, the integration indicated in Eq. (2-28) can be simplified by considering $G(H_s)$ to be an impulse at $H_s = H_o$, the value of field that divides in half the area under the curve, and having an area equal to the area under $G(H_s)$. Such an approximation yields

$$\int_{H_c}^H (H - H_s) G(H_s) dH_s = N_T (H - H_o) \quad (2-29)$$

where N_T is the area under the $G(H_s)$ curve and the total number of nucleation sites available in the reactor core. In this

case, Eq. (2-28) can be simplified to

$$f \left(\frac{r}{K_2 N_T} \right) \frac{dr}{dt} = K_1 K_2 N_T (H - H_o) \quad (2-30)$$

When the time τ_s required to completely reverse the reactor flux is desired, it can be found by integrating Eq. (2-30); because, when the flux is at residual, $r = 0$; and when the flux is completely reversed, $r = 1$. Performing this integration yields:

$$\int_0^1 f \left(\frac{r}{K_2 N_T} \right) dr = K_1 K_2 N_T (H - H_o) \tau_s \quad (2-31)$$

Since the left-hand side of this expression is a constant, a plot of $1/\tau_s$ as a function of applied field should yield a linear plot like that shown in Fig. 2-15. Experimental results of this type have been reported by Menyuk and Good-enough³² and later by Menyuk³³ for permalloy cores made from tapes of 1/8-mil to 1-mil thickness. In these experiments the field H_o was approximately 1.5 to 2 times the d-c coercive field, while the applied field ranged up to ten times the d-c coercive. Thus the representation is capable of describing the switching characteristics of saturable reactors at high field strengths.

According to the discussion of Section 2.2.2, the range of fields over which the function $G(H)$ has an appreciable value is an indication of the uniformity of the grain structure of a specimen. Since the field H_o obtained by extrapolating a high-field, constant-current switching characteristic, as shown in Fig. 2-15, is a measure of the range of fields

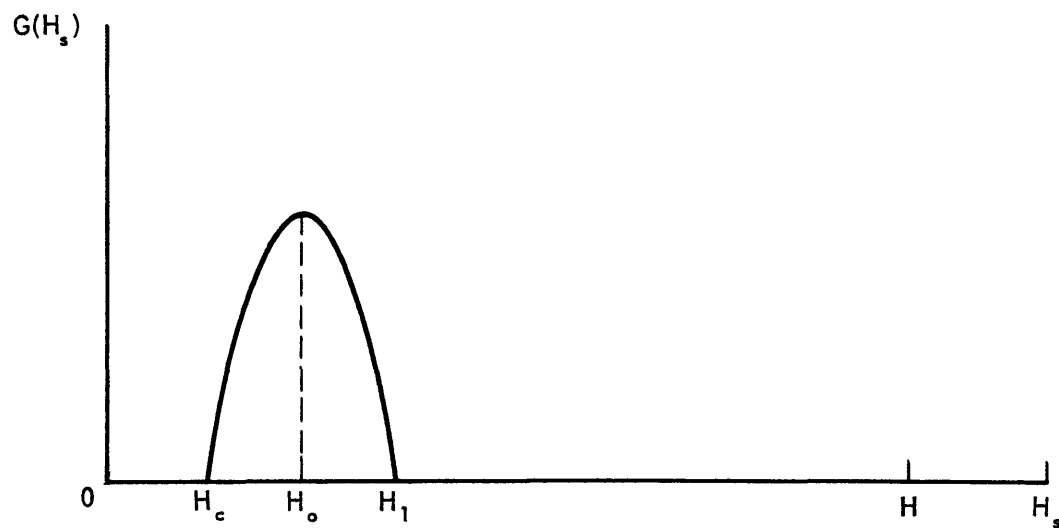


Fig. 2.14. One type of distribution of starting fields

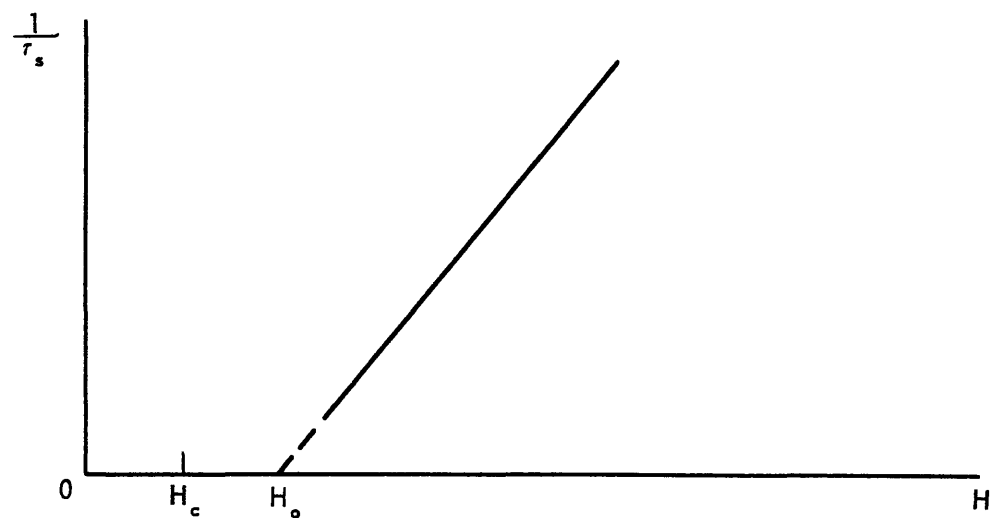


Fig. 2.15. Switching characteristics at high applied fields

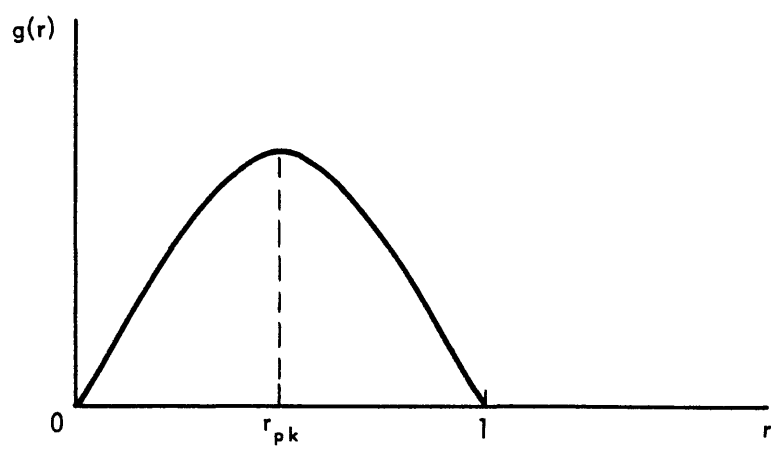


Fig. 2.16. Shape of voltage pulse for constant applied field

over which $G(H)$ has an appreciable value, as shown in Fig. 2-14, such a switching characteristic could be used as a measure of the uniformity of the grain structure in a material.

2.3.2 Switching With Small Constant Field

When the flux in a reactor is reset with a small field which occurs in the range of starting fields, the switching does not show the simple linear relation of the preceding section. This occurs because the number of domain walls moving depends on the applied field. When a constant field is applied, regardless of its size so long as it is greater than the d-c coercive field H_c , Eq. (2-21) reduces to

$$f \left(\frac{r}{K_2 \int_{H_c}^H G(H_s) dH_s} \right) \frac{dr}{dt} = K_1 K_2 \int_{H_c}^H (H - H_s) G(H_s) dH_s \quad (2-28)$$

while the rate of change of flux in the reactor is given by Eq. (2-27):

$$\frac{d\phi}{dt} = 2B_s g(r) \frac{dr}{dt} \quad (2-27)$$

The first problem in solution at low fields is the evaluation of the integrals in Eq. (2-31).

In order to facilitate evaluation of the integrals in question, the distribution $G(H_s)$ must be known. It is impossible at the present time to determine this function by examining the detailed structure of the material; consequently, $G(H_s)$ must be determined from electrical measurements on the reactor in question. In order to allow approximate correlation of the representation with experiments, the function $G(H_s)$ can be approximated by a power series over the range of

fields of interest. Since $G(H_s)$ is zero for $H_s < H_c$, it can be represented by the series:

$$G(H_s) = (H_s - H_c)^p \sum_{n=0}^{\infty} a_n (H_s - H_c)^n \quad (2-32)$$

where

$$H_s > H_c$$

$$-1 < p \leq 0$$

$$n \text{ an integer}$$

When the function of Eq. (2-32) is substituted into the right-hand side of Eq. (2-28), and the integral is evaluated, there results

$$\begin{aligned} K_1 K_2 \int_{H_c}^H (H - H_s) G(H_s) dH_s &= \\ &= K_1 K_2 \sum_{n=0}^{\infty} \frac{a_n}{(n + p + 1)(n + p + 2)} (H - H_c)^{n+p+2} \end{aligned} \quad (2-33)$$

The number of domain walls moving at any particular field strength H is

$$N_d = \int_{H_c}^H G(H_s) dH_s = \sum_{n=0}^{\infty} \frac{a_n}{n + p + 1} (H - H_c)^{n+p+1} \quad (2-34)$$

The second problem in the solution is that some information about the function

$$f\left(\frac{r}{K_2 N_d}\right)$$

must be known. This function is the damping constant; and, if the domains are expanding cylinders, this function will contain a constant term due to spin-relaxation damping [see

Eq. (2-9)] and a variable term due to eddy-current damping [see Eq. (2-7)]. Consequently, this function can be rewritten as:

$$f\left(\frac{r}{K_2 N_d}\right) = 1 + f_1\left(\frac{r}{K_2 N_d}\right) \quad (2-35)$$

When Eq. (2-28) is solved for $\frac{dr}{dt}$ and the result is substituted into the expression for rate of change of flux, Eq. (2-30), there results:

$$\frac{d\phi}{dt} = 2B_s K_1 K_2 \frac{g(r)}{1 + f_1\left(\frac{r}{K_2 N_d}\right)} \int_{H_c}^H (H - H_s) G(H_s) dH_s \quad (2-36)$$

For switching with constant field at low field strengths, where the number of domain walls N_d that are moving varies with applied field, the expression of Eq. (2-36) indicates that the shape of the switching voltage pulse will vary with applied field through the function f_1 . Experiments indicate that, to a good degree of approximation, for the materials and tape thicknesses commonly used in magnetic amplifiers, the shape of the switching voltage pulse remains the same over a wide range of applied fields; thus the assumption is made that

$$f_1\left(\frac{r}{K_2 N_d}\right) \ll 1 \quad (2-37)$$

Of course the degree of validity of this approximation varies among materials and tape thicknesses. Since the approximation of Eq. (2-37) is neglecting at least part of the eddy-current damping with respect to the spin-relaxation damping, it is expected that the inequality of Eq. (2-37) will be more nearly fulfilled for the thinner tapes and for those materials with

higher resistivity. In addition, the initial part of the waveform, which is of the most interest in magnetic-amplifier analysis, is dependent mostly on spin-relaxation damping²⁷; thus the approximation of Eq. (2-37) is more accurate for the initial part of the waveform.

With the restriction of constant applied field, and with the approximations of Eqs. (2-32) and (2-37), Eq. (2-28) reduces to

$$\frac{dr}{dt} = K_1 K_2 \sum_{n=0}^{\infty} \frac{a_n}{(n+p+1)(n+p+2)} (H - H_c)^{n+p+2} \quad (2-38)$$

while Eq. (2-36) becomes

$$\frac{d\phi}{dt} = 2B_s K_1 K_2 g(r) \sum_{n=0}^{\infty} \frac{a_n}{(n+p+1)(n+p+2)} (H - H_c)^{n+p+2} \quad (2-39)$$

In the representation described by Eqs. (2-38) and (2-39), the application of a constant field H results in a linear variation of the normalized dimension r with time. Consequently, the variation of $d\phi/dt$ with time is the same as the variation of $g(r)$ with r , with the amplitude and time scales dependent on the applied field. Thus, if the function $g(r)$ has a shape as shown in Fig. 2-16, with the peak occurring at r_{pk} , then the peak value of the rate of change of flux is given by:

$$\left(\frac{d\phi}{dt}\right)_{pk} = 2B_s K_1 K_2 g(r_{pk}) \sum_{n=0}^{\infty} \frac{a_n}{(n+p+1)(n+p+2)} (H - H_c)^{n+p+2} \quad (2-40)$$

The time τ_{pk} from the application of the field to the peak rate of change of flux is given by Eq. (2-38) as

$$\frac{1}{\tau_{pk}} = \frac{K_1 K_2}{r_{pk}} \sum_{n=0}^{\infty} \frac{a_n}{(n+p+1)(n+p+2)} (H - H_c)^{n+p+2} \quad (2-41)$$

Since the flux is completely switched for $r = 1$, the switching time is given by Eq. (2-38) as:

$$\frac{1}{\tau_s} = K_1 K_2 \sum_{n=0}^{\infty} \frac{a_n}{(n+p+1)(n+p+2)} (H - H_c)^{n+p+2} \quad (2-42)$$

A set of switching tests for a reactor can be used in conjunction with any one of the last three equations to determine the constants of the reactor. In addition, all three quantities can be plotted and compared to obtain a measure of how well the mathematical representation describes the reactor.

The interpretation of the mathematical representation of Eqs. (2-38) and (2-39) in terms of the domain pattern and domain wall motion that it implies is interesting. Consider the case of switching with a constant applied field. The expression of Eq. (2-38) describes all domain wall motion; thus all domains have the same behavior. Furthermore, all of the domain walls move against a constant damping force through the same distance, with each wall contributing a switching voltage pulse of the same shape and the same area. Thus the representation of Eqs. (2-38) and (2-39) could have been obtained by assuming a uniform distribution of identical domains, as shown in Fig. 2-10, with the number of domain walls moving given by the distribution function $G(H_s)$. Then each moving domain wall would contribute the same pulse of voltage, as illustrated in Fig. 2-16, and the net rate of change of flux would be the pulse for a single domain multiplied by the number of moving

walls. According to the original equation of motion, Eq. (2-12), domain wall motion is linear with applied field; consequently, the nonlinearity of Eqs. (2-38) and (2-39) is caused by the variation of the number of moving walls with applied field. In spite of the simplicity that could have been achieved by making the simplifying assumptions initially, the more general treatment is preferred here because it indicates points for future generalization of the representation as more detailed information about ferromagnetic materials becomes available.

The necessary constants for inclusion in the representation in a magnetic-amplifier analysis could be determined by finding the coefficients a_n and the exponent p which make the representation best fit an experimental plot of one of the three equations, Eq. (2-40), (2-41), or (2-42). The inclusion of such a result in a magnetic-amplifier analysis would entail cumbersome mathematics. A less accurate but more easily handled model can be obtained by approximating the series in these equations by a single term. The accuracy of such a representation, as well as the necessary constants, can be determined by plotting the experimental curves on a log-log plot. If the resulting plot is a straight line, the approximation of a single term is a good one. The accuracy of this approximation can be seen for three thicknesses of 50% Ni-50% Fe material in the plots of Fig. 2-17. These results are in good agreement with similar experimental plots given in the literature by Huhta.²¹

The analysis of the behavior of a reactor for other than

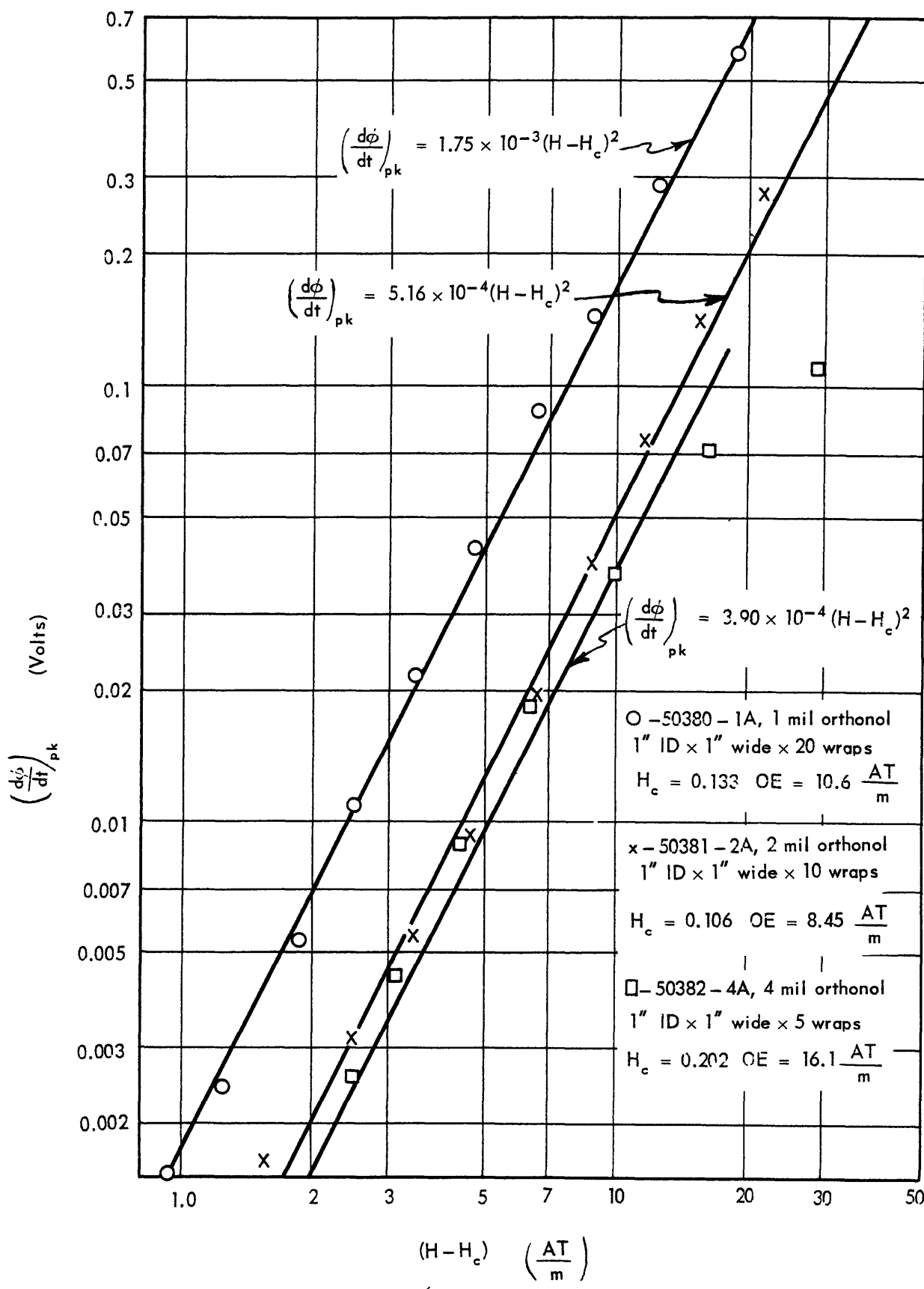


Fig. 2.17. Plots of $\left(\frac{d\phi}{dt} \right)_{pk}$ vs. $(H - H_c)$ for three reactors

constant applied fields is enhanced if the exponent p is zero. Thus, if the log-log plot of one of the three variables of Eqs. (2-40), (2-41), or (2-42) is approximated by a straight line with a slope equal to an integer, the resulting expression can easily be applied to the analysis of a magnetic amplifier. The error introduced into the analysis by this further approximation will depend on how well the model fits the original plot of one of the three switching variables as a function of applied field.

2.3.3 Switching With Slowly Varying Field

To be applicable to magnetic-amplifier analysis, the mathematical model must hold for variable applied fields. One of the simplest methods of applying a variable field is with the circuit arrangement of Fig. 2-18. When switch S is closed, the voltage of the battery V_g supplies current through the winding N_g to saturate the reactor strongly enough to satisfy the initial conditions of Section 2.2.0 of this chapter. When the switch S is opened at $t = 0$, the flux in the reactor is reset under the action of the voltage V_r acting through the resistance R_r . When the resistance R_r is high enough, the resetting source appears as a current source of value V_r/R_r ; however, as the resistance R_r is decreased, the current i_r will vary during the resetting process, thus applying variable field to the reactor. Of course, when the resistance R_r is made so low that the necessary exciting current causes negligible voltage drop across R_r , the rate of change of flux will be constant and equal to V_r/N_r .

For very high values of R_r , the field is constant during the resetting; consequently, the term containing dH/dt in Eq.(2-21) goes to zero. As the resistance R_r decreases from this high value, the rate of change of applied field with time will increase. For the values of resistance of interest in magnetic-amplifier analysis, the assumption is made that the field changes slowly enough so that the term containing dH/dt in Eq.(2-21) can still be neglected. Thus the equations describing the reactor material are Eqs.(2-38) and (2-39).

To check the validity of this representation, consider the one-mil Orthonol core for which the peak switching voltage is plotted in Fig. 2-17. The curve for this core is well approximated by assuming the exponents and coefficients in Eqs.(2-38) and (2-39) to be

$$\begin{aligned} n + p &= 0 \\ a_n &= 0 \quad \text{for } n \geq 1 \end{aligned} \tag{2-43}$$

With the constants thus specialized, Eqs.(2-41) and (2-42) become

$$\frac{dr}{dt} = K_1 K_2 \frac{a_0}{2} (H - H_c)^2 \tag{2-44}$$

$$\frac{d\phi}{dt} = B_s K_1 K_2 a_0 g(r) (H - H_c)^2 \tag{2-45}$$

The approximation that the switching characteristics vary as the square of the effective field implies that the function $G(H)$, which describes the distribution of starting fields, is a constant, as illustrated in Fig. 2-19. In terms of the representation being used, the fact that $G(H)$ is a constant means

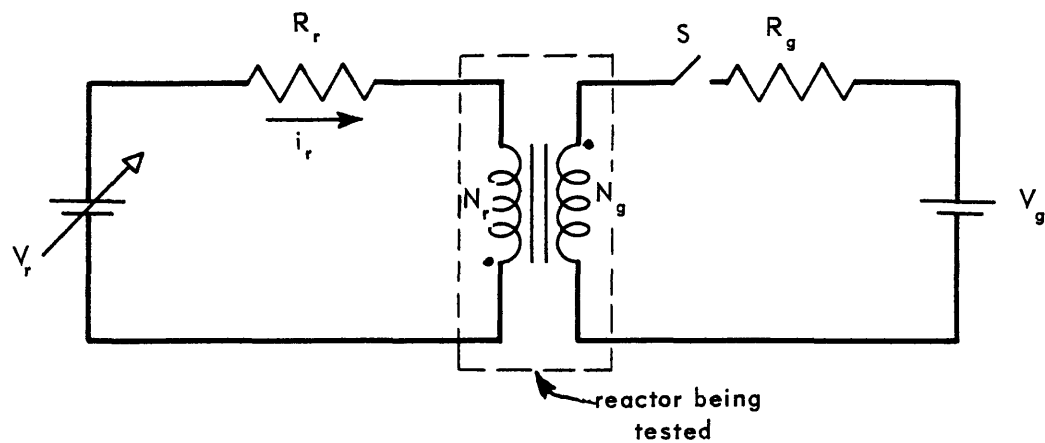


Fig. 2.18. Circuit for checking model with slowly varying field

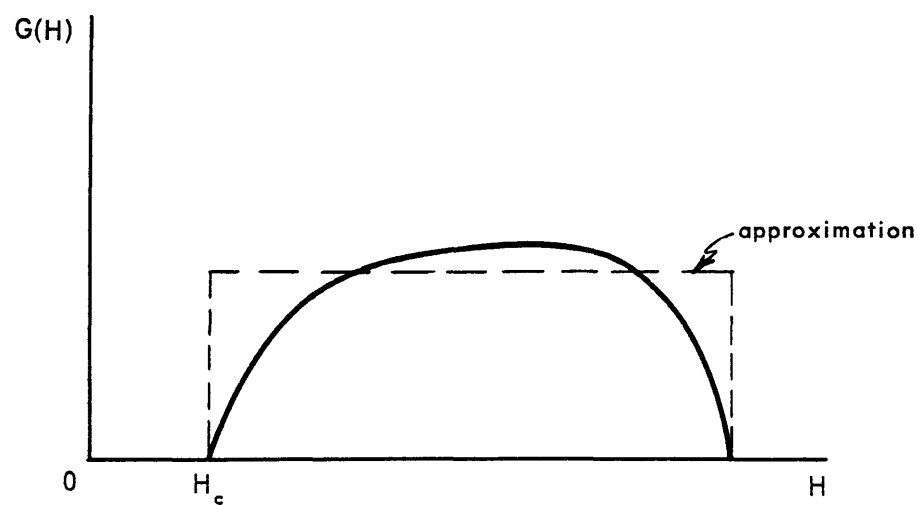


Fig. 2.19. Approximation for function $G(H)$ to yield switching characteristics that vary as the square of the effective field

that all the types of nucleating sites are present in equal numbers. The equation describing the resetting circuit of Fig. 2-18 with the switch opened at $t = 0$ is:

$$\frac{N_r V_r}{\lambda_m R_r} = H + \frac{N_r^2}{\lambda_m R_r} \frac{d\phi}{dt} \quad (2-46)$$

where λ_m is the mean length of the magnetic path and in rationalized mks units,

$$H = \frac{N_r i_r}{\lambda_m} \quad (2-47)$$

Implicit in Eq.(2-47) is the assumption that the field does not vary appreciably across the core. For the core presently being considered, the ratio of inside diameter to outside diameter is:

$$\frac{ID}{OD} = 0.99$$

Thus the assumption of constant field across the thickness of the specimen is well justified. When such an assumption cannot be justified, recourse must be had to the methods discussed below in Section 2.4.0.

A prediction of the switching characteristics of the reactor with slowly varying fields can be made by simultaneously solving Eqs.(2-44), (2-45), and (2-46). Such a solution yields for the rate of change of flux as a function of the normalized domain dimension r :

$$\frac{d\phi}{dt} = B_s K_1 K_2 a_o g(r) \left[\frac{-1 + \sqrt{1 + 4B_s K_1 K_2 a_o \frac{N_r^2}{\lambda_m R_r} g(r) \left(\frac{N_r V_r}{\lambda_m R_r} - H_c \right)}}{2B_s K_1 K_2 a_o \frac{N_r^2}{\lambda_m R_r} g(r)} \right]^2 \quad (2-48)$$

When the function $g(r)$ has only one peak, such as that shown in Fig. 2-16, the peak of $d\phi/dt$ will occur at the same value of r - that is, at r_{pk} - regardless of the relative resistance in the resetting circuit as indicated by the factor $\frac{N^2}{R_r}$. Thus the peak voltage from the switching pulse will be given by:

$$\left(\frac{d\phi}{dt}\right)_{pk} = \frac{B_s K_1 K_2 a_o g(r_{pk})}{\left[\frac{-1 + \sqrt{1 + 4B_s K_1 K_2 a_o \frac{N^2}{L_m R_r} g(r_{pk}) \left(\frac{N_r V_r}{L_m R_r} - H_c \right)}}{2B_s K_1 K_2 a_o \frac{N^2}{L_m R_r} g(r_{pk})} \right]^2} \quad (2-49)$$

The factor $B_s K_1 K_2 a_o g(r_{pk})$ is simply the coefficient in the approximation to Eq.(2-40) in which $n = p = 0$, and it can be found from the plot of Fig. 2-17. Designating this constant by

$$B_s K_1 K_2 a_o g(r_{pk}) = A, \quad (2-50)$$

Eq.(2-49) becomes:

$$\left(\frac{d\phi}{dt}\right)_{pk} = A \left[\frac{-1 + \sqrt{1 + 4A \frac{N^2}{L_m R_r} \left(\frac{N_r V_r}{L_m R_r} - H_c \right)}}{2A \frac{N^2}{L_m R_r}} \right]^2 \quad (2-51)$$

Equation (2-51) can be used to check the mathematical representation against experimental results for various values of $\frac{N^2}{L_m R_r}$, and for various resetting signal levels $\frac{N_r V_r}{L_m R_r}$. In fact, a normalized family of curves can be plotted using Eq. (2-51) to obtain a prediction of core switching characteristics for other than constant-current excitation.

In Fig. 2-20, experimental results obtained with the one-mil Orthonol core for which the constants were determined from

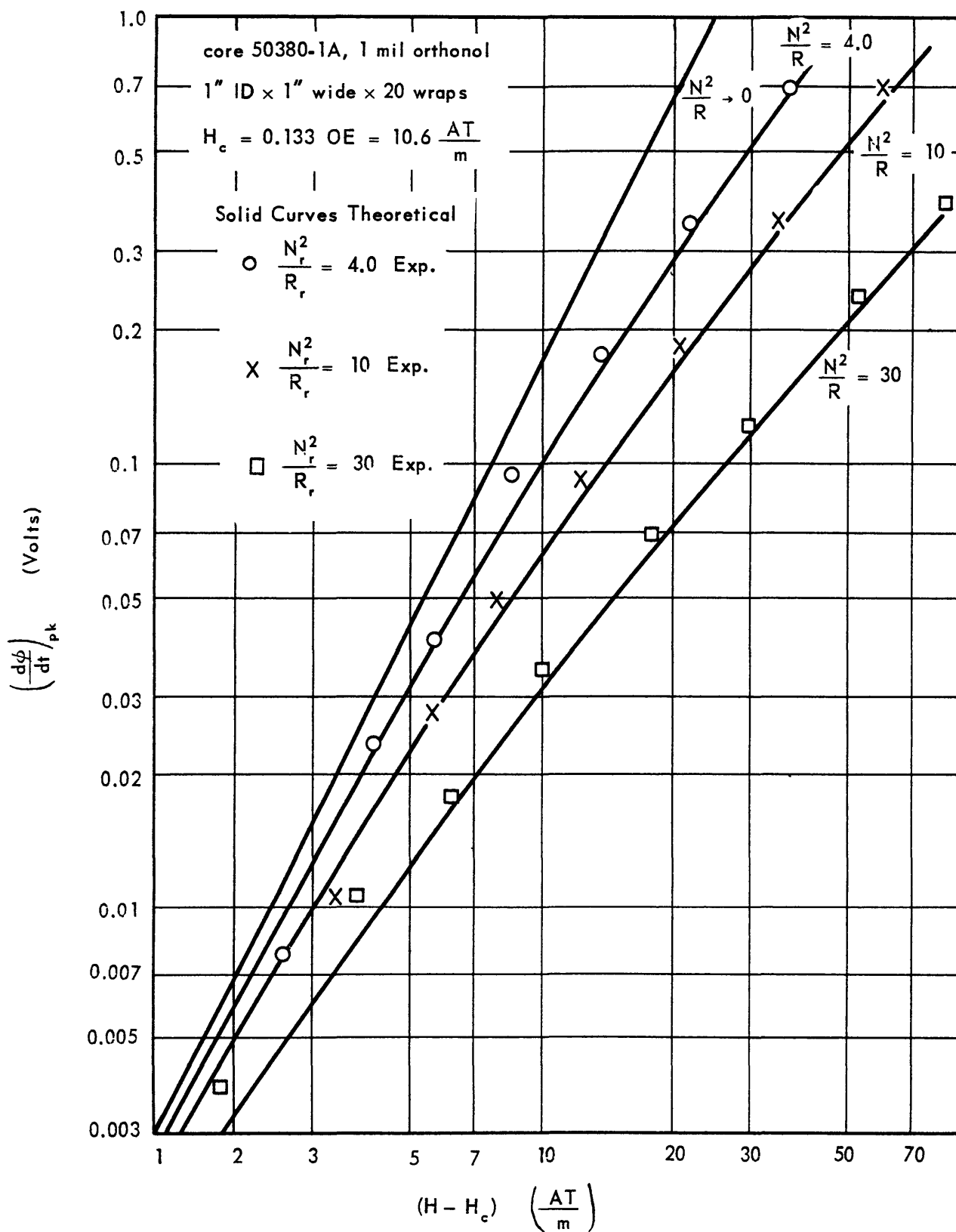


Fig. 2.20. Plots of $\left(\frac{d\phi}{dt} \right)_{pk}$ vs. $(H - H_c)$ for various values of $\frac{N_r^2}{R_r}$

the plot of Fig. 2-17 are plotted for four values of $\frac{N^2}{R_r}$ and are compared with the prediction of Eq.(2-51). The agreement between the representation and the experimental results is seen to be good.

The type of excitation used in the tests of Fig. 2-20 is the type used in many magnetic-amplifier circuits; consequently the reactor representation of Eqs.(2-44) and (2-45) is suitable for the analysis of most magnetic amplifiers. Since the assumption was made that the rate of change of applied field is small, the best quantitative results should be obtained for excitation conditions most closely approximating constant current excitation. In cases where the applied field varies rapidly, the representation of Eqs.(2-44) and (2-45) should still yield useful qualitative results when applied to a magnetic amplifier analysis.

2.4.0 Variation of ID/OD Ratio

The preceding treatment has been restricted to those cases where the ID/OD ratio is sufficiently close to unity so that the field can be considered constant across the thickness of the reactor core.

Consider the core structure shown in Fig. 2-21 with the definitions shown. Even though the core may be toroidally wound of thin tape, the resultant air gap introduced into an annular ring of thickness $d\rho$ is neglected. It is reasonable to expect that each small ring of thickness $d\rho$ will behave the same; thus the simplified model for slowly varying fields given by Eqs.(2-38) and (2-39) will hold for a ring of radius ρ .

and thickness $d\rho$, but the applied field will be a function of ρ . Thus the average normalized domain dimension r becomes a function of the radius ρ , from Eq.(2-38), in the following way:

$$\frac{dr}{dt} = K_1 K_2 \sum_{n=0}^{\infty} \frac{a_n}{(n+p+1)(n+p+2)} \left(\frac{N_i}{2\pi\rho} - H_c \right)^{n+p+2} \quad (2-52)$$

If the constants in Eq.(2-39) represent the rate of change of flux for a specimen of the same cross-sectional area as the specimen in question, then the proportion of the area in a ring of thickness $d\rho$ is

$$\frac{d}{R_o - R_i}$$

and the total rate of change of flux is:

$$\frac{d\phi}{dt} =$$

$$\frac{2B_s K_1 K_2}{R_o - R_i} \int_{R_i}^{R_o} g(r) \sum_{n=0}^{\infty} \frac{a_n}{(n+p+1)(n+p+2)} \left(\frac{N_i}{2\pi\rho} - H_c \right)^{n+p+2} d\rho \quad (2-53)$$

In order to apply Eqs.(2-52) and (2-53), the function $g(r)$ must be known. In addition, r must be known as a function of time and of N_i ; but, in general, N_i is an unknown variable in the solution of a problem. Thus the only case for which these equations can readily be solved is the case of constant current excitation, which does not have great practical interest. Even in this case, the function $g(r)$ must be selected both to approximately fit the core switching characteristic and to allow evaluation of the integral in Eq.(2-53). Thus it appears impractical to try to include the effect of ID/OD ratio in the present representation.

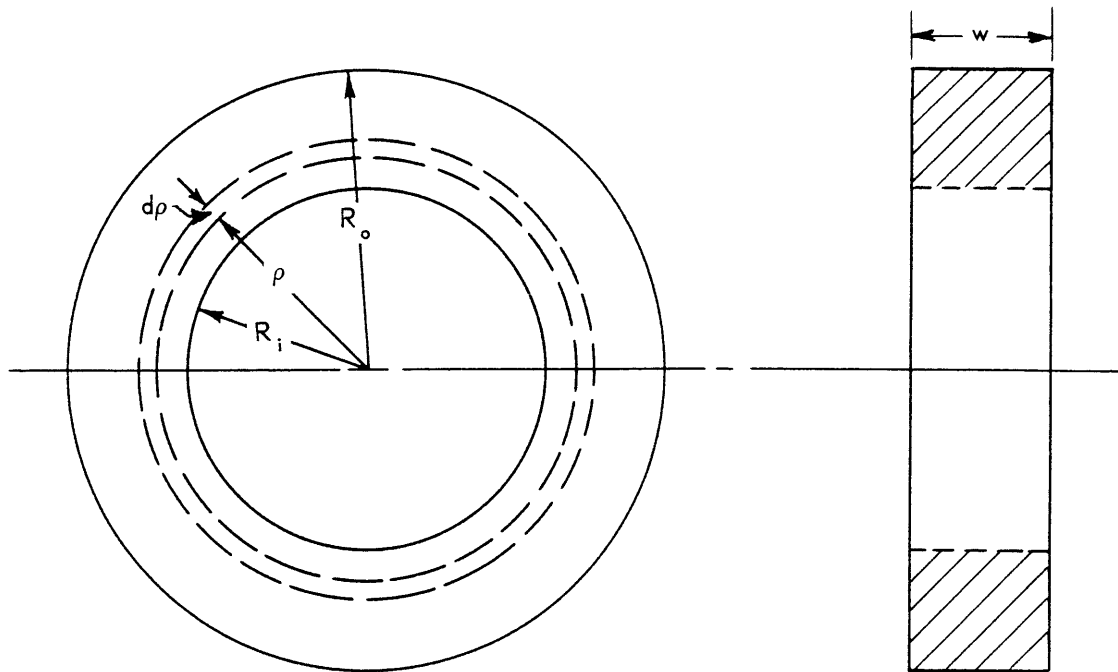


Fig. 2.21. Core configuration for investigating the effects of $\frac{ID}{CD}$ ratio

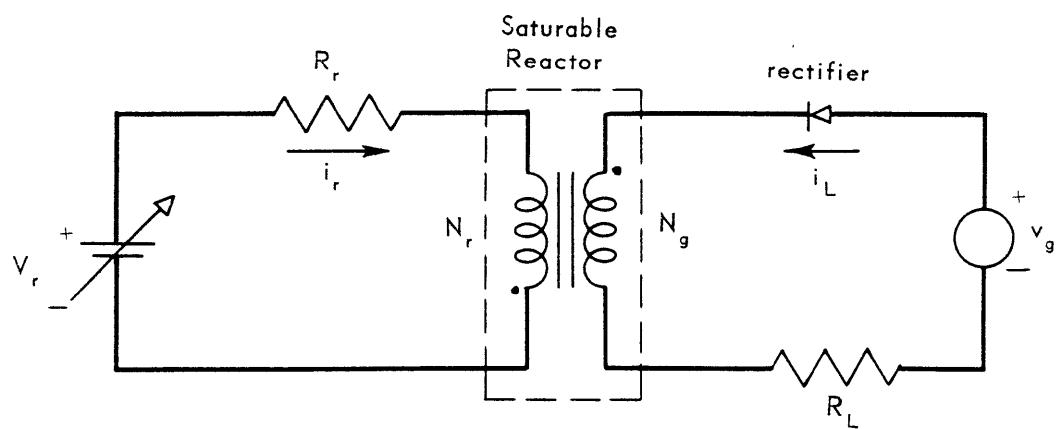


Fig. 3.1. Single-core self-saturating magnetic amplifier circuit

Roberts and Van Nice³⁷ have made a study of the influence of ID/OD ratio on the performance of magnetic amplifiers. Their results indicate that the performance at 60 and 400 cps is unaffected for ID/OD ratios from 0.8 to 1.0. Their results also indicate that the range of ID/OD ratios over which there is no change in performance increases with frequency. This is reasonable; because at higher frequencies, larger fields are necessary to reset the reactor faster, and consequently the difference between the net field ($H - H_c$) at the inner and outer surfaces of the core becomes decreased. Thus, since most practical cores have ID/OD ratios in the range of 0.8 to 1.0, the simple representation of Eqs.(2-38) and (2-39) can be used. When a core having a smaller ID/OD ratio must be used, an estimate of the decrement in gain to be expected can be obtained from the paper by Roberts and Van Nice.³⁷

Chapter III

MAGNETIC AMPLIFIER ANALYSIS USING THE REACTOR REPRESENTATION

3.0.0 Introduction

The single-core, self-saturating magnetic-amplifier circuit to be analyzed is shown schematically in Fig. 3-1. The rectifier is assumed ideal: that is, the reverse resistance is assumed infinite and the forward resistance is assumed zero. The resistance R_L includes all resistance in the load circuit and is assumed constant. The gate supply voltage v_g is an alternating voltage having a symmetrical waveform. The exact nature of the wave form will be discussed below. The reset voltage source V_r is a battery of variable voltage, and the resistance R_r includes all series resistance in the reset circuit. When the saturable reactor is unsaturated, unity coupling exists between the two windings; and when the reactor is saturated, the rate of change of flux is assumed identically zero.

Since a magnetic amplifier is controlled through the medium of a flux, which is a volt-time integral, it is most readily characterized by average values: that is, the input-output characteristic of the device is usually a plot of average load current as a function of average control voltage or some variable linearly related to it, such as average control ampere turns. During a negative alternation of the supply voltage v_g , the control or reset voltage V_r causes the reactor flux to be reset to some level Φ_0 , as shown on the

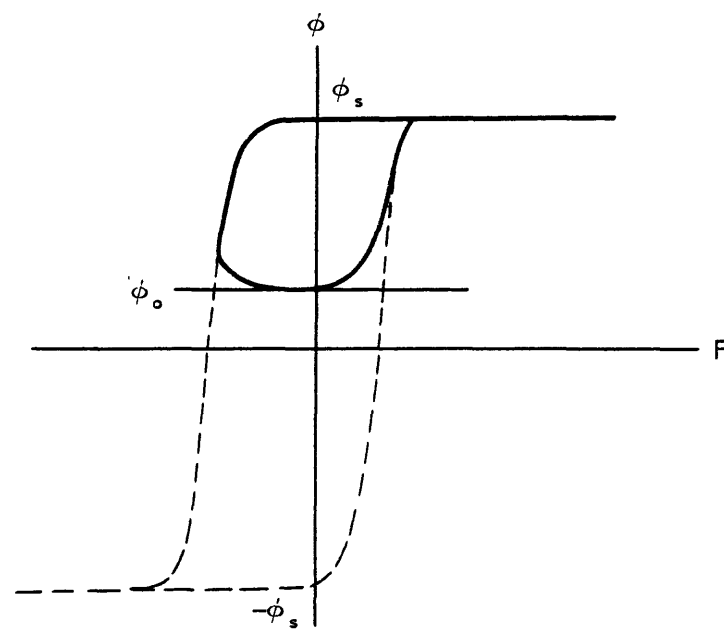


Fig. 3.2. Operating ϕ - F loop

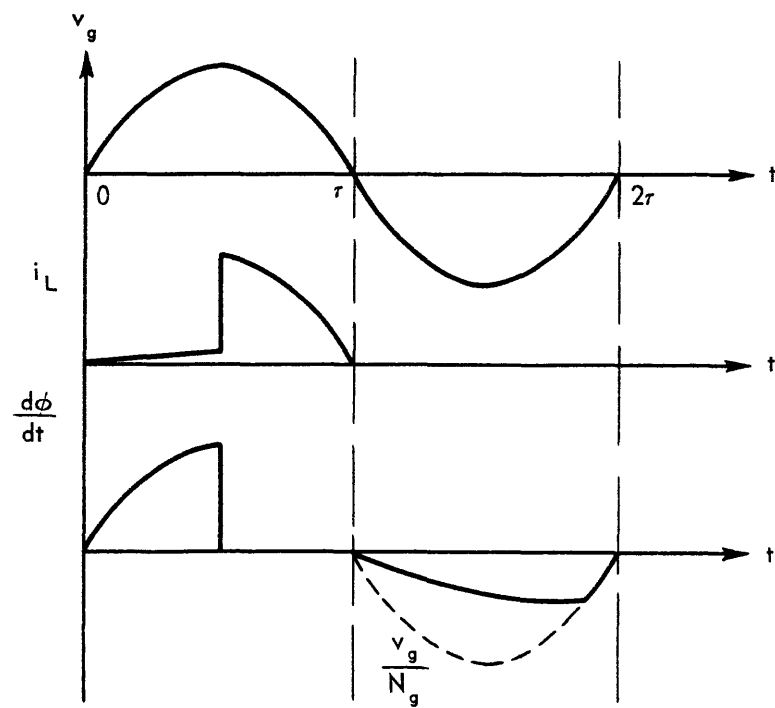


Fig. 3.3. Typical waveforms in circuit

Φ -F loop of Fig. 3-2. At the start of the next positive alternation of the supply voltage, enough mmf must be supplied by the load circuit to overcome the control-circuit mmf before the flux can increase. When the load-circuit resistance R_L is assumed small enough so that unsaturated exciting current, plus any reflected current from the control circuit, causes negligible drop across R_L , the flux will start changing in the positive direction at the instant the supply voltage becomes positive. Thus, with reference to the waveforms of Fig. 3-3, the load-circuit loop equation can be written:

$$v_g = i_L R_L + N_g \frac{d\phi}{dt} \quad (3-1)$$

When this expression is divided by R_L and integrated over the positive period of the supply, there results:

$$\int_0^{\tau} \frac{v_g}{R_L} dt = \int_0^{\tau} i_L dt + \int_0^{\tau} \frac{N_g}{R_L} \frac{d\phi}{dt} dt \quad (3-2)$$

Division of this result by the full period 2τ of the supply voltage yields:

$$\frac{1}{2\tau} \int_0^{\tau} \frac{v_g}{R_L} dt = \frac{1}{2\tau} \int_0^{\tau} i_L dt + \frac{1}{2\tau} \int_0^{\tau} \frac{N_g}{R_L} \frac{d\phi}{dt} dt \quad (3-3)$$

The term on the left-hand side of Eq. (3-3) is the half-wave rectified average current flowing through a load resistance R_L from a source v_g ; thus this term represents the maximum value of average load current that can be drawn from the circuit of Fig. 3-1. This quantity is defined as

$$I_{Lm} = \frac{1}{2\tau} \int_0^{\tau} \frac{v_g}{R_L} dt \quad (3-4)$$

The first term on the right-hand side of Eq. (3-3) is the average load current, and is denoted:

$$I_L = \frac{1}{2\tau} \int_0^\tau i_L dt \quad (3-5)$$

The last term on the right-hand side of Eq. (3-3) is simply

$$\frac{1}{2\tau} \int_0^\tau \frac{N_g}{R_L} \frac{d\varphi}{dt} dt = \frac{N_g}{2\tau R_L} (\varphi_s - \varphi_o) \quad (3-6)$$

When the flux change from saturation is defined as $\Delta\varphi$,

$$\Delta\varphi = \varphi_s - \varphi_o \quad (3-7)$$

Equation (3-3) can be written simply as:

$$I_L = I_{Lm} - \frac{N_g}{2\tau R_L} \Delta\varphi \quad (3-8)$$

In order to complete the description of the magnetic amplifier of Fig. 3-1, the flux reset from saturation must be found in terms of the reset signal.

Before consideration of the reset flux, the expression of Eq. (3-8) can be further simplified by normalization with respect to I_{Lm} ; thus

$$\frac{I_L}{I_{Lm}} = 1 - \frac{N_g}{2\tau R_L I_{Lm}} \Delta\varphi \quad (3-9)$$

From Eq. (3-4), the quantity

$$2\tau R_L I_{Lm} = \int_0^\tau v_g dt \quad (3-10)$$

Thus the expression of Eq. (3-9) becomes:

$$\frac{I_L}{I_{Lm}} = 1 - \frac{\Delta\varphi}{\int_0^\tau \frac{v_g}{N_g} dt} \quad (3-11)$$

In the experimental verification of the analysis of this chapter, normal excitation of the reactor will be assumed. Normal excitation is defined as that excitation which drives the reactor between positive and negative saturation when the rectifier is shorted and the control circuit is opened in the circuit of Fig. 3-1. In terms of the instantaneous supply voltage v_g , normal excitation is defined by

$$2B_s A_c = \int_0^\tau \frac{v_g}{N_g} dt \quad (3-12)$$

Substitution of this expression into Eq.(3-11) yields the expression for normalized output current for normal reactor excitation:

$$\frac{I_L}{I_{Lm}} = 1 - \frac{\Delta\varphi}{2B_s A_c} \quad (3-13)$$

Normal excitation has been assumed because this level of excitation yields the widest possible control range for a given reactor. The normalization process carried out above can be carried out with equal ease for any level of reactor excitation.

The flux in the reactor is reset during a negative alternation of the supply voltage v_g . Since there is no rate of change of flux while the reactor is saturated, the reset circuit current will reach its steady-state value of V_r/R_r while the reactor is saturated just prior to $t = \tau$ (see Fig. 3-3). Thus the reactor may become unsaturated before $t = \tau$; however, with the assumption of relatively small R_L made above, this exit from saturation will occur so close to $t = \tau$ that

negligible error will be introduced by assuming that the resetting action starts at $t = \tau$, the instant the supply voltage goes negative. If the rectifier operated as an independently controlled switch to open the load circuit during the reset half-cycle, then it would only be necessary to compute the flux change from saturation occurring during the length of time τ due to the reset voltage. However, the rectifier is an open circuit only when the instantaneous supply voltage is greater than the voltage $N_g \frac{d\phi}{dt}$. If this condition is not fulfilled, the rectifier unblocks; and with the low value of load resistance assumed previously, the rate of change of flux becomes

$$\frac{d\phi}{dt} = \frac{V_g}{N_g} \quad (3-14)$$

Thus, in computing the reset flux change $\Delta\phi$, the sensitivity of the rectifier to its terminal voltage must be taken into account.

The reset flux and hence the amplifier input-output characteristic will be computed and experimentally verified for two types of reset: constant current, and constant voltage with finite resistance. First, the analysis for constant-current reset will be completed in a fairly "exact" manner in which the solution is made graphically to account for the rectifier unblocking discussed in conjunction with Eq.(3-14) above. Second, because of mathematical difficulties involved in the "exact" solution, a simplified approximate solution will be made in which the rectifier unblocking is not accounted

for. After the result of the approximate solution is checked against the result for the "exact" solution, in the case of constant-current reset, the approximate solution will be extended to cover the case of constant-voltage reset with finite resistance. In this case, the relative reset circuit conductance for which maximum power gain occurs will be found, and the input-output characteristic will be normalized with respect to this quantity.

3.1.0 "Exact" Analysis, Constant-Current Reset

Before the reset flux $\Delta\varphi$ can be computed for the circuit of Fig. 3-1, the equations describing the reactor under reset conditions must be known. The mathematical representation of Chap. II in its most general form cannot be applied in a simple manner in this analysis; consequently, some simplification of the general representation is necessary. In Chap. II, it was found that a simple approximation worked well with the one-mil Orthonol core tested in that chapter. This simplified representation will be applied to the analysis in this section. When, by the methods of Chap. II, a different simplification of the general representation gives a better reactor description, then that representation can be applied to the analysis in a manner similar to the method to be used. Most practical reactors exhibit the same type of behavior; thus, in most cases, the performance of a particular reactor in a single-core magnetic-amplifier circuit can be obtained to a good degree of accuracy simply by specializing the constants in the results of this chapter.

In Chap. II, the one-mil Orthonol core used was found to be described by two equations of the form [see Eqs.(2-44 and (2-45)]:

$$\frac{dr}{dt} = K_1 K_2 \frac{a_o}{2} (H - H_c)^2 \quad (3-15)$$

$$\frac{d\phi}{dt} = 2B_s g(r) \frac{dr}{dt} \quad (3-16)$$

The form of the function $g(r)$ was not considered in Chap. II. Most reactor cores that are used in high-performance magnetic amplifiers exhibit nearly rectangular B-H loops under sinusoidal voltage excitation. This indicates that when the flux is driven from saturation to saturation sinusoidally, the exciting current remains essentially constant. Conversely, when the flux in one of these reactors is reversed by a current-pulse of constant amplitude, the resulting pulse of $d\phi/dt$ is very nearly sinusoidal. Consequently, for the "exact" analysis of this section the function $g(r)$ will be assumed sinusoidal, and the expression of Eq.(3-16) becomes:

$$\frac{d\phi}{dt} = \pi B_s A_c \sin \pi r \frac{dr}{dt} \quad (3-17)$$

where A_c is the cross-sectional area of the core. When a constant reset current I_r is applied to the reactor, simultaneous solution of Eqs.(3-15) and (3-17) yields the rate of change of flux:

$$\frac{d\phi}{dt} = \frac{\pi}{2} B_s A_c K_1 K_2 a_o (H - H_c)^2 \sin [\pi K_1 K_2 a_o (H - H_c)^2 t] \quad (3-18)$$

with the definition

$$H = \frac{N_r I_r}{\ell_m} \quad (3-19)$$

where ℓ_m is the mean length of the magnetic path.

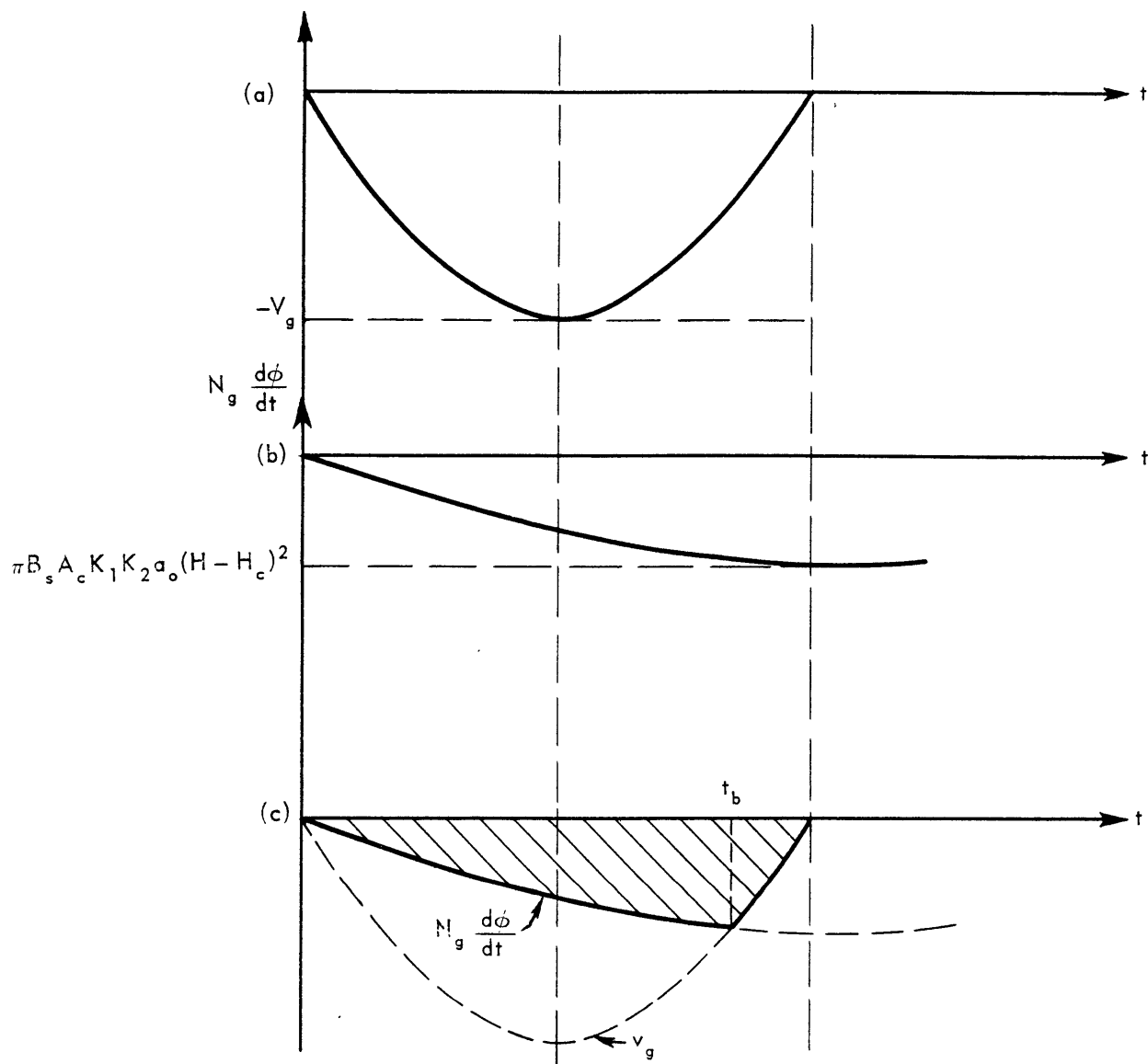


Fig. 3.4. Reset wave forms

3.1.1 Calculation of Reset Flux

During the resetting period the supply voltage, which is assumed sinusoidal,

$$v_g = V_g \sin \omega t, \quad (3-20)$$

has the waveform shown in Fig. 3-4a. For a particular applied resetting field H , the rate of change of flux, with the load circuit held open, is shown in Fig. 3-4b. The rectifier remains blocked or open, however, only as long as the magnitude of the instantaneous supply voltage is greater than the reflected rate of change of flux $N_g (d\varphi/dt)$. When the voltage $N_g (d\varphi/dt)$ tends to become larger than the supply voltage, the rectifier conducts; and in the presence of the low resistance of the load circuit, the rate of change of flux is determined by the supply voltage. Thus the rate of change of flux during the resetting period is that shown in Fig. 3-4c, and the cross-hatched area represents $N_g \Delta\varphi$. When this reset flux is related to the applied field H , the input-output characteristic of the amplifier can be obtained by substituting the result in Eq.(3-13) for normal reactor excitation.

In order to evaluate the cross-hatched area of Fig. 3-4c, the time t_b at which the rectifier unblocks must be known. With the functions being used, this intersection can be found only graphically; however, for any particular level of v_g , only one set of solutions is necessary. In Appendix II, a set of solutions is obtained for the case of normal excitation.

3.1.2 Calculation of Normalized Input-Output Characteristic

The load current as a function of the reset flux for normal excitation is given in Eq.(3-13). In Appendix II, the reset flux is substituted into this equation to obtain the normalized input-output characteristic shown plotted as the theoretical curve in Fig. 3-6. The input variable for the plot is H_e/H_{em} , where H_e is the effective applied field, which is given by:

$$H_e = (H - H_c) \quad (3-21)$$

and H_{em} is the effective applied field for minimum output current as expressed in Eq.(II-7) of Appendix II:

$$H_{em} = \sqrt{\frac{2\omega}{\pi K_1 K_2 a_0}} \quad (3-22)$$

3.1.3 Experimental Verification of "Exact" Analysis

Also shown in Fig. 3-6 are experimental points obtained using the experimental arrangement shown in Fig. 3-7. The values of H_{em} for the excitation frequencies which were necessary for normalization of the experimental curves are given in Table II-2 of Appendix II. The constant describing the reactor core was obtained from the constant-current switching characteristic plotted in Fig. 2-17 of Chap. II.

It is evident, from a comparison of the theoretical and experimental results shown plotted in Fig. 3-6, that although the agreement is not exact, the prediction is relatively invariant with frequency. The error at high levels of output is caused principally by the neglect of the flux change after saturation in the mathematical representation. The error at

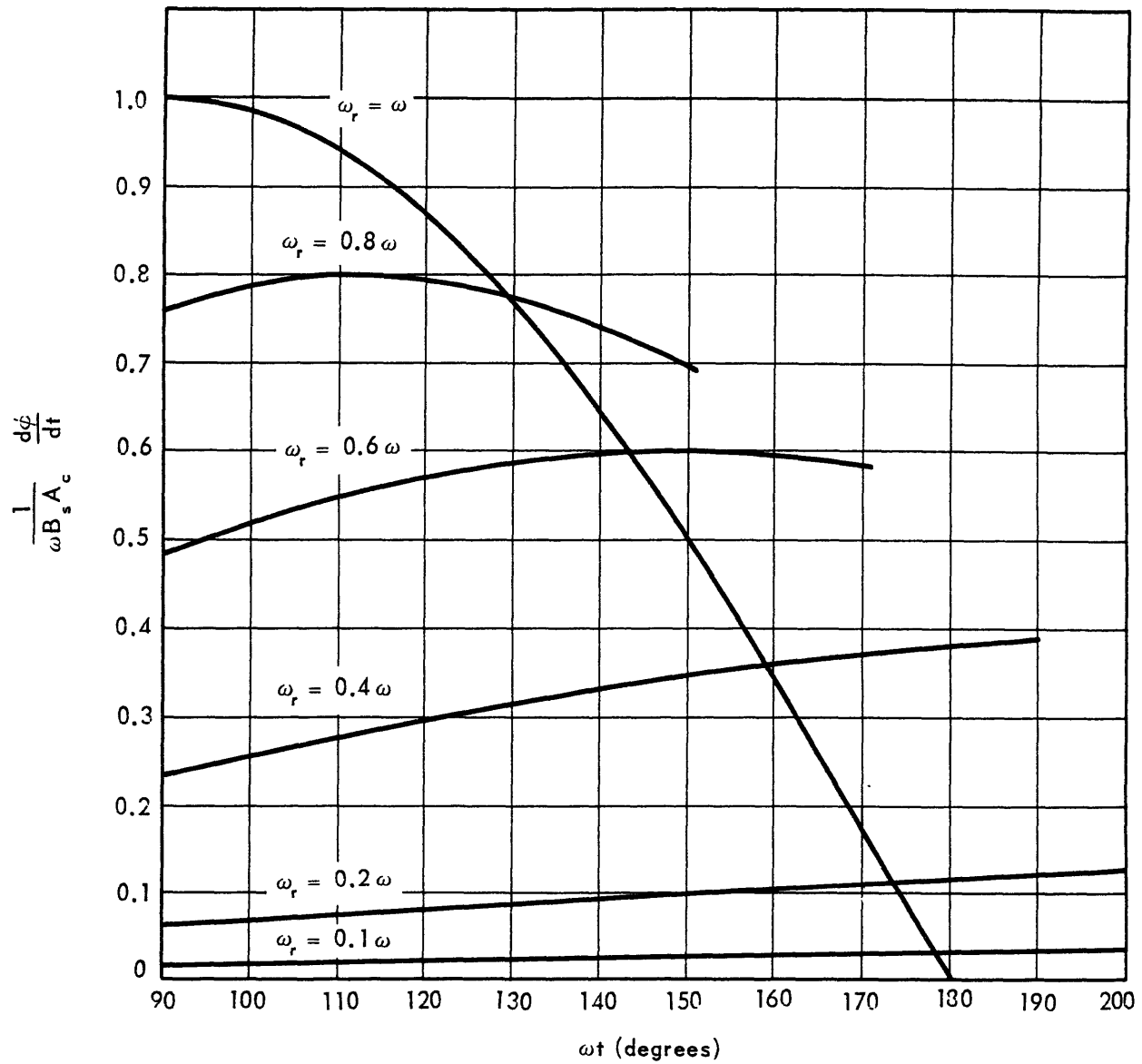


Fig. 3.5. Normalized rate of change of flux as a function of ωt for various values of ω_r

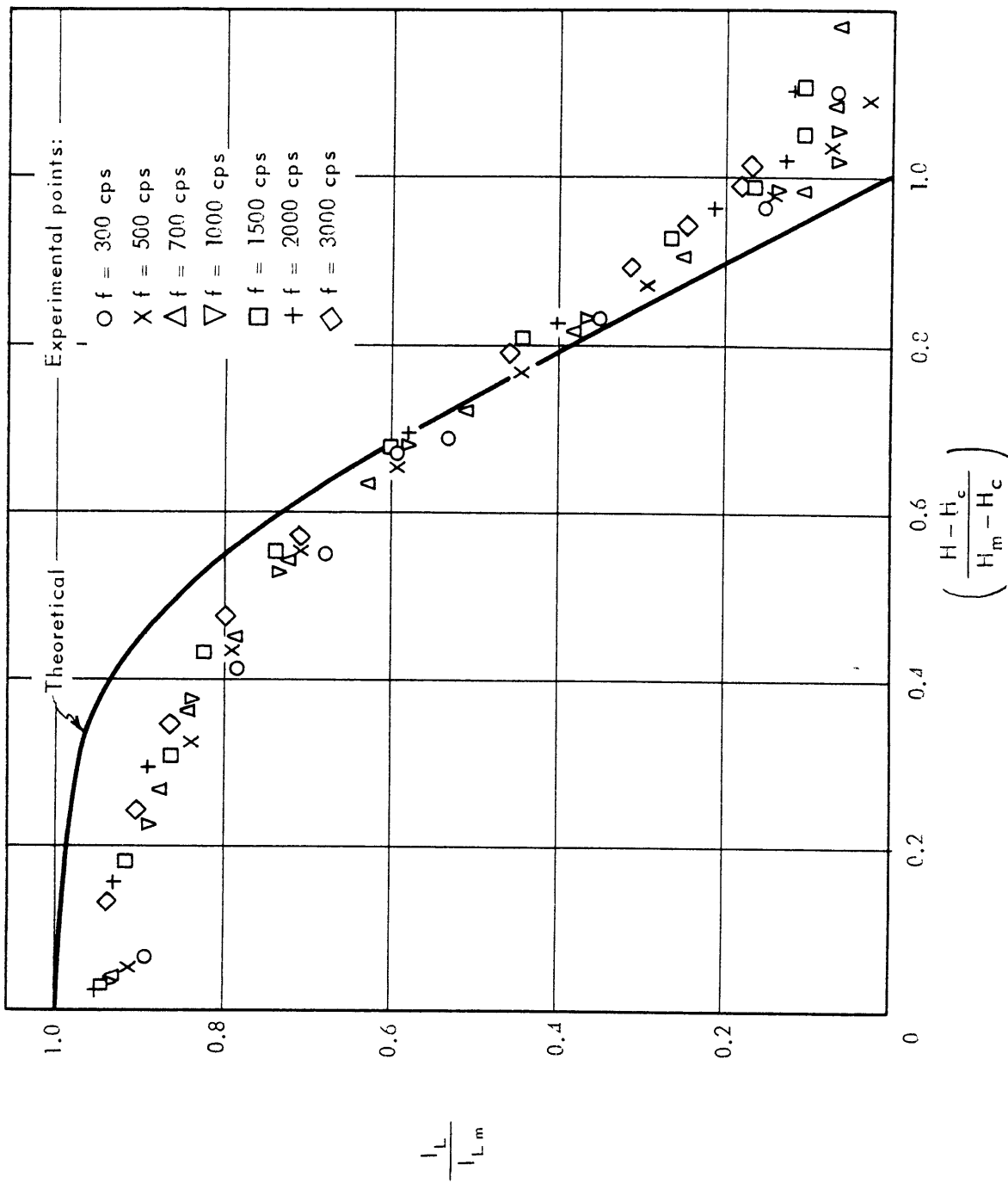
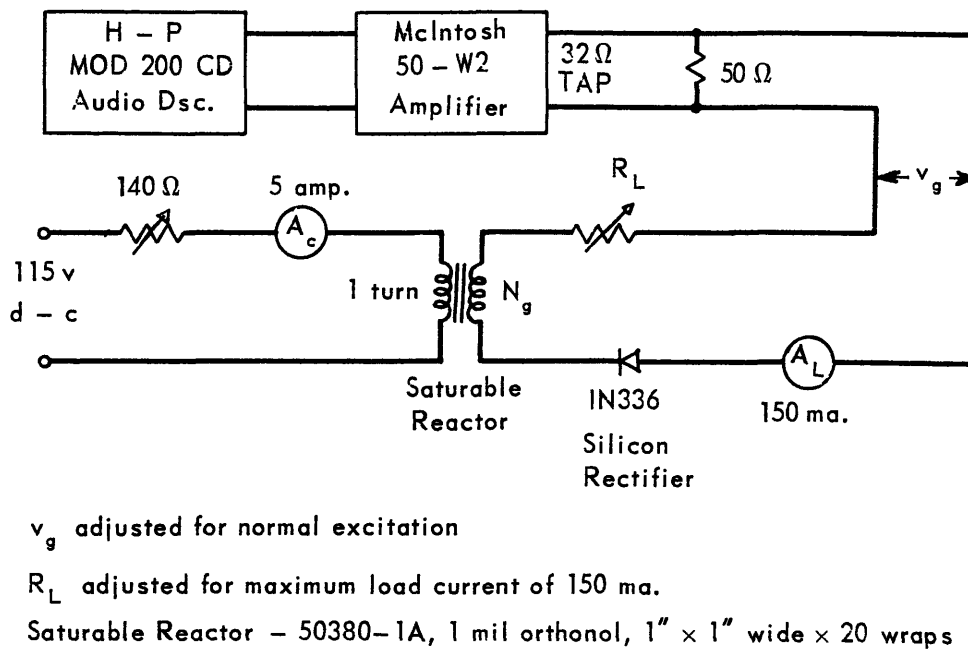


Fig. 3.6. Normalized input - output characteristic of the amplifier.



Supply Frequency (cps)	300	500	700	1000	1500	2000	3000
N_g (turns)	800	800	550	400	250	200	150

Fig. 3.7. Experimental arrangement for input-output characteristics with constant current reset and variable frequency

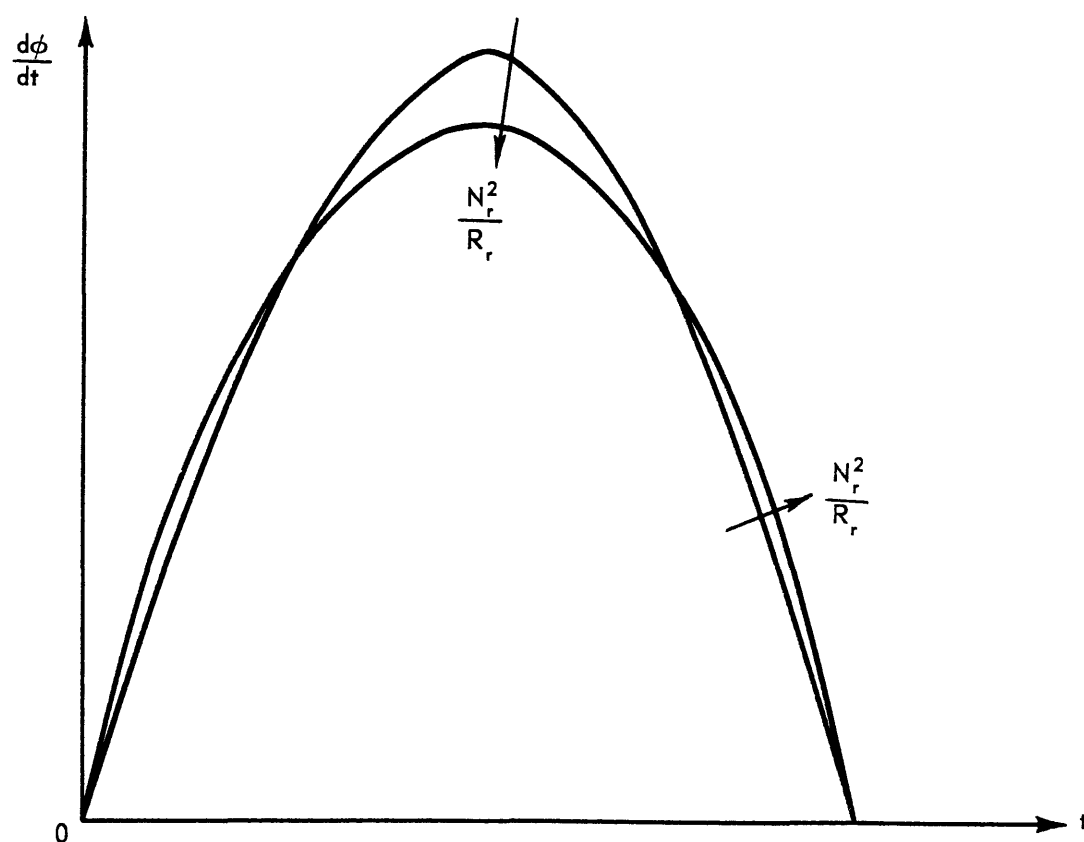


Fig. 3.8. Illustrating the flattening of the reset waveform with increasing reset $\frac{N^2}{R}$

low levels of output is caused by the neglect of the exciting current during the gating half-cycle in the analysis. Additional error is introduced by the departure of the function $g(r)$ in the mathematical representation from a pure sinusoid, as well as by the accuracy with which the representation describes the reactor with respect to applied field, as indicated by the straight-line approximation of Fig. 2-17 of Chap. II. The analysis predicts quite accurately the field at which minimum output occurs (see Fig. 3-6). The predicted slope of the transfer characteristic is approximately 25 per cent higher than the measured slopes of the experimental curves at half of full output.

3.2.0 Approximate Analysis

The analysis of the preceding section, while being fairly exact with respect to the details of waveforms, is complicated by the necessity for graphical solutions. In addition, this analysis is limited to the constant-current reset case, which is of little practical interest. An attempt to generalize that analysis to include the case of finite reset resistance would require machine computation for reasonably rapid solution. Although such a process is not unreasonable, it is the purpose here to obtain simple expressions which will have engineering applicability. Consequently, some complicating features of the preceding analysis will be removed in order to obtain a simple approximate analysis of the single-core self-saturating magnetic amplifier.

The mathematical representation to be used in the approximate analysis is the form obtained in Chap. II for the one-mil

Orthonol reactor and given as Eqs.(3-15) and (3-16):

$$\frac{dr}{dt} = K_1 K_2 \frac{a_o}{2} (H - H_c)^2 \quad (3-15)$$

$$\frac{d\varphi}{dt} = 2B_s g(r) \frac{dr}{dt} \quad (3-16)$$

The part of this representation which complicates the analysis is the function $g(r)$. In the "exact" analysis of Section 3.1.0, this function was assumed to be a sinusoid, an assumption well founded on experimental evidence. Since most practical power supplies are sinusoidal, the function $g(r)$ has the same waveform as the power-supply voltage.

The power supply to be used in the experimental verification of this analysis will be sinusoidal; in the analysis, however, the supply voltage will be assumed to have a square waveform of period 2τ and amplitude V_g . The function $g(r)$ will also be assumed to be a square wave, and it will have the definition:

$$g(r) = \begin{cases} A_c & , \text{ for } 0 < r < 1 \\ 0 & , \text{ elsewhere} \end{cases} \quad (3-23)$$

Thus, in the approximate analysis, the function $g(r)$ has the same shape as the power-supply waveform assumed in the analysis. This is done to remove some of the errors introduced by assuming a square wave for $g(r)$. Reference to the "exact" analysis of Section 3.1.0 and to Fig. 3-5 shows that, at minimum output, full control of the reactor flux is obtained with no rectifier unblocking. This is a direct result of the assumption that $g(r)$ and the supply voltage have the same waveform. Thus the assumption that both have the same waveform in the approximate analysis makes the analysis correct

at one point, minimum output, and thereby the error occurring at other points is reduced. With the function $g(r)$ defined by Eq.(3-23), Eqs.(3-15) and (3-16) can be combined to yield a single equation which describes the reactor under resetting conditions:

$$\frac{d\varphi}{dt} = B_s A_c K_1 K_2 a_o (H - H_c)^2, \text{ for } -B_s A_c < \varphi < B_s A_c \quad (3-24)$$

The foregoing simplified representation leads to two major sources of error in the magnetic-amplifier analysis. When the reset voltage V_r is a constant, no rectifier unblocking occurs during the resetting period, because the square-wave supply voltage keeps the rectifier blocked throughout the resetting period. When the relative resistance (N^2/R) of the control circuit becomes appreciable, the waveform of the $d\varphi/dt$ in the actual reactor due to the reset circuit becomes flattened, as shown in Fig. 3-8. With this flattening of the resetting waveform, the load rectifier will begin to unblock at the start of the resetting period at high levels of reset flux, thereby reducing the amount of reset flux obtainable at a given level of resetting signal. In the approximate representation given by Eq.(3-24), this waveform change with reset N^2/R is neglected; consequently, the expected error should increase with reset N^2/R . In spite of these errors, the $g(r)$ assumed in Eq.(3-23) leads to the simplest expressions describing the reactor which still retain the necessary variation of reset voltage with applied field.

The constant of the core, $K_1 K_2 a_o$, is best determined from constant-current switching tests. The assumption of a

square wave for $g(r)$ means that the constant-current switching waveform is being replaced by its average value over the switching time. Thus, if the constant is determined from a plot of the peak switching voltage, as it is in Fig. 2-17 of Chap. II, it must be multiplied by the ratio of average value to peak value of the switching waveform, before it can be used in the approximate analysis. Most reactor cores used in high-performance magnetic amplifiers have very nearly rectangular B-H loops for sinusoidal voltage excitation; thus their constant current switching waveforms are very nearly sinusoidal. Consequently, if the core constant determined from a plot of peak switching voltage (see Fig. 2-17 of Chap. II) is multiplied by $2/\pi$, the resulting constant will give good results in the approximate analysis. In essence, the approximation used considers that the switching time for a given applied field is the same for the approximate representation and for the "exact" representation. This allows an accurate prediction of the applied field required for minimum output.

3.2.1 Constant-Current Reset

In order to obtain a measure of the accuracy of the approximate analysis, the magnetic amplifier of Fig. 3-1 will be analyzed with constant-current reset and the approximate reactor representation of Eq.(3-24). The result of this analysis will be compared with the results of the "exact" analysis and with the experimental results given previously in Fig.3-6.

The supply voltage has been assumed a square wave; consequently, the rectifier remains blocked throughout the reset

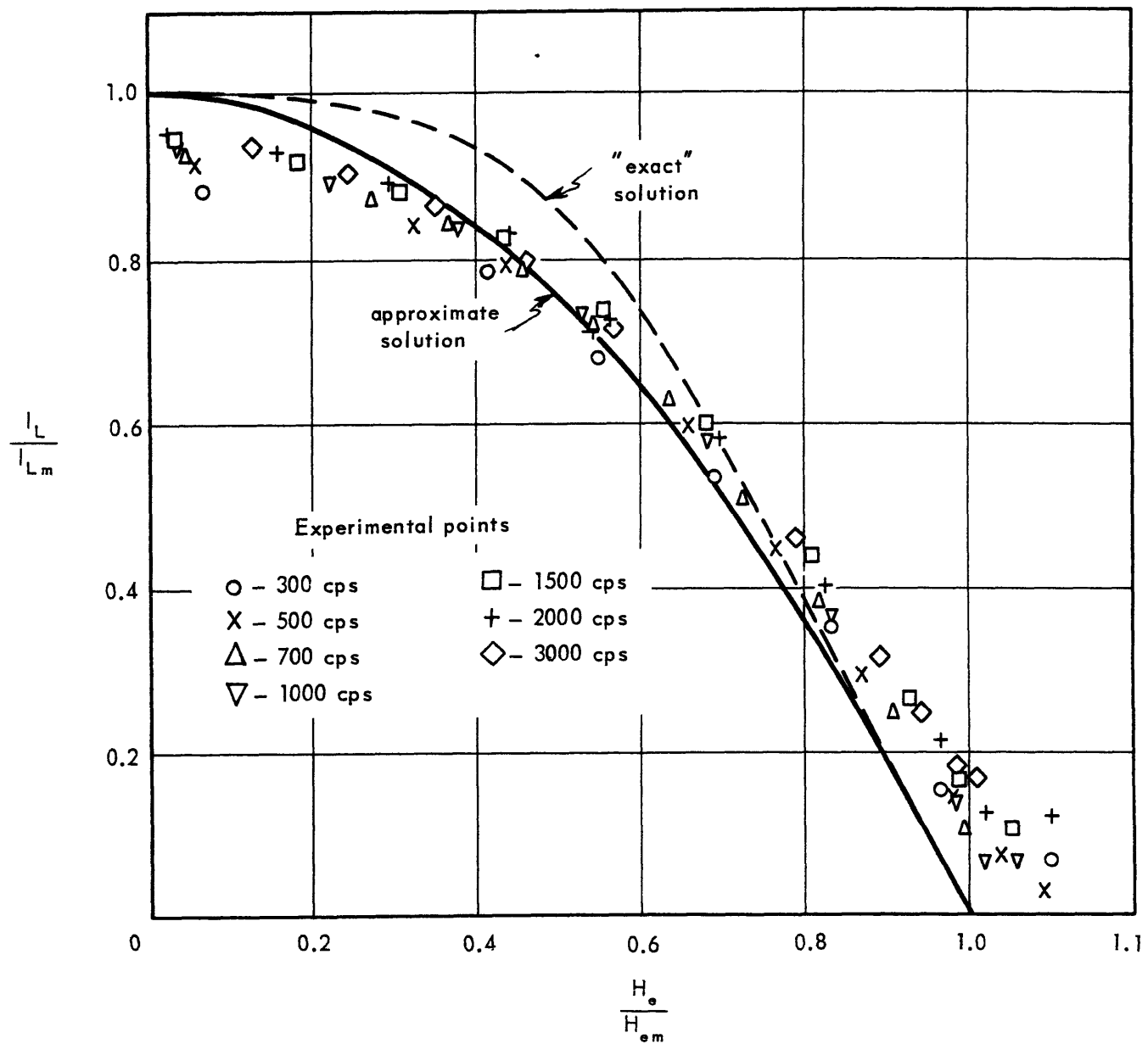


Fig. 3.9. Comparison of theoretical and experimental input-output characteristics for constant-current reset, approximate analysis

interval. With constant-current reset, the rate of change of flux during the resetting interval is constant and is given by Eq.(3-24); therefore the reset flux is given simply by

$$\Delta\varphi = K_3 \tau H_e^2 \quad (3-25)$$

where

$$K_3 = B_s A_c K_1 K_2 a_0$$

$$H_e = H - H_c$$

$$H = \frac{N_r I_r}{l_m}$$

The effective applied field H_{em} necessary to produce minimum output for normal reactor excitation is given by

$$H_{em} = \sqrt{\frac{2B_s A_c}{K_3 \tau}} \quad (3-26)$$

which reduces identically to Eq.(3-22) in the "exact" analysis. Thus Eq.(3-25) can be normalized to:

$$\frac{\Delta\varphi}{2B_s A_c} = \left(\frac{H_e}{H_{em}} \right)^2 \quad (3-27)$$

Substitution of Eq.(3-27) into the magnetic-amplifier output equation for normal reactor excitation, Eq.(3-13), yields the normalized input-output relation resulting from the approximate analysis:

$$\frac{I_L}{I_{Lm}} = 1 - \left(\frac{H_e}{H_{em}} \right)^2 \quad (3-28)$$

This relation is shown plotted in Fig. 3-9, along with the theoretical curve derived by the "exact" method of Section 3.1.0 and the experimental points previously plotted in Fig. 3-6. In Fig. 3-9, the approximate solution fits the experimental points better than the "exact" solution does; however,

this is merely coincidence. The error between the "exact" solution and the experimental points at high levels of output is principally due to the additional flux change after saturation, a phenomenon which occurs during the gating period. The error between the "exact" and the approximate solutions at high output levels is a consequence of the different waveforms assumed in the two cases during the reset half-cycle. Thus, although the added accuracy of the approximate solution is just coincidence, it will occur with most reactors. At any rate, the accuracy of the approximate method, as indicated by the results plotted in Fig. 3-9, is such that an extension of the approximate analysis to the case of finite reset resistance seems justified.

3.2.2 Constant-Voltage Reset With Finite Resistance

The circuit under consideration is shown schematically in Fig. 3-1, and the reactor is described during reset by Eq.(3-24). During the resetting period, the supply voltage (assumed to be a square wave) keeps the load-circuit rectifier blocked; consequently, during reset the circuit of Fig. 3-1 is described by the equation

$$\frac{N_r V_r}{\lambda_m R_r} = H + \frac{N_r^2}{\lambda_m R_r} \frac{d\phi}{dt} \quad (3-29)$$

where

$$H = \frac{N_r i_r}{\lambda_m}$$

Simultaneous solution of Eqs.(3-24) and (3-29) for the rate of change of flux yields:

$$\frac{d\varphi}{dt} = K_3 \left[\frac{-1 + \sqrt{1 + 4K_3 \frac{N_r^2}{\lambda_m R_r} H_e}}{2 \frac{N_r^2}{\lambda_m R_r} K_3} \right]^2 \quad (3-30)$$

where

$$K_3 = B_s A_c K_1 K_2 a_o$$

and the average effective applied resetting field H_e is given by

$$H_e = \frac{N_r V_r}{\lambda_m R_r} - H_c \quad (3-31)$$

The expression of Eq.(3-30) is a constant; thus the reset flux $\Delta\varphi$ occurring during the resetting period is simply:

$$\Delta\varphi = K_3 \tau \left[\frac{-1 + \sqrt{1 + 4K_3 \frac{N_r^2}{\lambda_m R_r} H_e}}{2 K_3 \frac{N_r^2}{\lambda_m R_r}} \right]^2 \quad (3-32)$$

When the reset flux of Eq.(3-32) is substituted into the magnetic-amplifier equation for normal reactor excitation, Eq.(3-13), there results:

$$\frac{I_L}{I_{Lm}} = 1 - \frac{K_3 \tau}{2 B_s A_c} \left[\frac{-1 + \sqrt{1 + 4K_3 \frac{N_r^2}{\lambda_m R_r} H_e}}{2 K_3 \frac{N_r^2}{\lambda_m R_r}} \right]^2 \quad (3-33)$$

For any particular reactor K_3 , supply frequency $\frac{1}{2\tau}$, and relative reset circuit resistance N_r^2/R_r , the input-output characteristic could be plotted; however, more general information can be obtained by normalizing this expression with respect to the average effective applied field necessary for

minimum output, and with respect to the relative reset-circuit resistance for maximum power gain. Before this normalization is done in Section 3.2.4, the value of relative reset resistance for maximum power gain will be derived.

3.2.3 Maximization of the Power Gain

Before the power gain can be maximized, several definitions must be made. First, only incremental input and output quantities will be considered. This type of treatment is consistent with methods used with other types of amplifiers.

Since the input-output characteristic is nonlinear, the incremental gain is not constant. Consequently, to fix ideas and define a basis for comparison of different circuits, the incremental gain will always be considered for half of full output: i.e., $\frac{I_L}{I_{Lm}} = 0.5$. The power gain is defined as

$$K_p = \left(\frac{\partial I_L}{\partial I_r} \right)_L^{\frac{1}{2}} \frac{R_L}{2} \quad (3-34)$$

where I_L and I_r are average quantities and the partial derivative is taken at $(I_L/I_{Lm}) = 0.5$. Equation (3-34) does not give the true power gain; however, since the waveforms do not vary drastically among magnetic-amplifier circuits of the same type, the power gain defined in Eq.(3-34) gives a good index for comparison among amplifiers of the same type.

Starting with Eq.(3-33), the power gain defined by Eq. (3-34) is derived in Appendix III, and is:

$$K_p = \frac{\frac{K_3 B_s A_c}{\tau} \frac{N_g^2}{L_m R_L} G}{\left[2K_3 G \sqrt{\frac{B_s A_c}{K_3 \tau}} + 1 \right]^2} \quad (3-35)$$

with the definition

$$G = \frac{N_r^2}{\lambda_m R_r} \quad (3-36)$$

The value of G_m for which maximum power gain occurs is found in Appendix III to be:

$$G_m = \frac{1}{2K_3} \sqrt{\frac{K_3}{B_s A_c}} \quad (3-37)$$

The resulting maximum power gain K_{pm} is:

$$K_{pm} = \frac{1}{8} \frac{N_g^2}{\lambda_m R_L} \sqrt{\frac{K_3 B_s A_c}{\tau}} \quad (3-38)$$

Note, from Eq.(3-37), that the value of N_r^2/R_r for maximum power gain with a given reactor varies inversely with the square root of supply frequency. This means that although a control source may appear to have relatively high resistance at a low supply frequency, the same resistance will appear relatively lower at a higher supply frequency. It is evident from Eq.(3-38), that the maximum power gain varies directly with the square root of supply frequency. In this case, the supply voltage must vary linearly with frequency to maintain normal reactor excitation with the same value of N_g .

When the ratio γ is defined as:

$$\gamma = \frac{G}{G_m} = 2K_3 \sqrt{\frac{B_s A_c}{K_3 \tau}} \frac{N_r^2}{\lambda_m R_r} \quad (3-39)$$

the power gain of Eq.(3-35) can be normalized to:

$$\frac{K_p}{K_{pm}} = \frac{4\gamma}{(\gamma + 1)^2} \quad (3-40)$$

The normalized power gain of Eq.(3-40) is plotted as a function of γ in Fig. 3-10. Also shown in this plot are experimental points obtained using the experimental arrangement of Fig. 3-11. Note that, while the theory yields an optimistic prediction of the level of the power gain, the location of the peak-power gain and the shape of the variation with respect to γ are predicted very well. Thus the expression of Eq.(3-37) can be used to accurately predict the reset circuit N^2/R necessary for maximum power gain, and Eq.(3-38) can be used to predict the maximum power gain within 25 percent of the actual power gain.

3.2.4 Normalized Input-Output Characteristics, Finite Resistance

In order to obtain a simplified and orderly method of describing the input-output characteristic of a magnetic amplifier with finite reset resistance, the expression of Eq. (3-33) is normalized, in Appendix IV, to the result:

$$\frac{I_L}{I_{Lm}} = 1 - \frac{1}{2} \left[\frac{-1 + \sqrt{1 + [(\sqrt{2}\gamma + 1)^2 - 1] \frac{H_e}{H_{em}}}}{\gamma} \right]^2 \quad (3-41)$$

The ratio γ is the relative reset-circuit conductance per unit mean length normalized with respect to the value that gives maximum power gain at half output. The ratio γ is defined by Eq.(3-39). The quantity H_e is the average effective applied field, and was defined previously in Eq.(3-31). The quantity H_{em} is the average effective applied field necessary for minimum output, and is given by Eq.(IV-8) of Appendix IV as:

$$H_{em} = \sqrt{\frac{B_s A_c}{K_3 \tau}} \frac{(\sqrt{2}\gamma + 1)^2 - 1}{2\gamma} \quad (3-42)$$

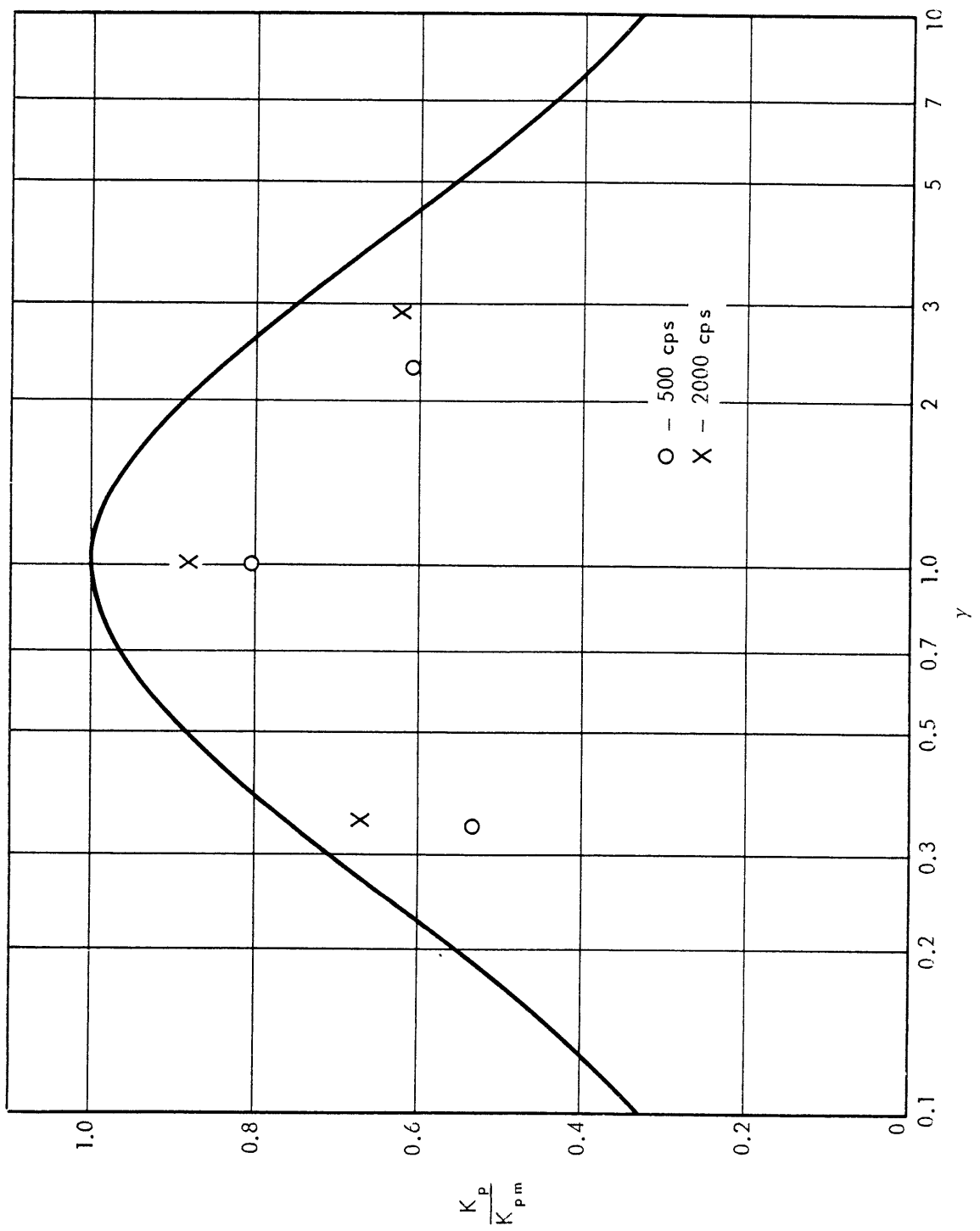
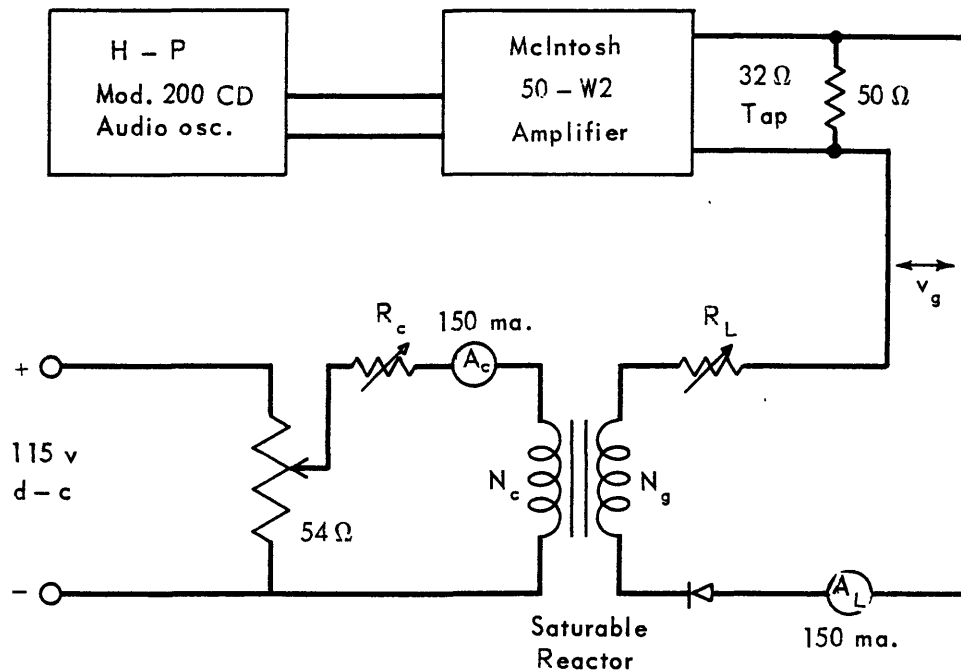


Fig. 3.10. Theoretical and experimental power gain as a function of the relative noise $\frac{N^2}{R}$



v_g adjusted for normal excitation

R_L adjusted for maximum load current of 150 ma.

Saturable Reactor - 50380-1A, 1 mil Orthonol, 1" ID x 1" wide x 20 wraps

Frequency (cps)	R_e (Ω)						N_c (T)
	N_g (T)	R_L (Ω)	$\gamma = 1$	$\gamma = 0.343$	$\gamma = 2.29$	$\gamma = 2.86$	
500	800	114	356	1067	160		80
2000	200	129	732	2133		256	80

Fig. 3.11. Experimental arrangement for input-output characteristics with variable reset $\frac{N^2}{R}$ and variable frequency

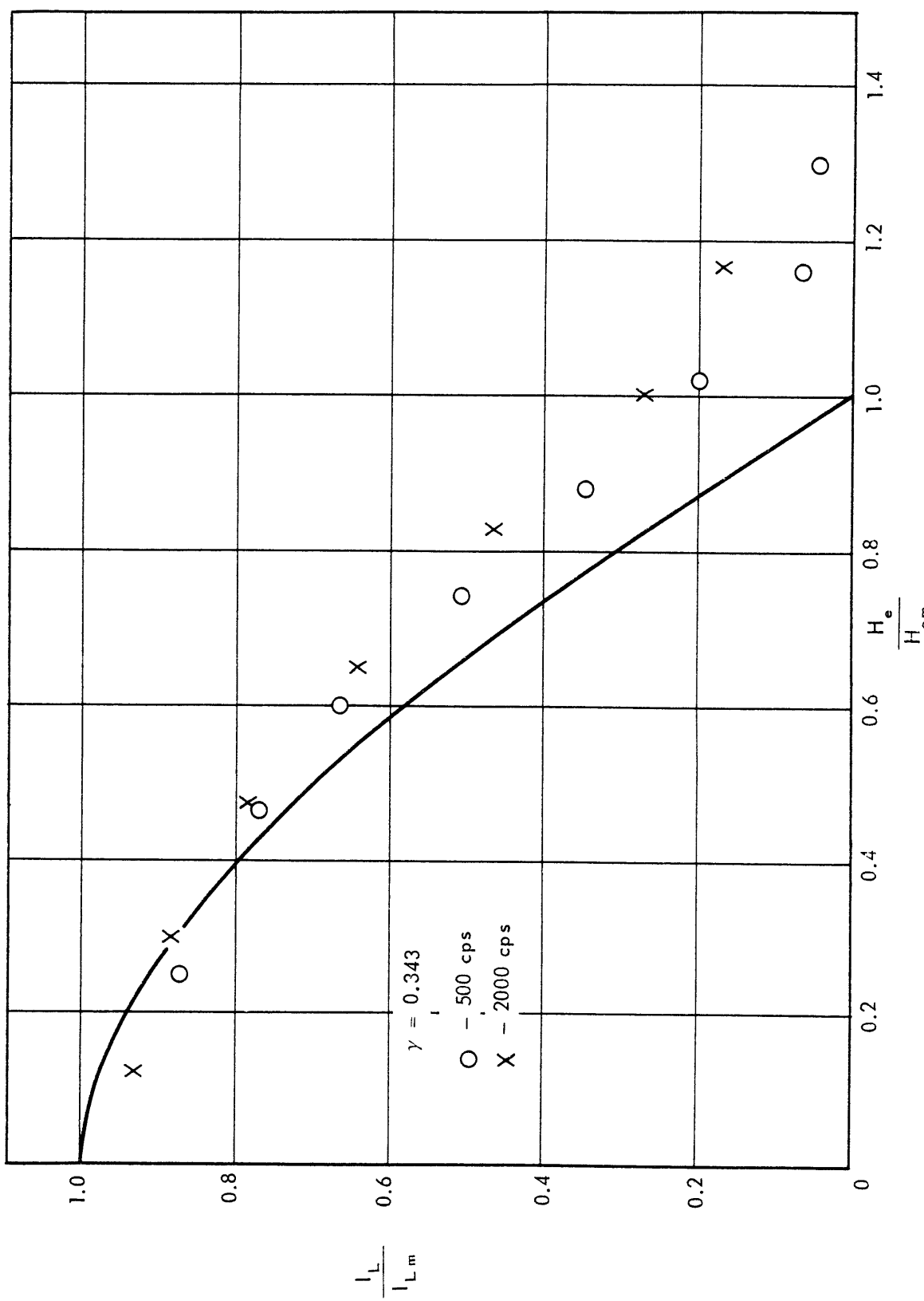


Fig. 3.12. Theoretical and experimental input-output characteristics for $\gamma = 0.343$.

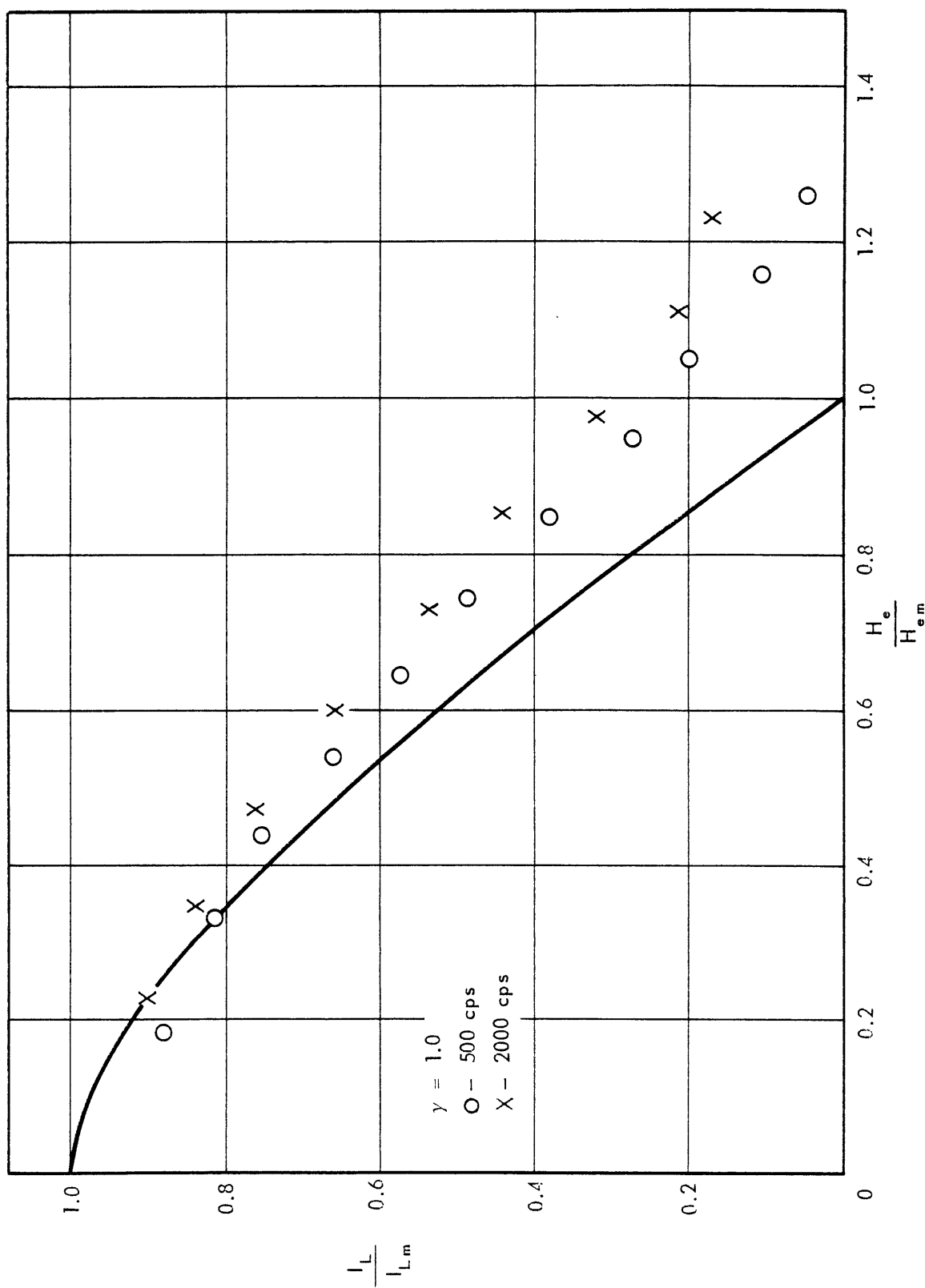


Fig. 3.13. Theoretical and experimental input-output characteristics for $\gamma = 1.0$

The expression of Eq.(3-41) is independent of frequency; thus a family of input-output characteristics could be plotted with γ as parameter, and then the curves could be used to predict amplifier behavior by the substitution of reactor and circuit constants into the expressions of Eqs.(3-39) and (3-42).

The expression of Eq.(3-41) is plotted for two values of γ as the solid curves of Figs. 3-12 and 3-13. The experimental points on the plots were obtained by the use of the experimental arrangement of Fig. 3-11. The constants necessary for normalizing the experimental points are calculated in Appendix IV. The experimental points of Figs. 3-12 and 3-13 were used to obtain four of the experimental points plotted in the normalized power-gain plot of Fig. 3-10. In Figs. 3-12 and 3-13, the prediction is fairly good and relatively independent of supply frequency. The predicted gain in all cases is too high; the error for $\gamma = 1.0$ is approximately 35 per cent. The principal source of this error is the change in reset rate of change of flux waveform with γ , which is neglected in the approximate analysis. This error shows up mostly at low output where the change in waveform causes appreciable rectifier unblocking and hence reduced gain in the actual amplifier. Further evidence of this unblocking is the larger applied signal necessary to produce minimum output than is predicted theoretically. This error in signal required for minimum output increases with γ , as shown by a comparison of the experimental points of Figs. 3-12 and 3-13.

The normalized result of the approximate analysis provides a useful answer to the long-debated question of what

determines whether the control or reset circuit resistance in a magnetic amplifier is high or low: i.e., whether the reset source acts as a current source or as a voltage source. When the normalized reset conductance γ is unity, maximum power gain results, and the reset source is neither a voltage source nor a current source, but the input impedance of the reactor is matched to the external resistances in the circuit. For values of γ greater than unity, the reactor input impedance is greater than the external circuit resistance, and hence the reset source behaves more like a voltage source. On the other hand, for values of γ less than unity, the reactor input impedance is less than the external circuit resistance; therefore, the reset source behaves more like a current source. This discussion is illustrated best by a consideration of the slope of the normalized input-output characteristic of Eq.(3-41) at half output. When the normalized current gain K_i is defined as

$$K_i = \sqrt{\frac{B_s A_c}{K_3 \tau}} \left[\frac{\partial \left(\frac{I_L}{I_{Lm}} \right)}{\partial H_e} \right] \frac{I_L}{I_{Lm}} = 0.5 \quad (3-43)$$

then, from Eq.(III-5) of Appendix III, this gain becomes:

$$K_i = \frac{1}{\gamma + 1} \quad (3-44)$$

This expression is plotted in Fig. 3-14. For very small values of γ , the curve approaches the asymptote of current control; while for very large values of γ , the curve approaches the asymptote for voltage control. As indicated by Eq.(3-39),

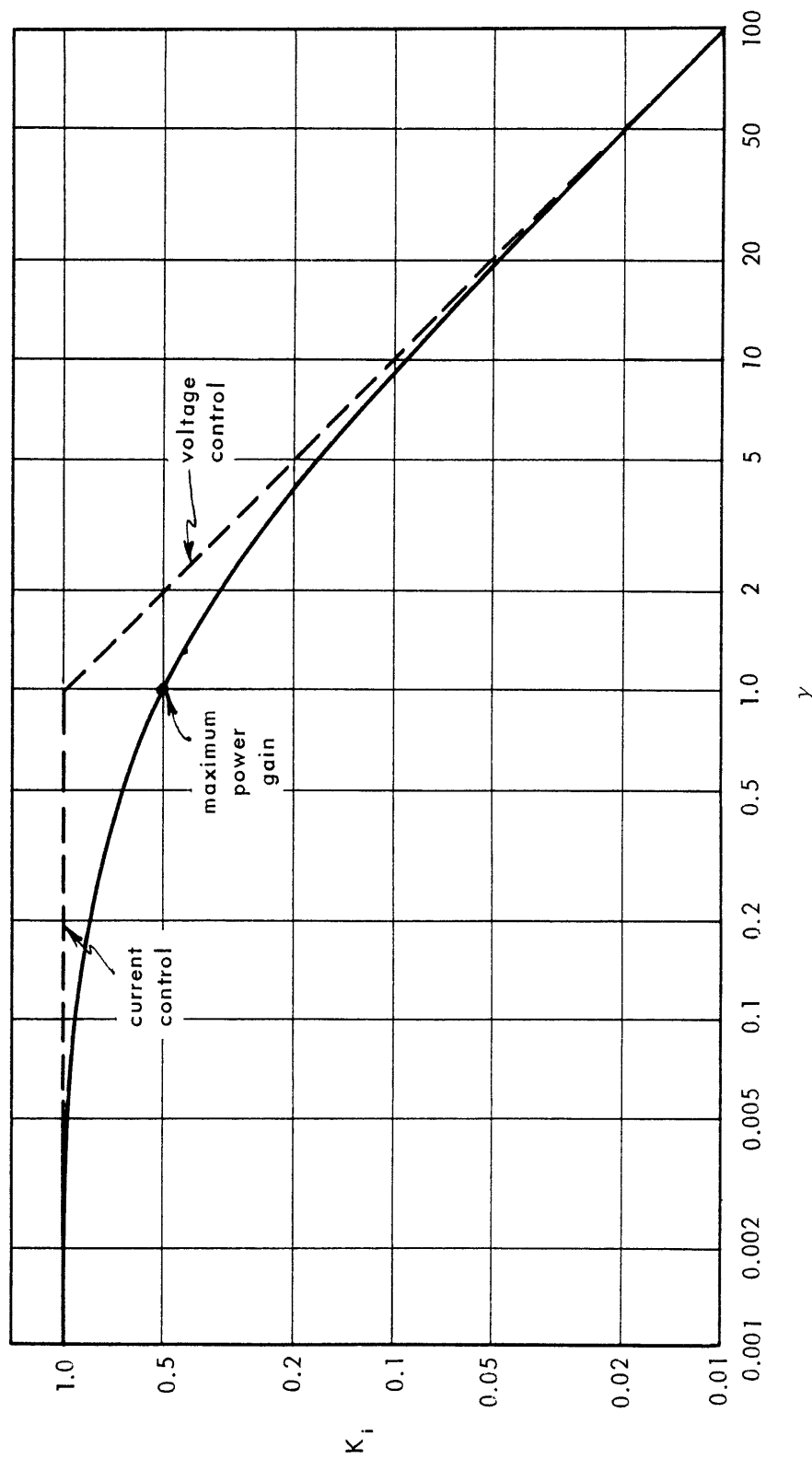


Fig. 3.14. Normalized current gain as a function of relative reset conductance

a knowledge of the reactor constants and supply frequency will allow calculation of the relative reset conductance per unit mean length for any type of control indicated in the plot of Fig. 3-14.

In the approximate analysis, the reset waveform distortion and rectifier unblocking that were neglected make the error in the analysis increase with increasing γ . Thus the accuracy of the plot of Fig. 3-14 decreases with increasing γ .

Chapter IV

RESULTS AND CONCLUSIONS

4.0.0 Introduction

In brief summary, the results of this research are the following: A mathematical representation for a polycrystalline, thin-tape, ferromagnetic metal is derived for the operating conditions found during flux resetting in a magnetic amplifier. The starting point for the derivation of the representation is the dynamic behavior of ferromagnetic single crystals as reported in the literature. All mobile domain walls are assumed to have the same equation of motion on the average, but each domain wall is assumed to have a different starting field. The general representation obtained in this manner is not checked experimentally; however, two simplified versions which are suitable for magnetic-amplifier analysis are checked experimentally. The simplified reactor representation contains constants and a function which could be determined from material properties if sufficient detailed information were available, but such information is not available at present. Consequently, the constants and function of the mathematical representation must be determined by an empirical fit to a suitable terminal characteristic of the reactor. As pointed out in Chap. I, this, in essence, has been the method used in determining reactor characteristics for magnetic-amplifier analyses in the past. The reasons the representation derived in this research represents an improvement are: first, the new mathematical representation is more

general than those used in the past, in that it accounts - in at least an approximate way - for the processes believed to be active in a ferromagnetic material during a flux change; second, being more general, the representation requires a more descriptive terminal characteristic than a normal magnetization curve or symmetrical hysteresis loop for the determination of the constants and function. The terminal characteristic used in this research is a constant-current switching characteristic and a typical switching waveform. The particular switching characteristic used here is a plot of peak switching voltage as a function of effective applied field, as shown in Fig. 2-17.

As an example of the application of the reactor representation to magnetic-amplifier analysis, the simplified representation is applied to the analysis of a single-core, self-saturating magnetic amplifier with constant reset voltage and variable reset resistance. The results of the analysis are compared with experimental results, and indicate that, with the reactor representation derived in this research, reasonably accurate prediction of magnetic-amplifier characteristics over a wide range of supply frequency and reset resistance is obtained. An additional result of importance is the derivation of the relative reset resistance necessary for maximum power gain, and the calculation of the maximum power gain for a particular reactor with specified gate circuit constants. Although some analyses have been made in the past for a single supply frequency and for the limiting cases of high reset resistance (current-source control) and low reset resistance

(voltage control), no analyses have been reported in the literature in which an independently determined reactor representation has been used to predict magnetic-amplifier characteristics simultaneously over a wide frequency range and over the range of reset resistances from current to voltage control. In fact, the results of this research are used to define, in terms of reactor and circuit constants, the regions of current and voltage control. The definition of these regions has been the subject of much discussion in the past, and no analytical definition is available in the literature.

The reactor representation which was used in the magnetic amplifier analysis was simplified with reference to the characteristics of a one-mil Orthonol* reactor. Most of the reactor materials, such as Orthonol and Permalloy in the tape thicknesses (one, two, and four mil) normally used in magnetic amplifiers, behave in approximately the same manner over the range of applied fields found in magnetic amplifiers operating at normal power frequencies (60 cps to 3000 cps). Thus the analysis is useful in describing magnetic-amplifier characteristics with other reactors. The degree of accuracy is, of course, governed by how well the reactor representation used fits the reactor under consideration over the range of operating conditions of interest. It is pointed out that the application of the techniques developed here to single-core magnetic-amplifier circuits with other than constant

* See Table I, Chap. II.

voltage control, and to multi-core magnetic amplifiers with any form of control voltage, will require further analytical work.

In the following sections, the results of the several parts of this research will be given, along with the essential steps leading to the results, along with important conclusions to be drawn from the results. The limitations of the techniques will be pointed out. Suggested topics for future work to strengthen and extend the concepts used here will be given, with some discussion.

4.1.0 The Mathematical Representation for a Reactor

The derivation of the mathematical representation for the reactor in Chap. II is based on the following steps. First, the form of the equations governing the dynamics of a single-domain wall in an arbitrarily shaped, single-crystal specimen is determined from a consideration of the processes (eddy-current damping and spin-relaxation damping) that impede domain wall motion, and of the dynamics of domain wall motion in simplified crystal shapes. The form of these equations is given in Eqs.(2-12) and (2-16):

$$f(\bar{\delta}) \frac{d\bar{\delta}}{dt} = K_1 (H - H_s) \quad (2-12)$$

$$\frac{d\varphi_1}{dt} = 2B_s g'(\bar{\delta}) \frac{d\bar{\delta}}{dt} \quad (2-16)$$

where*

* Throughout this research, all equations are written using the rationalized mks system of units.

- δ = the average distance of the domain wall from the nucleating site
 H = applied field
 H_s = minimum field required to make the domain wall move
 φ_1 = the flux enclosed by the domain wall
 $f(\delta)$ = the positional dependence of the wall damping factor
 K_1 = constant of the material related to the wall damping
 B_s = saturation flux density of the material
 $g'(\delta)$ = rate of change of cross-sectional area enclosed by the domain wall with respect to the average wall position
 t = time

Next, the motion of a typical domain wall in a polycrystalline specimen is assumed to be governed by equations of the same form as Eqs.(2-12) and (2-16). Because of the inhomogeneity of polycrystalline materials, the starting field H_s is assumed to vary among domains; thus the number of domains moving for any applied field strength will vary. In general, a large number of domains participate in the flux reversal process; consequently, the number of domain walls N_d which move is considered as a continuous function of the applied field. Thus the distribution function $G(H_s)$, which describes the number of walls which start to move for applied fields between H_s and $H_s + dH_s$, is defined by Eq.(2-18):

$$G(H_s)dH_s = \frac{dN_d(H_s)}{dH_s} dH_s \quad (2-18)$$

The significance of the function $G(H)$ will be discussed later.

By using the distribution function $G(H)$, the equation of motion for a typical domain wall, Eq.(2-12), is averaged over the distribution of starting fields; as a result, the average domain dimension \bar{x} , obtained by averaging over all the domain walls that are moving, is defined in Eq.(2-19). This dimension is then used to define the average normalized domain dimension r in Eq.(2-20). The dimension r is defined in such a way that, regardless of the applied field strength or how the field varies during a flux reversal, the variable r is zero at the start of a flux reversal and is unity at the end of a flux reversal. In terms of the normalized dimension r , the equation of motion which describes domain wall motion throughout the polycrystalline specimen is derived as Eq. (2-21). This expression contains a term in dH/dt , the rate of change of applied field. In all the considerations of this research, the applied field is assumed to change slowly enough during the flux reversal so that this term containing dH/dt can be neglected. Thus the most general form of the domain wall equation of motion used in this research is given by Eq.(2-28).

$$f \left(\frac{r}{K_2 \int_{H_c}^H G(H_s) dH_s} \right) \frac{dr}{dt} = K_1 K_2 \int_{H_c}^H (H - H_s) G(H_s) dH_s \quad (2-28)$$

where K_2 is a constant relating the maximum distance moved by an average domain wall to the number of domain walls moving [see Eq.(2-20)]. The other equation in the mathematical representation for the reactor is obtained by essentially a summation of Eq.(2-16) over all domains participating in the

flux reversal. The final result is given by Eq.(2-27):

$$\frac{d\varphi}{dt} = 2B_s g(r) \frac{dr}{dt} \quad (2-27)$$

where $g(r)$ describes the rate of change of area of reversed magnetization with respect to the dimension r as given by Eq.(2-26).

Equations (2-27) and (2-28) can be interpreted in terms of the domain configuration they imply; thus some of the limitations of the representation will be apparent. The use of a single equation to describe all domain wall motion means that all domains are assumed to be identical and uniformly distributed over the specimen. The shape of the constant-current switching voltage pulse resulting from a single domain is independent of the number of domains participating in the reversal, but the magnitude and duration of the pulse are dependent on the number of domain walls that are moving. In a polycrystalline specimen, all domain walls do not behave identically, and the shape of the voltage pulse resulting from the constant-current switching of a single domain should depend on the number of domains moving. However, as pointed out in Section 2.2.3 of Chap. II, the initial part of the voltage pulse will have a shape relatively independent of the number of domains moving, because the small nucleated domains will be relatively far removed from one another. The shape of the final part of the voltage pulse is determined by the rate of annihilation of domain walls. Since annihilation occurs because a domain wall collides with other domain walls or the crystalline surfaces, the shape of the final part of

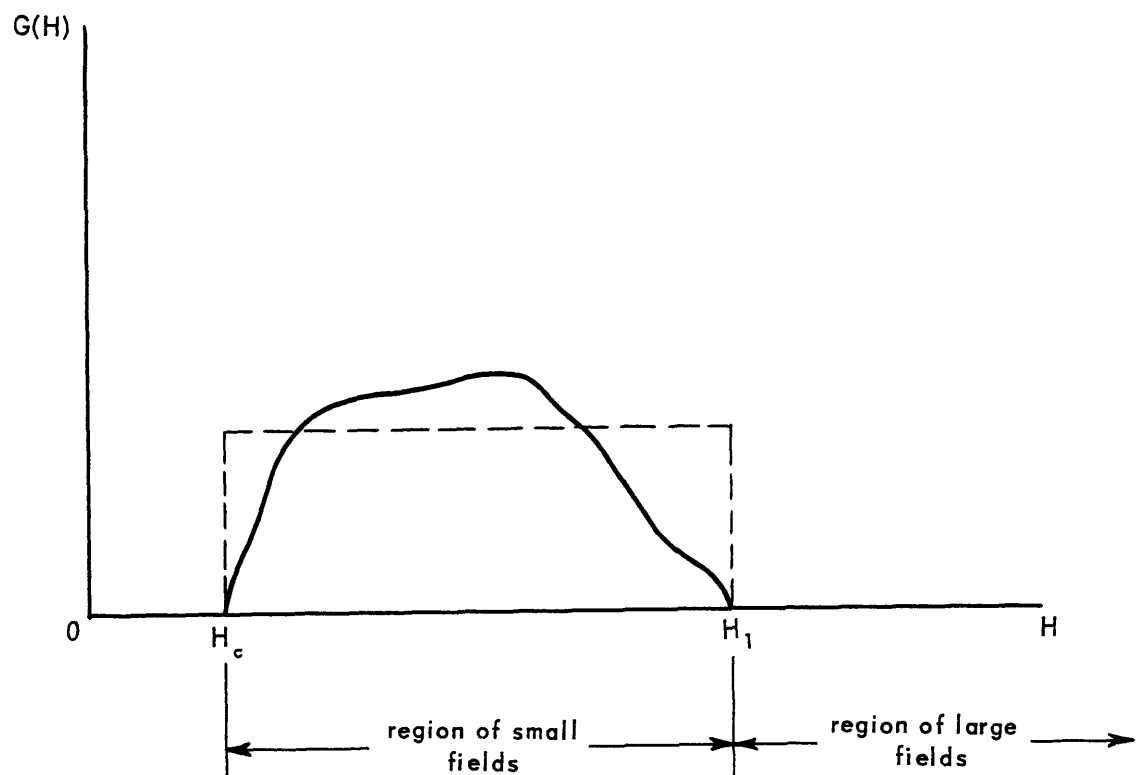


Fig. 4.1. Qualitative plot of the distribution of domain wall starting fields.

the waveform should be dependent on the number of domain walls moving. Although the present representation is suitable for magnetic-amplifier analysis where the initial part of the re-setting voltage waveform is of primary importance, it may not be suitable for applications where the final part of the re-setting waveform must be accurately known.

In Chap. II, the mathematical representation given by Eqs.(2-27) and (2-28) is shown to describe adequately the characteristics of saturable reactors for three types of switching excitation: large constant field, small constant field, and small slowly varying field. The relative size of the field is best defined in terms of the distribution of domain-wall starting fields described by the function $G(H_s)$ in Eq.(2-18). In general, a reactor will have a distribution of starting fields similar to the curve shown qualitatively in Fig. 4-1. Of course, no domains will move for fields less than the coercive force H_c . For fields slightly greater than the coercive field, the number of domain walls that move will vary rapidly with applied field; while at a field strength H_1 practically all of the possible nucleation sites supply domain walls that move. For fields greater than H_1 , the number of domain walls participating in a flux reversal does not vary with applied field. Thus, as shown in Fig. 4-1, the region of small fields is from H_c to H_1 , while the region of large fields is beyond H_1 .

4.1.1 Switching with Large Constant Field

When the applied field is much greater than H_1 (see Fig. 4-1), the distribution function $G(H)$ can be considered

as an impulse in the integration of Eq.(2-28): in other words, for such a large field, all possible domain walls move, and the effective field propelling each wall - the applied field minus the starting field - is approximately the same. It is shown in Section 2.3.1 of Chap. II that consideration of $G(H)$ as an impulse leads to the result that the inverse of the constant-field switching time varies linearly with applied field, in agreement with experiments performed in the computer field and reported in the literature.^{32,33} Thus the mathematical representation is adequate for describing constant-field switching characteristics for large applied fields.

4.1.2 Switching with Small Fields

For an analytical consideration of switching at small fields ($H_c < H < H_1$ in Fig. 4-1), the function $G(H)$ must be known. The lack of detailed information about nucleating sites and starting fields makes it impossible to determine the function $G(H)$ from considerations of material constants and structure. Thus, to obtain analytical expressions that can be empirically fit to experimental curves, the function $G(H)$ is assumed to be a power series given by Eq.(2-32):

$$G(H_s) = \sum_{n=0}^{\infty} a_n (H_s - H_c)^{n+p} \quad (2-32)$$

$$H_s > H_c, \quad -1 < p \leq 0$$

Using this approximation of $G(H)$ and the assumption that the damping of the domain walls is not position-dependent [see Eqs.(2-35) and (2-37)], the mathematical representation for the reactor simplifies to Eqs.(2-38) and (2-39):

$$\frac{dr}{dt} = K_1 K_2 \sum_{n=0}^{\infty} \frac{a_n}{(n+p+1)(n+p+2)} (H - H_c)^{n+p+2} \quad (2-38)$$

$$\frac{d\phi}{dt} = 2B_s K_1 K_2 g(r) \sum_{n=0}^{\infty} \frac{a_n}{(n+p+1)(n+p+2)} (H - H_c)^{n+p+2} \quad (2-39)$$

When a constant-current switching characteristic is plotted for a reactor in terms of one of the three variables - peak switching voltage $(d\phi/dt)_{pk}$, time to reach peak voltage τ_{pk} , or time for complete switching τ_s - the reactor constants can be determined by fitting the power series of Eq.(2-40), (2-41), or (2-42) to the experimental result. In general, several terms in the power series may be necessary to obtain a good empirical fit over a wide range of applied fields; however, for inclusion in a circuit analysis it is better to use the best approximation over the range of fields of interest afforded by a single term of the power series. The graph of Fig. 2-17 shows plots of peak switching voltage as a function of the effective applied field for three reactors. Also shown in Fig. 2-17 are approximations to the three plots made by assuming $n = p = 0$ in the power series of Eqs.(2-38) and (2-39). It is evident, from Fig. 2-17, that the approximation is very good for the one-mil reactor, but is less accurate for the other two. Similar results reported by Huhta²¹ indicate that this is a good approximation for all materials commonly used in high-performance magnetic amplifiers. In subsequent work, the representation using the approximation of $n = p = 0$ is used, and experimental verification is made

with the one-mil core, with the reactor constant determined from the approximation of Fig. 2-17.

The approximation of $n = p = 0$ in the power series means that the distribution of starting fields described by the function $G(H)$ is a constant from the coercive field H_c up to the operating field, as shown by the dotted curve in Fig. 4-1.

The approximation of $n = p = 0$ for the power series in the mathematical representation of Eqs. (2-38) and (2-39) leads to the simplified representation of Eqs. (2-44) and (2-45):

$$\frac{dr}{dt} = K_1 K_2 \frac{a_0}{2} (H - H_c)^2 \quad (2-44)$$

$$\frac{d\varphi}{dt} = B_s K_1 K_2 a_0 g(r) (H - H_c)^2 \quad (2-45)$$

When this representation is applied to the analysis of switching with constant voltage and finite resistance, as shown schematically in Fig. 2-18, the peak switching voltage is given by Eq. (2-49). This expression is shown plotted in Fig. 2-20, along with experimental points obtained with the one-mil Orthonol reactor with three values of reset circuit N^2/R . The agreement between theory and experiment is good over a wide range of applied fields. Thus, when the constants of the reactor representation are specialized to obtain an empirical fit with a set of constant-current switching characteristics, the resulting representation can be used to predict a switching characteristic obtained by the use of a constant switching voltage with a finite switching or reset circuit resistance. In this mode of operation, the field applied to the core varies during the switching.

4.2.0 Magnetic-Amplifier Analysis

In the treatment up to this point, no consideration has been given to the function $g(r)$ in the mathematical representation for the reactor. Control in a magnetic amplifier is obtained essentially by controlling the amount of flux reset in the reactor during a given interval of time. The amount of flux reset varies from zero to twice the reactor saturation flux; consequently, when the representation is included in the analysis of a magnetic amplifier, the instantaneous rate of change of flux must be known at all times during the resetting period. Thus, if the mathematical representation of Eqs. (2-38) and (2-39) is to be applied in a magnetic-amplifier analysis, the function $g(r)$ must be specified.

In the approximate representation of Eqs. (2-38) and (2-39), for which the assumption has already been made that the domain wall damping is position-independent, the application of a constant field H makes the dimension r vary linearly with time. In this case, the function $g(r)$, plotted as a function of r , has the same shape as the switching voltage plotted as a function of time. Thus the function $g(r)$ can be obtained by approximating a switching voltage waveform by some analytical function.

Most reactors used in magnetic amplifiers exhibit so-called rectangular B-H loops when the reactor is excited by a sinusoidal voltage source. This means that when the rate of change of flux is sinusoidal, the exciting current is constant. Conversely, when such a reactor is switched with a

constant current, the resulting induced voltage pulse is very nearly sinusoidal. Thus, for those reactors operated in a range of fields for which the B-H loop is rectangular for sinusoidal excitation, the function $g(r)$ can be assumed a sinusoid.

In all the magnetic-amplifier analyses of this research the representation used is the single-term approximation to the power series of Eqs.(2-38) and (2-39) given in Eqs.(2-44) and (2-45). While the variation in the behavior of reactors in general may vary appreciably, the reactors commonly used in magnetic amplifiers when operated over the limited range of fields found in magnetic amplifiers will exhibit similar behavior. Consequently, while the magnetic-amplifier analyses to follow are based on the representation for a particular reactor, the results will be applicable to magnetic amplifiers utilizing most of the common types of reactors. Naturally, caution must be exercised in making such a generalization.

4.2.1 "Exact" Magnetic-Amplifier Analysis

In Section 3.1.0 of Chap. III, the magnetic amplifier shown schematically in Fig. 3-1 is analyzed for constant current reset $[(N_r^2/R_r) \rightarrow 0]$, using the mathematical representation of the reactor given by Eqs.(2-44) and (2-45) with the function $g(r)$ a sinusoid. The analysis requires some graphical solutions, which are made in Appendix II. The resulting normalized input-output characteristic is plotted in Fig. 3-6, where I_L/I_{Lm} is plotted as a function of H_e/H_{em} . I_L is the average load current, I_{Lm} is the maximum average load current,

H_e is the effective applied field,

$$H_e = \frac{N_r I_r}{\lambda_m} - H_c ,$$

and H_{em} is the field required for minimum output given by Eq.(3-22):

$$H_{em} = \sqrt{\frac{2\omega}{\pi K_1 K_2 a_o}} \quad (3-22)$$

with ω the radian frequency of the supply, and $K_1 K_2 a_o$ the reactor constant. Also plotted in Fig. 3-6 are experimental points obtained at various supply frequencies from the experimental arrangement of Fig. 3-7. The normalizing constant for the input of each experimental curve, H_{em} , is calculated from Eq.(3-22) in Appendix II.

A comparison of the theoretical curve and the experimental points in Fig. 3-6 shows that, although the agreement is not exact, the error is relatively invariant with frequency. At high levels of output, the error is mainly due to the neglect in the mathematical representation of the flux change after saturation. The size of the error due to this flux change should remain fairly constant down to half output, and below half output it should decrease to zero at minimum output. At low levels of output, the principal source of error is the neglect of the exciting current in the analysis of the gating half-cycle. This error is a maximum at minimum output, and decreases as the output increases. These two sources of error account for practically all of the nearly 25 percent difference between the theoretical and experimental gains at half-output. As demonstrated by the results of Fig. 3-6, the

mathematical representation derived in Chap. II allows reasonably accurate prediction of magnetic-amplifier input-output characteristics over a frequency range of a decade for constant current reset. No such prediction has been attempted in the literature up to the present time, the reason being that the mathematical representations for the reactors used previously were not general enough to allow such a prediction.

4.2.2 Approximate Magnetic-Amplifier Analysis

When the reset circuit resistance in the single-core, self-saturating magnetic-amplifier circuit of Fig. 3-1 is made finite, the field applied to the reactor will vary during the resetting process. Under such a set of conditions, the use of the mathematical representation of Eqs.(2-44) and (2-45) with $g(r)$ a sinusoid to describe the reactor, leads to expressions requiring machine computation for rapid solution. To remove the difficulty and allow simplified, though somewhat less accurate solutions, the representation is further simplified in Section 3.2.0 of Chap. III by the assumption that the function $g(r)$ in Eq.(2-45) is a square wave. To compensate partially for this assumption, the supply voltage is also assumed to be a square wave, in spite of the fact that the supply voltage used in the experimental verification is sinusoidal. These two assumptions are reasonable, because in the actual amplifier the supply voltage and the function $g(r)$ have the same shape. The errors introduced by these assumptions arise because, with a constant reset voltage, the change of resetting waveshape with reset circuit N^2/R , illustrated in Fig. 3-8, no longer occurs, and the rectifier

unblocking that takes place in the actual amplifier during the resetting period does not occur in the simplified analysis.

The analysis of the circuit with constant-current reset and the simplified reactor representation is carried out in Section 3.2.1 of Chap. III. The resulting input-output characteristic is plotted in Fig. 3-9, where a comparison is made both with the theoretical result of the more exact analysis of Section 3.1.0 and with the experimental results first plotted in Fig. 3-6. According to the plot of Fig. 3-9, the approximate analysis gives better agreement with experiment than the "exact" analysis does. This, however, is coincidence because the sources of error between the "exact" analysis and experiment manifest themselves during the gating period, while the error between the "exact" and the approximate analysis occurs because of waveform differences during the resetting period. In spite of the errors, the plot of Fig. 3-9 shows that the approximate analysis yields a good prediction of the magnetic-amplifier characteristic over a supply frequency range of a decade for constant-current reset. This extremely simple analysis yields the result expressed as Eq.(3-28):

$$\frac{I_L}{I_{Lm}} = 1 - \left(\frac{H_e}{H_{em}} \right)^2 \quad (3-28)$$

The factors in this expression are defined in the same way as those for the "exact" analysis given above.

The approximate analysis for finite reset resistance and constant reset voltage is carried out in Section 3.2.2, and the input-output characteristic is obtained in Eq.(3-33) in

terms of the average effective applied field H_e ,

$$H_e = \frac{N_r V}{\mathcal{L}_m R_r} - H_c , \quad (3-31)$$

the reset conductance per unit mean length,

$$G = \frac{N_r^2}{\mathcal{L}_m R_r} , \quad (3-36)$$

the supply period 2π , and the reactor constants. The input-output characteristic of Eq.(3-33) is rather unwieldy to use, but the expression can be put into very useful form by normalizing it with respect to the average effective field required for minimum output and with respect to the value of reset conductance per unit mean length required for maximum power gain. Thus, before this input-output characteristic is treated further, the power gain is maximized in Section 3.2.3.

The power gain is defined as an incremental quantity at half-output in Eq.(3-34):

$$K_p = \left(\frac{\partial I_L}{\partial I_r} \right)_{\frac{1}{2}} \frac{R_L}{R_r} \quad (3-34)$$

Since the variables involved are average values, Eq.(3-34) does not give the true power gain; however, this expression gives a good index of comparison among amplifiers of the same type, which is a much simpler expression than the true power gain.

The value of the reset conductance per unit mean length necessary for maximum power gain at half-output is derived in Appendix III, and is given by Eq.(3-37):

$$G_m = \frac{1}{2K_3} \sqrt{\frac{K_3 \tau}{B_s A_c}} \quad (3-37)$$

and the resulting maximum power gain is

$$K_{pm} = \frac{1}{8} \frac{N_g^2}{\lambda_m R_L} \sqrt{\frac{K_3 B_s A_c}{\tau}} \quad (3-38)$$

In these expressions,

$$K_3 = B_s A_c K_1 K_2 a_o$$

With the definition of the relative reset conductance γ given by Eq.(3-39),

$$\gamma = \frac{G}{G_m} = 2K_3 \sqrt{\frac{B_s A_c}{K_3 \tau}} \frac{N_r^2}{\lambda_m R_r} \quad (3-39)$$

the power gain at half-output for any level of G can be found from the expression:

$$\frac{K_p}{K_{pm}} = \frac{4\gamma}{(\gamma+1)^2} \quad (3-40)$$

This normalized power gain is plotted in Fig. 3-10, along with some experimental points obtained using the experimental arrangement of Fig. 3-11. From the results shown in Fig. 3-10, it is apparent that, while the predicted power gain is too high, the prediction of the reset N^2/R at which maximum power gain occurs is very good. This result provides one form of a solution to the problem of whether the reset circuit resistance is relatively high or low. Another form of the same solution will be given below.

In Appendix IV, the relative reset conductance γ is used to normalize the input-output characteristic of the amplifier with constant reset voltage. The result is given in Eq.(3-41):

$$\frac{I_L}{I_{Lm}} = 1 - \frac{1}{2} \left[\frac{-1 + \sqrt{1 + [(\sqrt{2} \gamma + 1)^2 - 1] \frac{H_e}{H_{em}}}}{\gamma} \right]^2 \quad (3-41)$$

with H_{em} the average effective applied field now given by:

$$H_{em} = \sqrt{\frac{B_s A_c}{K_3 \tau}} \frac{(\sqrt{2} \gamma + 1)^2 - 1}{2\gamma} \quad (3-42)$$

The expression for the input-output characteristic, Eq.(3-41), is independent of supply frequency; consequently, a family of input-output characteristics could be plotted with γ as parameter; then the performance of a particular reactor at a given supply frequency could be found by substituting the reactor and circuit constants into the normalizing expressions, Eqs. (3-39) and (3-42). The expression of Eq.(3-41) is plotted for two values of γ in Figs. 3-12 and 3-13. Experimental points obtained at two values of supply frequency with the circuit of Fig. 3-11 are shown in Figs. 3-12 and 3-13. Although the predicted slopes of the two curves are optimistic, the error is relatively independent of frequency. The error at high values of output is due to the flux change after saturation which was neglected in the reactor representation. At low levels of output, the error is caused by the neglect of exciting current during the gating period, and in addition by the neglect of the waveform change with γ and rectifier unblocking in the simplified representation. Reference to Fig. 3-10, where the constant-current reset characteristic was plotted, shows that the prediction of H_{em} , the field required for minimum output, was very good. Reference to Figs. 3-12 and 3-13 shows that the prediction of H_{em} increases in

error as γ increases. This is to be expected, because the waveform distortion and the consequent decrement in reset flux due to rectifier unblocking increase with γ . The waveform distortion and rectifier unblocking were disregarded in the approximate analysis. In spite of the errors involved, the approximate analysis gives a reasonably accurate prediction of magnetic-amplifier behavior over a range of frequency and a range of relative reset resistance values. Such a prediction has never been attempted in the literature up to the present time.

The normalized current gain K_i at half-output is defined in Eq.(3-43) as:

$$K_i = \sqrt{\frac{B_s A_c}{K_3 \tau}} \left[\frac{\partial \left(\frac{I_L}{I_{Lm}} \right)}{\partial H_e} \right] \frac{I_L}{I_{Lm}} = 0.5 \quad (3-43)$$

In terms of the normalized conductance γ , the current gain K_i is given as:

$$K_i = \frac{1}{\gamma+1} \quad (3-44)$$

This expression, shown plotted in Fig. 3-14, provides a quantitative measure of the approach to voltage or current control in terms of the reactor constants and supply frequency. By comparison of the actual curve with the current-control and voltage-control asymptotes in Fig. 3-14, the accuracy of either approximation can be obtained. Of course, the optimum operating point with respect to power gain occurs at $\gamma = 1$ where the asymptotes intersect.

In the approximate analysis the reset waveform distortion and rectifier unblocking that were neglected cause the error in the analysis to increase with increasing γ . Thus the accuracy of the plot of Fig. 3-14 decreases with increasing γ . The accuracy of the experimental power gain shown plotted in Fig. 3-10 does not change appreciably up to $\gamma = 3$; consequently, the plot of Fig. 3-14 is useful for values of γ on both sides of the optimum of $\gamma = 1$.

4.3.0 Conclusions

In this section the conclusions to be drawn from the results of this research will be discussed along with the limitations of the techniques. This discussion will be broken into two parts: how the material quality can be specified in terms of the mathematical representation, and how the representation can be useful in the application of existing reactors in magnetic amplifiers.

4.3.1 Material Quality

Before material quality can be discussed, the meaning of the term must be known. As it is used here, material quality means how well a magnetic amplifier performs with a reactor using the core material. Most amplifiers are characterized by gain-bandwidth products. Magnetic amplifiers are usually characterized by a similar factor called the figure of merit, which is the ratio of power gain to time constant. The single-core self-saturating magnetic amplifier exhibits a time delay of one half-cycle of the supply frequency; consequently, the maximum power gain obtainable is

a direct measure of the figure of merit for this amplifier. The maximum obtainable power gain will be used as a measure of the material quality in this section.

The maximum power gain is given by Eq.(3-38):

$$K_{pm} = \frac{1}{8} \frac{N_g^2}{\lambda_m R_L} \sqrt{\frac{K_3 B_s A_c}{\tau}} \quad (3-38)$$

Methods of achieving maximum power gain by adjusting core dimensions and operating conditions are straightforward; thus, in the discussion of material quality, a reactor of given dimensions, and material are assumed. Since Eq.(3-38) was derived for normal reactor excitation, the fixing of the supply frequency leaves only the reactor constant K_3 to affect the power gain. Included as factors in K_3 are the constants K_1 and $K_2 a_0$. Reference to Eq.(2-12) shows that the constant K_1 is a measure of the damping of domain wall motion. An increase of K_1 means a decrease in the damping on the domain wall. The damping is caused by both eddy currents and spin relaxation. The eddy-current damping can be reduced by making the material thinner, but the spin-relaxation damping is a property of the material itself; consequently, there exists a limit to the improvement possible by using thinner material.

Reference to Eqs.(2-20) and (2-32) indicates that the constant $K_2 a_0$ depends on the number of domain walls participating in the flux reversal process. It should be evident that if the number of walls is increased, the velocity of each wall for a given rate of change of flux will be decreased. Thus, less field will be required to drive the walls. The

number of walls available for flux reversal undoubtedly depends on the grain structure in the material, because nucleation is considered to occur (at least in part) at grain boundaries. It might seem reasonable that a reduction in grain size would improve the material by providing more domain walls. However, the process of nucleation at grain boundaries is not simple nor well understood because of a lack of detailed knowledge of just how nucleation takes place in a polycrystalline specimen. The constant $K_2 a_0$ can be increased by improving the uniformity of the grain structure throughout the specimen. This has the effect of reducing the variation of starting fields to a minimum; as a result, for a given change in applied field, a greater number of domain walls start to move.

4.3.2 Application of Existing Reactors

The analyses and experimental results given in Chap. III indicate that the mathematical representation can be used to predict magnetic-amplifier characteristics over a wide range of supply frequency and reset circuit impedance. In addition, the representation allows a calculation of the reset circuit impedance at which maximum power gain occurs. Such predictions have not been possible with reactor representations used in the past. By the use of this representation to describe a given reactor, a constant-current switching characteristic can be measured and Eqs.(2-38) and (2-39) can be fitted to the characteristics. This representation can then be used to predict single-core, self-saturating magnetic-amplifier characteristics. If the switching characteristic

can be approximated by the simplified representation of Eqs. (2-44) and (2-45), the results of Chap. III are applicable to the reactor.

It must be remembered that all the analyses of Chap. III have been made with a constant resetting voltage; consequently, if magnetic-amplifier characteristics are desired for other types of resetting signals - for instance, reset pulses - , the analysis of Chap. III will have to be generalized to include the particular type of reset used. In the case of pulse reset, caution must be exercised in applying the simplified representation because the dH/dt term neglected in the simplification may no longer be negligible.

The reactor representation used in this research can be used to establish a model theory for application with the Roberts core test.¹⁸ In the Roberts core test, a normalized input-output characteristic of the reactor, operating in a single-core, self-saturating magnetic-amplifier circuit, is obtained at one supply frequency. Thus, by using the reactor representation of Chap. II, the results of a Roberts core test could be used to obtain the characteristics of the reactor operating at different levels of reset circuit impedance. As Roberts points out,¹⁸ when current pulse reset is used, the results of his core test are changed from the result obtained by using constant current reset; however, by proper application of the reactor representation, a magnetic amplifier model theory could be developed for each of several common types of reset signals.

The problem of matching reactors for use in balanced amplifiers has not been wholly solved. The representation developed in this research indicates the necessary condition that two reactors be matched. The condition is simply that both reactors shall have the same constants and constant-current switching waveforms. The switching waveform is very important because, as Roberts points out,¹⁸ a change in resetting waveform can make a profound difference in magnetic-amplifier characteristics.

4.4.0 Areas of Future Work

One area that needs to be investigated thoroughly is the problem of how well the mathematical representation of the material actually describes the processes in the reactor. Although the representation has proved useful in the prediction of magnetic-amplifier characteristics, there is no way at present of verifying whether or not the representation does describe the detailed behavior accurately. The questions to be answered are: Where does nucleation occur, and what constitutes a nucleation site? How do grain size and structure affect nucleation and wall motion? What is the domain wall configuration during flux change? The answers to these questions will go a long way toward determining the accuracy of the representation already developed, and will probably indicate methods for obtaining an improved representation. In addition, the answers to these questions will indicate to the metallurgist what variables to control in producing better and more consistent magnetic materials. Also it might then

be possible to determine the constants of a reactor from more fundamental considerations than a terminal characteristic of the reactor.

Future work of value can be performed in the area of application of the representation developed in this research to conditions of magnetic-amplifier operation other than those covered here. Examples of the problems still unsolved are: the application to single-core amplifiers with resetting voltage waveforms other than the constant used in Chap. III, and the application of the representation to the analysis of multi-core, self-saturating amplifiers. The solution of the latter problem would provide a large step in the solution of the problem which has faced magnetic-amplifier designers for many years: namely, how does one design a magnetic amplifier with specified operating characteristics, having available only independent information on cores and rectifiers? The stumbling block to the solution of this problem has been an inability to state what information about the reactor is necessary for such a design. The representation developed in this research can be used to indicate the type of core information needed for a practical magnetic-amplifier synthesis. Since the core information is obtained from a set of constant-current switching characteristics, a type of test performed in the computer field for some time, the information may already be available; but, if it is not available, it is easily obtainable from simple test procedures.

Appendix IDERIVATION OF SINGLE-DOMAIN BEHAVIORA. Plane-Wall, Rectangular Specimen
Eddy-Current Damping

The physical structure treated in this derivation is shown in Figs. 2-1 and 2-2. The material is assumed to have constant conductivity σ over all the material, and the starting field H_0 is assumed to be constant for all wall positions. The domain wall velocity will be found by equating the eddy-current power losses to the input power.

The saturation moment is so great that $\mu_0 H$ can be neglected; consequently, the rate of change of flux is zero everywhere except at the domain wall

$$\nabla_x \vec{E} = - \frac{\partial \vec{B}}{\partial t} = 0 \quad (I-1)$$

where \vec{E} is the electric-field intensity and \vec{B} is the flux density. Since there is symmetry in the y -direction, and since the current density \vec{J} is given by

$$\vec{J} = \vec{i} J_x + \vec{j} J_y + \vec{k} J_z = \sigma \vec{E} \quad (I-2)$$

where \vec{i} , \vec{j} , and \vec{k} are unit vectors in the right-hand coordinate system xyz, then:

$$\frac{\partial^2 J_x}{\partial x^2} + \frac{\partial^2 J_x}{\partial z^2} = 0 \quad (I-3)$$

$$\frac{\partial^2 J_z}{\partial x^2} + \frac{\partial^2 J_z}{\partial z^2} = 0 \quad (I-4)$$

The boundary conditions are: that the normal component of the current density is zero at the specimen boundaries:

$$\begin{aligned} J_x &= 0 \quad \text{at } x = -\delta \\ x &= w - \delta \end{aligned} \tag{I-5}$$

$$J_z = 0 \quad \text{at } z = \pm \frac{d}{2}$$

At the domain wall,

$$\begin{aligned} J_z(0-) &= -\sigma v B_s \\ J_z(0+) &= \sigma v B_s \end{aligned} \tag{I-6}$$

The solution of Eqs. (I-3) and (I-4), subject to the boundary conditions, Eqs. (I-5) and (I-6), is:

for $-\delta \leq x < 0$

$$J_x = - \sum_{n \text{ odd}} A_n \sin \frac{n\pi z}{d} \sinh \frac{n\pi(\delta+x)}{d} \tag{I-7}$$

$$J_z = - \sum_{n \text{ odd}} A_n \cos \frac{n\pi z}{d} \cosh \frac{n\pi(\delta+x)}{d} \tag{I-8}$$

$$A_n = \pm \frac{4\sigma v B_s}{n\pi \cosh \frac{n\pi\delta}{d}} \tag{I-9}$$

with + sign for $n = 1, 5, 9, \dots$

- sign for $n = 3, 7, 11, \dots$

for $0 < x \leq w - \delta$

$$J_x = - \sum_{n \text{ odd}} B_n \sin \frac{n\pi z}{d} \sinh \frac{n\pi(w-\delta-x)}{d} \tag{I-10}$$

$$J_z = \sum_{n \text{ odd}} B_n \cos \frac{n\pi z}{d} \cosh \frac{n\pi(w-\delta-x)}{d} \tag{I-11}$$

$$B_n = \pm \frac{4\sigma v B_s}{n\pi \cosh \frac{n\pi(w-\delta)}{d}} \tag{I-12}$$

with + sign for $n = 1, 5, 9, \dots$

- sign for $n = 3, 7, 11, \dots$

The power dissipated by the eddy currents is

$$P_e = \frac{1}{\sigma} \int_{\text{volume}} (\vec{J} \cdot \vec{J}) d(\text{volume}) \quad (I-13)$$

The eddy-current power dissipated per unit length of the specimen is:

$$P_e = \frac{2}{\sigma} \left[\int_0^{\frac{d}{2}} \int_0^{w-\delta} (J_x^2 + J_z^2) dx dz + \int_0^{\frac{d}{2}} \int_{-\delta}^0 (J_x^2 + J_z^2) dx dz \right] \quad (I-14)$$

Substitution of the values for J_x and J_z into Eq. (I-14), and evaluation of the integral lead to:

$$P_e = \frac{16 \sigma v^2 B_s^2 d^2}{\pi^3} F(\delta) \quad (I-15)$$

$$F(\delta) = \sum_{n \text{ odd}} \frac{1}{n^3} \frac{\sinh \frac{n\pi w}{d}}{\cosh \frac{n\pi w}{d} + \cosh \frac{n\pi(2\delta-w)}{d}} \quad (I-16)$$

The electrical input power per unit length is:

$$P_{el} = (H - H_o) \frac{d\phi}{dt} = 2B_s v d(H - H_o) \quad (I-17)$$

Equating electrical input power to eddy-current power loss, and solving for the domain wall velocity v , yield:

$$v = \frac{\pi^3}{8B_s d F(\delta)} (H - H_o) \quad (I-18)$$

B. Plane-Wall, Rectangular Specimen Spin-Relaxation Damping

The physical structure considered is shown in Fig. 2-1. The thickness d is very small compared to the radius r_i ; therefore the applied field is constant over the thickness of the specimen. Considering the unit length of material with a domain wall moving as shown in Fig. 2-2, the retarding force

on the wall per unit length of material is

$$f_{\text{retard}} = \beta_r v d \quad (\text{I-19})$$

Thus the power dissipated in spin-relaxation damping per unit length of material is:

$$p_r = \beta_r v^2 d \quad (\text{I-20})$$

The electrical input power per unit length of material is given by Eq.(I-17):

$$p_{\text{el}} = 2B_s v d (H - H_0) \quad (\text{I-17})$$

Setting Eq.(I-17) equal to Eq.(I-20) yields the velocity:

$$v = \frac{2B_s}{\beta_r} (H - H_0) \quad (\text{I-21})$$

C. Cylindrical Wall, Cylindrical Specimen, Eddy-Current Damping

The physical structure considered is shown in Figs. 2-4 and 2-5. The applied field H , as well as the starting field H_0 , is the same throughout the structure. As shown in Fig. 2-5, a single, concentric, cylindrical domain wall is expanding with velocity v .

The cross-sectional area enclosed by the domain wall is

$$A_{\text{domain}} = \pi \delta^2 \quad (\text{I-22})$$

Thus the rate of change of flux, which all occurs at the domain wall, is:

$$\frac{d\varphi}{dt} = 2B_s \frac{dA_{\text{domain}}}{dt} = 4\pi B_s \delta \frac{d\delta}{dt} \quad (\text{I-23})$$

where φ is considered positive pointing into the plane of the paper in Fig. 2-5. Using Faraday's Law,

$$\oint \vec{E} \cdot d\vec{s} = - \frac{d\varphi}{dt} \quad (\text{I-24})$$

and integrating around a concentric path of radius r (see Fig. 2-5), the tangential electric field is:

$$E_\theta = \begin{cases} -\frac{1}{2\pi r} \frac{d\phi}{dt} & \text{for } r > \delta \\ 0 & \text{for } r < \delta \end{cases} \quad (\text{I-25})$$

Since the electric field possesses only a tangential component, the current density is given by:

$$J_\theta = \sigma E_\theta = -\frac{\sigma}{2\pi r} \frac{d\phi}{dt} \quad \text{for } r > \delta \quad (\text{I-26})$$

Substitution of Eq. (I-23) into (I-26) yields:

$$J_\theta = -\frac{2B_s \sigma \delta}{r} \frac{d\phi}{dt} \quad \text{for } r > \delta \quad (\text{I-27})$$

The total eddy-current losses per unit length of the specimen are found by evaluating the integral

$$P_e = \int_{\delta}^{r_m} \frac{J_\theta^2}{\sigma} 2\pi r dr \quad (\text{I-28})$$

The result is:

$$P_e = 8\pi B_s^2 \sigma \delta^2 \ln \frac{r_m}{\delta} \left(\frac{d\delta}{dt} \right)^2 \quad (\text{I-29})$$

The electrical input power per unit length of material is

$$P_{el} = 4\pi B_s \delta \frac{d\delta}{dt} (H - H_o) \quad (\text{I-30})$$

Thus, equating electrical input power to power loss in eddy currents yields the differential equation:

$$\delta \ln \frac{r_m}{\delta} \frac{d\delta}{dt} = \frac{1}{2B_s \sigma} (H - H_o) \quad (\text{I-31})$$

D. Cylindrical Wall, Cylindrical Specimen, Spin-Relaxation Damping

The physical structure assumed in the derivation is described in Figs. 2-4 and 2-5. The wall is assumed to be moving

and retarded only by a spin-relaxation damping force characterized by the damping constant β_r . Thus, in unit length of the material, the retarding force on the domain wall is:

$$f_{\text{retard}} = 2\pi\delta \beta_r \frac{d\delta}{dt} \quad (\text{I-32})$$

The power dissipated in spin-relaxation damping per unit length of material is then

$$p_r = f_{\text{retard}} v = 2\pi\delta\beta_r \left(\frac{d\delta}{dt} \right)^2 \quad (\text{I-33})$$

Setting this power loss equal to the electrical power input given by Eq.(I-30) yields:

$$\frac{d\delta}{dt} = \frac{2B_s}{\beta_r} (H - H_0) \quad (\text{I-34})$$

This equation, in conjunction with the rate of change of flux given by Eq.(I-23), relates flux to applied field in the specimen.

Appendix II

INPUT-OUTPUT CHARACTERISTIC, "EXACT" ANALYSIS, CONSTANT-CURRENT RESET

The rate of change of flux in the reactor when constant-current reset is applied and the load circuit of Fig. 3-1 is open, is given by Eq.(3-13) as

$$\frac{d\phi}{dt} = \frac{\pi}{2} B_s A_c K_1 K_2 a_o (H - H_c)^2 \sin [\pi K_1 K_2 a_o (H - H_c)^2 t] \quad (\text{II-1})$$

This expression can be simplified by defining a reset frequency ω_r :

$$\omega_r = \frac{\pi}{2} K_1 K_2 a_o (H - H_c)^2 \quad (\text{II-2})$$

Substitution of this expression into Eq.(II-1) yields the simplified expression:

$$\frac{d\phi}{dt} = B_s A_c \omega_r \sin \omega_r t \quad (\text{II-3})$$

The supply voltage v_g is given by:

$$v_g = V_g \sin \omega t \quad (\text{II-4})$$

With normal excitation, the amplitude of the supply voltage is given by:

$$V_g = \omega N_g B_s A_c \quad (\text{II-5})$$

Substitution of this expression into Eq.(II-4) and division of both sides by N_g yield:

$$\frac{v_g}{N_g} = B_s A_c \omega \sin \omega t \quad (\text{II-6})$$

It is evident that when the resetting field H has a value such that $\omega_r = \omega$, the reactor flux is reset to negative saturation, and the reactor will not saturate on the next gating

half-cycle. This is the condition of minimum average load current which in the practical case is the exciting current of the reactor, but in this analysis the exciting current is neglected in its contribution to the load current; thus the minimum load current from the analysis will be zero. Definition of the field H_m necessary to give minimum load current leads to the expression

$$H_m - H_c = \sqrt{\frac{2\omega}{\pi K_1 K_2 a_0}} \quad (\text{II-7})$$

For fields of magnitude less than H_m , the shaded area shown in Fig. 3-4c must be evaluated to determine the reset flux. The time t_b must be found graphically; consequently, a family of curves of Eq.(II-3) is plotted for various values of ω_r in Fig. 3-5. Also included on this graph is a plot of v_g/N_g , Eq.(II-6). The time t_b at which the rectifier unblocks (see Fig. 3-4c) for each value of ω_r is given in Table II-1.

The reset flux can be computed as:

$$\Delta\Phi = \int_0^{t_b} \frac{d\Phi}{dt} dt + \int_{t_b}^{\pi/\omega} \frac{v_g}{N_g} dt \quad (\text{II-8})$$

Substitution of $\frac{d\Phi}{dt}$ from Eq.(II-3), and v_g/N_g from Eq.(II-6), into Eq.(II-8), and evaluation of the integrals yield:

$$\Delta\Phi = B_s A_c (1 - \cos \omega_r t_b) + B_s A_c (1 + \cos \omega_r t_b) \quad (\text{II-9})$$

The normalized value of $\Delta\Phi$ is tabulated for each value of ω_r in Table II-1.

When the effective applied field H_e is defined as

$$H_e = H - H_c, \quad (\text{II-10})$$

TABLE II-1

$\frac{\omega_r}{\omega}$	ωt_b degrees	$\cos \omega t_b$	$\omega_r t_b$ degrees	$\cos \omega_r t_b$	$\frac{\Delta\phi}{B_s A_c}$	$\frac{\omega_r}{\omega} = \frac{H_e}{H_{em}}$	$\frac{I_L}{I_{Lm}} =$ $1 - \frac{\Delta\phi}{2B_s A_c}$
0.1	178.3	-0.999	17.83	0.953	0.048	0.316	0.976
0.2	173.5	-0.993	34.7	0.822	0.185	0.448	0.907
0.4	159.0	-0.934	63.6	0.444	0.622	0.633	0.689
0.6	143.2	-0.800	85.9	0.072	1.128	0.776	0.436
0.8	129.0	-0.629	103.2	-0.228	1.599	0.896	0.200
1.0					2.000	1.000	0

the effective field H_{em} for minimum output is

$$H_{em} = H_m - H_c \quad (\text{II-11})$$

A combination of Eqs. (II-2) and (II-7) yields the result

$$\frac{H_e}{H_{em}} = \sqrt{\frac{\omega_r}{\omega}} \quad (\text{II-12})$$

This ratio gives the effective applied field in terms of the effective applied field for minimum output, and it will be used as the input variable in the normalized plot of the input output characteristic. This ratio is also tabulated in Table II-1.

The average load current is given by Eq. (3-13) of Chap. III:

$$\frac{I_L}{I_{Lm}} = 1 - \frac{\Delta\phi}{2B_s A_c}$$

Using the normalized values of the effective resetting field and reset flux given in Table II-1, a normalized input-output characteristic is plotted as the theoretical curve in Fig. 3-6.

The normalizing constant needed for the experimental points of Fig. 3-6 is the effective applied field for minimum output H_{em} , which is given by Eq.(II-7). The reactor used in the experimental tests is the one-mil Orthonol reactor tested previously in Chap. II. From Fig. 2-17 of Chap. II, the constant describing the reactor is

$$\cdot \frac{\pi}{2} B_s A_c K_1 K_2 a_o = 1.75 \times 10^{-3} \frac{vm^2}{a^2}, \quad (II-13)$$

$$B_s A_c = 1.87 \times 10^{-5} \text{ w}$$

The value of H_{em} for each excitation frequency is given in Table II-2.

TABLE II-2

Freq. (cps)	300	500	700	1000	1500	2000	3000
H_{em} (A/M)	4.50	5.70	6.87	8.21	10.1	11.6	14.2

Appendix III
MAXIMIZATION OF THE POWER GAIN

The input-output characteristic of the magnetic amplifier, using the approximate analysis, is given by Eq.(3-33) of Chap. III:

$$\frac{I_L}{I_{Lm}} = 1 - \frac{K_3 \tau}{2B_s A_c} \left[\frac{-1 + \sqrt{1 + 4K_3 G H_e}}{2K_3 G} \right]^2 \quad (\text{III-1})$$

where G is defined as:

$$G = \frac{N^2}{\lambda_m R_r} \quad (\text{III-2})$$

The incremental power gain will be obtained at half-output; thus the average effective field $H_{e\frac{1}{2}}$ required for this level of output is defined from Eq.(III-1) in the expression

$$\sqrt{1 + 4K_3 G H_{e\frac{1}{2}}} = 2K_3 G \sqrt{\frac{B_s A_c}{K_3 \tau}} + 1 \quad (\text{III-3})$$

Differentiation of Eq.(III-1) to obtain the slope of the input-output characteristic yields:

$$\frac{\partial \left(\frac{I_L}{I_{Lm}} \right)}{\partial H_e} = - \frac{\tau}{2B_s A_c G} \left[\frac{-1 + \sqrt{1 + 4K_3 G H_e}}{\sqrt{1 + 4K_3 G H_e}} \right] \quad (\text{III-4})$$

Substitution of Eq.(III-3) into Eq.(III-4) yields the slope at half-output:

$$\left[\frac{\partial \left(\frac{I_L}{I_{Lm}} \right)}{\partial H_e} \right] \frac{I_L}{I_{Lm}} = 0.5 = - \frac{\sqrt{\frac{K_3 \tau}{B_s A_c}}}{2K_3 G \sqrt{\frac{B_s A_c}{K_3 \tau}} + 1} \quad (\text{III-5})$$

The power gain defined by Eq.(3-34) of Chap. III is given

in terms of the derivative of Eq.(III-5) as:

$$K_p = \left(\frac{\partial I_L}{\partial I_r} \right)^2 \frac{R_L}{R_r} = \left[\frac{\partial \left(\frac{I_L}{I_{Lm}} \right)}{\partial H_e} \right]^2 \frac{I_L^2 R_L}{I_{Lm}^2} = 0.5 \frac{I_{Lm}^2 R_L}{\ell_m^2 R_r N_r^2} \quad (\text{III-6})$$

Remembering that for the assumed supply voltage square wave,

$$I_{Lm} = \frac{V_g}{2R_L} \quad (\text{III-7})$$

and for normal reactor excitation,

$$\frac{V_g}{N_g} = \frac{2B_s A_c}{\tau} \quad (\text{III-8})$$

substitution of Eq.(III-5) into Eq.(III-6) and subsequent simplification yield the incremental power gain at half-output for normal excitation:

$$K_p = \frac{\frac{K_3 B_s A_c}{\tau} \frac{N_g^2}{\ell_m R_L} G}{\left[2K_3 G \sqrt{\frac{B_s A_c}{K_3 \tau}} + 1 \right]^2} \quad (\text{III-9})$$

Differentiation of Eq.(III-9) with respect to G yields the value of this variable for which maximum power gain occurs:

$$G_m = \frac{1}{2K_3} \sqrt{\frac{K_3 \tau}{B_s A_c}} \quad (\text{III-10})$$

The resulting maximum power gain is:

$$K_{pm} = \frac{1}{8} \frac{N_g^2}{\ell_m R_L} \sqrt{\frac{K_3 B_s A_c}{\tau}} \quad (\text{III-11})$$

When the ratio γ is defined as:

$$\gamma = \frac{G}{G_m} = 2K_3 \sqrt{\frac{B_s A_c}{K_3 \tau}} \frac{N_r^2}{L_m R_r} \quad (\text{III-12})$$

the power gain of Eq.(III-9) can be normalized to:

$$\frac{K_p}{K_{pm}} = \frac{4\gamma}{(\gamma+1)^2} \quad (\text{III-13})$$

Appendix IV

NORMALIZATION OF INPUT- OUTPUT CHARACTERISTICS

The input-output characteristic for the magnetic amplifier of Fig. 3-1 is described, from the approximate analysis in Eq.(3-33) of Chap. III, as:

$$\frac{I_L}{I_{Lm}} = 1 - \frac{K_3 \tau}{2B_s A_c} \left[\frac{-1 + \sqrt{1 + 4K_3 G H_e}}{2K_3 G} \right]^2 \quad (\text{IV-1})$$

where H_e is the average effective applied field

$$H_e = \frac{N_r V_r}{\lambda_m R_r} - H_c \quad (\text{IV-2})$$

and G is the relative reset conductance per unit mean length:

$$G = \frac{N_r^2}{\lambda_m R_r} \quad (\text{IV-3})$$

The value of G which makes the power gain at half-output a maximum is given by Eq.(3-37) of Chap. III:

$$G_m = \frac{1}{2K_3} \sqrt{\frac{K_3 \tau}{B_s A_c}} \quad (\text{IV-4})$$

The ratio γ , defined in Eq.(3-39) of Chap. III, is:

$$\gamma = \frac{G}{G_m} = 2K_3 \sqrt{\frac{B_s A_c}{K_3 \tau}} \frac{N_r^2}{\lambda_m R_r} \quad (\text{IV-5})$$

From this expression there results

$$G = \gamma G_m = \frac{\gamma}{2K_3} \sqrt{\frac{K_3 \tau}{B_s A_c}} \quad (\text{IV-6})$$

Substitution of Eq.(IV-6) into Eq.(IV-1) yields the first step in the normalization:

$$\frac{I_L}{I_{Lm}} = 1 - \frac{1}{2} \left[\frac{-1 + \sqrt{1 + 2\gamma \sqrt{\frac{K_3 \tau}{B_s A_c} H_e}}}{\gamma} \right]^2 \quad (\text{IV-7})$$

The average effective applied field H_{em} necessary for minimum output is found, by setting Eq.(IV-7) to zero, to be:

$$H_{em} = \frac{(\sqrt{2} \gamma + 1)^2 - 1}{2\gamma \sqrt{\frac{K_3 \tau}{B_s A_c}}} \quad (\text{IV-8})$$

Then, in terms of this field for minimum output, the average effective applied field becomes:

$$H_e = \frac{H_e}{H_{em}} \left[\frac{(\sqrt{2} \gamma + 1)^2 - 1}{2\gamma \sqrt{\frac{K_3 \tau}{B_s A_c}}} \right] \quad (\text{IV-9})$$

Substitution of Eq.(IV-9) into Eq.(IV-7) yields the second and last step in the normalizing process. The result is:

$$\frac{I_L}{I_{Lm}} = 1 - \frac{1}{2} \left[\frac{-1 + \sqrt{1 + [(\sqrt{2} \gamma + 1)^2 - 1] \frac{H_e}{H_{em}}}}{\gamma} \right]^2 \quad (\text{IV-10})$$

The normalizing constants for the experimental points of Figs. 3-12 and 3-13 are found in the following way. In Eq. (II-13) of Appendix II, the constant for the reactor used in the experiments was found to be

$$K_3 = B_s A_c K_1 K_2 a_o = 1.12 \times 10^{-3} \frac{v_m^2}{a^2} \quad (\text{IV-11})$$

and

$$B_s A_c = 1.87 \times 10^{-5} \text{ webers} \quad (\text{IV-12})$$

Then, using Eq.(IV-8), the values of H_{em} in Table IV-1 result. These values were used in normalizing the experimental points shown plotted in Figs. 3-12 and 3-13.

TABLE IV-1

freq. (cps)	$H_{em} \frac{a}{m}$ $\gamma = 1.00$	$H_{em} \frac{a}{m}$ $\gamma = 0.343$
500	9.79	7.16
2000	19.6	14.3

BIOGRAPHICAL NOTE

Herbert H. Woodson was born on April 5, 1925, in Stamford, Texas. After attending public schools in Slaton, Texas; Oklahoma City, Oklahoma; and Lubbock, Texas; he was graduated from Lubbock High School in 1942. He joined the United States Navy in 1942; and, after attending the Navy Radio Materiel School At Treasure Island, California, he served aboard ship in the Pacific Area for twenty months. After his discharge from the Navy in 1946, Mr. Woodson entered M.I.T. as a freshman in 1947. He was accepted for the Co-operative Course in Electrical Engineering, performing his work assignments with the Naval Ordnance Laboratory at Silver Spring, Maryland. He received the S.B. and S.M. degrees in Electrical Engineering from M.I.T. in January, 1952. While still a graduate student, Mr. Woodson married Blanche E. Sears, of Rockport, Massachusetts, in 1951.

Upon his graduation from M.I.T., Mr. Woodson accepted a position as Electrical Engineer in the Magnetics Division of the Naval Ordnance Laboratory. He remained in this position until January, 1954, at which time he was re-admitted to the Graduate School at M.I.T. for the purpose of working toward the Sc.D. degree in Electrical Engineering.

BIBLIOGRAPHY

1. AIEE Committee Report, "Progress Report of the AIEE Magnetic Amplifier Subcommittee," Trans. AIEE, 70, Part I, 1951, pp. 445-9.
2. Alexanderson, E.F.W., "A Magnetic Amplifier for Radio Telephony," Proc. IRE, 4, No. 2, April 1916, 101-29.
3. Boyajian, A., "Theory of D-C Excited Iron-Core Reactors," Trans. AIEE, 43, October 1924, 919-36.
4. Boyajian, A., "Mathematical Analysis of Nonlinear Circuits," Gen. Elec. Review, 34, September 1931, 531-7.
5. Johannessen, P.R., "Analysis of Magnetic Amplifiers by the Use of Difference Equations," Trans. AIEE, 73, Part I (Comm. and Elec.), January 1955, 700-11.
6. Storm, H.F., "Series-Connected Saturable Reactor with Control Source of Comparatively Low Impedance," Trans. AIEE, 69, Part II, 1950, 756-65.
7. Storm, H.F., "Series-Connected Saturable Reactor with Control Source of Comparatively High Impedance," Trans. AIEE, 69, Part II, 1950, 1299-1309.
8. Lamm, A.U., "Some Fundamentals of the Transductor or Magnetic Amplifier," Trans. AIEE, 66, 1947, 1078-85.
9. Black, A.O., Jr., "Effect of Core Materials on Magnetic Amplifier Design," Proc. of the Nat. Elec. Conf., 4, Chicago, Ill., 1948, 427-35.
10. Geyger, W.A., "Magnetic Amplifiers with Orthonol Tape Cores," Proc. of the Nat. Elec. Conf., 6, Chicago, Ill., 1950, 59-67.
11. Milnes, A.G., "Magnetic Amplifiers," Proc. IEE, 96, Part I, London, England, 1949, 89-98.
12. Finzi, L.A. and Beaumariage, D.C., "General Characteristics of Magnetic Amplifiers," Trans. AIEE, 69, Part II, 1950, 919-27.
13. Esselman, W.H., "Steady-State Analysis of Self-Saturating Magnetic Amplifiers Based on Linear Approximations of the Magnetization Curve," Trans. AIEE, 70, Part I, 1951, 451-9.
14. Krabbe, U., The Transductor Amplifier (book), Lindhska Boktryckeriet, Orebro, Sweden, 1947.

BIBLIOGRAPHY (continued)

15. Dornhoefer, W.J., "Self-Saturation in Magnetic Amplifiers," Trans. AIEE, 68, Part II, 1949, 835-50.
16. Smith, E.J., "Determination of Steady-State Performance of Self-Saturating Magnetic Amplifiers," Trans. AIEE, 69, Part II, 1950, 1309-17.
17. Lehman, H., "Predetermination of Control Characteristics of Half-Wave Self-Saturated Magnetic Amplifiers," Trans. AIEE, 70, Part II, 1951, 2097-2103.
18. Roberts, R.W., "Magnetic Characteristics Pertinent to the Operation of Cores in Self-Saturating Magnetic Amplifiers," Trans. AIEE, 73, Part I (Comm. and Elec.), January 1955, 682-9.
19. Lord, H.W., "Dynamic Hysteresis Loops of Several Core Materials Employed in Magnetic Amplifiers," Trans. AIEE, 72, Part I (Comm. and Elec.), March 1955, 85-8.
20. Lord, H.W., "The Influence of Magnetic-Amplifier Circuitry upon the Operating Hysteresis Loops," Trans. AIEE, 73, Part I (Comm. and Elec.), January 1954, 721-8.
21. Huhta, H., "Flux Resetting Characteristics of Several Magnetic Materials," Trans. AIEE, 73, Part I (Comm. and Elec.), May 1954, 111-4.
22. Bates, L.F., Modern Magnetism (Cambridge University Press, London, England, 1951), 281-4.
23. Kittel, C., "Physical Theory of Ferromagnetic Domains," Rev. of Mod. Phys., 21, No. 4, October 1949, 541-83.
24. Williams, H.J., "Magnetic Domains," Bell Lab. Rec., 30, No. 10, October 1952, 385-96.
25. Dijkstra, L.J., "A Nucleation Problem in Ferromagnetism," Thermodynamics in Physical Metallurgy, American Society for Metals, Cleveland, Ohio, 1950, 271-81.
26. Goodenough, J.B., "A Theory of Domain Creation and Coercive Force in Polycrystalline Ferromagnetics," Physical Review, 95, No. 4, August 15, 1954, 917-32.
27. Friedlander, F.J., "Flux Reversal in Magnetic Amplifier Cores," Trans. AIEE, 74, Part I (Comm. and Elec.), 1956.
28. Pittman, G.F., Jr., "A High-Accuracy Static Time Delay Device Utilizing Transistors," Trans. AIEE, 73, Part I (Comm. and Elec.), March 1955, 54-8.

BIBLIOGRAPHY (continued)

29. Landau, L. and Lifshitz, E., "On the Theory of the Dispersion of Magnetic Permeability in Ferromagnetic Bodies," Physikalische Zeitschrift der Sowjetunion, 8, 1935, 153-69.
30. Galt, J.K., "Motion of a Ferromagnetic Domain Wall in $\text{Fe}_{3/4}$," Physical Review, 85, No. 4, February 15, 1952, 664-9.
31. Williams, H.J., Shockley, W., and Kittel, C., "Studies of the Propagation Velocity of a Ferromagnetic Domain Boundary," Physical Review, 80, No. 6, December 15, 1950, 1090-94.
32. Menyuk, N., Goodenough, J.B., "Magnetic Materials for Digital-Computer Components. I. A Theory of Flux Reversal in Polycrystalline Ferromagnetics," Jour. of Applied Physics, 26, No. 1, January 1955, 8-18.
33. Menyuk, N., "Magnetic Materials for Digital-Computer Components. II. Magnetic Characteristics of Ultra-Thin Molybdenum Permalloy Cores," Jour. of Applied Physics, 26, No. 6, June 1955, 692-7.
34. Rado, G.F., Wright, R.W., and Emerson, W.H., "Ferromagnetism at Very High Frequencies. III. Two Mechanisms of Dispersion in a Ferrite," Physical Review, 80, No. 2, October 15, 1950, 273-80.
35. Batdorf, S.B. and Johnson, W.N., "An Instability of Self-Saturating Magnetic Amplifiers Using Rectangular Loop Core Materials," Trans. AIEE, 72, Part I (Comm. and Elec.), July 1953, 223-7.
36. Rodbell, D.S. and Bean, C.P., "The Influence of Pulsed Magnetic Fields on the Reversal of Magnetization in Square-Loop Metallic Tapes," Proc. of the Conf. on Magnetism and Magnetic Materials, AIEE, October 1955, 219-27.
37. Roberts, R.W. and Van Nice, R.I., "Influence of ID/OD Ratio on Static and Dynamic Magnetic Properties of Toroidal Cores," Trans. AIEE, 73, Part I (Comm. and Elec.), November 1955, 599-607.